ปฏิกิริยาไฮโดรจิเนชันแบบเลือกเกิดในวัฏภาคของเหลวของฟีนิลอะเซทิลีนบนตัวเร่งปฏิกิริยา
แพลเลเดียมบนตัวรองรับไทเทเนียขนาดไมโครเมตรและนาโนเมตร

นางสาวพัชราภรณ์ วีระชวนะศักดิ์

LIQUID-PHASE SELECTIVE HYDROGENATION OF PHENYLACETYLENE ON MICRON AND NANO-SIZED TiO₂ SUPPORTED Pd CATALYSTS

Miss Patcharaporn Weerachawanasak

A Thesis Submitted in Partial Fulfillment of the Requirements
for the Degree of Master of Engineering Program in Chemical Engineering
Department of Chemical Engineering
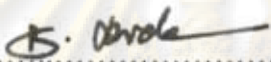Faculty of Engineering
Chulalongkorn University
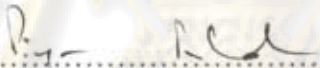Academic Year 2007
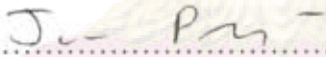
500335

Thesis Title	LIQUID-PHASE SELECTIVE HYDROGENATION OF PHENYLACETYLENE ON MICRON AND NANO-SIZED TiO$_2$ SUPPORTED Pd CATALYSTS
By	Miss Patcharaporn Weerachawanasak
Field of Study	Chemical Engineering
Thesis Advisor	Assistant Professor Joongjai Panpranot, Ph.D.

Accepted by the Faculty of Engineering, Chulalongkorn University in Partial Fulfillment of the Requirements for the Master's Degree

……………………………………Dean of the Faculty of Engineering

(Associate Professor Boonsom Lerdhirunwong, Dr.Ing.)

THESIS COMMITTEE

……………………………………Chairman

(Professor Piyasan Praserthdam, Dr.Ing.)

……………………………………Thesis Advisor

(Assistant Professor Joongjai Panpranot, Ph.D.)

……………………………………External Member

(Assistant Professor Okorn Mekasuwandamrong, Ph.D.)

……………………………………Member

(Assistant Professor Bunjerd Jongsomjit, Ph.D.)

……………………………………Member

(Associate Professor Muenduen Phisalaphong, Ph.D.)

พัชราภรณ์ วีระชวนะศักดิ์: ปฏิกิริยาไฮโดรจิเนชันแบบเลือกเกิดในวัฏภาคของเหลวของฟีนิลอะเซทิลีน บนตัวเร่งปฏิกิริยาแพลเลเดียมบนตัวรองรับไทเทเนียขนาดไมโครเมตรและนาโนเมตร (LIQUID-PHASE SELECTIVE HYDROGENATION OF PHENYLACETYLENE ON MICRON AND NANO-SIZED TiO$_2$ SUPPORTED Pd CATALYSTS) อ. ที่ปรึกษา: ผศ. ดร. จุงใจ ปั้นประณต, 106 หน้า

วิทยานิพนธ์นี้ศึกษาลักษณะเฉพาะและคุณสมบัติการเร่งปฏิกิริยาของตัวเร่งปฏิกิริยาแพลเลเดียมบน ตัวรองรับไทเทเนียขนาดไมโครเมตรและนาโนเมตรในปฏิกิริยาไฮโดรจิเนชันแบบเลือกเกิดของฟีนิลอะเซทิลีน ในวัฏภาคของเหลวและผลของอุณหภูมิที่ใช้ในการรีดิวซ์ต่ออันตรกิริยาระหว่างโลหะแพลเลเดียมและตัวรองรับ ไทเทเนีย โดยที่ตัวเร่งปฏิกิริยาแพลเลเดียมบนตัวรองรับไทเทเนียทั้งหมดเตรียมขึ้นโดยวิธีการเคลือบฝัง ไทเทเนีย ขนาดไมโครเมตรเป็นไทเทเนียทางการค้าในขณะที่ไทเทเนียขนาดนาโนเมตรเตรียมโดยวิธีโซลโวเทอร์มอล พบว่าเมื่อรีดิวซ์ด้วยไฮโดรเจนที่อุณหภูมิ 500 องศาเซลเซียส ตัวเร่งปฏิกิริยาแพลเลเดียมบนตัวรองรับไทเทเนีย ขนาดนาโนเมตรจะปรากฏอันตรกิริยาที่แข็งแรงระหว่างโลหะแพลเลเดียมและตัวรองรับไทเทเนียซึ่งส่งผลในการ เพิ่มประสิทธิภาพการเร่งปฏิกิริยาในปฏิกิริยาไฮโดรจิเนชันแบบเลือกเกิดของฟีนิลอะเซทิลีนในวัฏภาคของเหลว โดยทำให้ค่าการเลือกเกิดเป็นผลิตภัณฑ์ที่ต้องการคือสไตรีนสูงขึ้นที่ค่าการแปลงผันของฟีนิลอะเซทิลีน 100% ผลการวิเคราะห์ด้วยเทคนิคการดูดซับคาร์บอนมอนออกไซด์, เอ็กซ์เรย์โฟโตอิเล็คตรอนสเปกโทรสโกปี, กล้อง จุลทรรศน์อิเลคตรอนแบบส่องผ่านและการดูดซับคาร์บอนมอนนอกไซด์แบบโปรแกรมอุณหภูมิ พบว่าตัวเร่ง ปฏิกิริยาแพลเลเดียมบนตัวรองรับไทเทเนียขนาดไมโครเมตรที่ถูกรีดิวซ์ด้วยไฮโดรเจนที่อุณหภูมิ 500 องศา เซลเซียสจะไม่เกิดอันตรกิริยาระหว่างแพลเลเดียมและไทเทเนีย ทั้งนี้คาดว่าเป็นผลจากการที่ Ti^{3+} ที่อยู่ในผลึก ของไทเทเนียที่มีขนาดใหญ่เคลื่อนที่ไปยังพื้นผิวของแพลเลเดียมได้ยากกว่า Ti^{3+} ที่อยู่บนพื้นผิวของผลึกไท เทเนียขนาดเล็ก ทำให้เกิดการรวมตัวกันของโลหะแพลเลเดียมแทนการเกิดอันตรกิริยาระหว่างแพลเลเดียมและ ตัวรองรับไทเทเนีย เมื่อทำการศึกษาผลของขนาดผลึกของตัวรองรับไทเทเนียในช่วง 9 ถึง 23 นาโนเมตร พบว่า ตัวเร่งปฏิกิริยาที่เตรียมบนตัวรองรับไทเทเนียที่มีผลึกขนาดเล็กโลหะแพลเลเดียมจะมีขนาดเล็กกว่าตัวเร่ง ปฏิกิริยาที่เตรียมจากตัวรองรับไทเทเนียที่มีผลึกขนาดใหญ่ อย่างไรก็ตามตัวเร่งปฏิกิริยาบนไทเทเนียขนาดเล็กมี ความว่องไวในปฏิกิริยาไฮโดรจิเนชันต่ำกว่าตัวเร่งปฏิกิริยาบนตัวรองรับไทเทเนียขนาดใหญ่ โดยที่ค่าการเลือก เกิดของสไตรีนสูงขึ้นเมื่อรีดิวซ์ที่อุณหภูมิ 500 องศาเซลเซียส เนื่องมาจากผลของอันตรกิริยาที่แข็งแรงระหว่าง แพลเลเดียมและตัวรองรับไทเทเนีย โดยที่ผลของอันตรกิริยานี้จะปรากฏชัดเจนสำหรับตัวรองรับไทเทเนียที่ผลึก ขนาดเล็กมากกว่าตัวรองรับไทเทเนียที่มีผลึกขนาดใหญ่

ภาควิชา..........วิศวกรรมเคมี..........ลายมือชื่อนิสิต.....พัชราภรณ์ วีระชวนะศักดิ์........

สาขาวิชา..........วิศวกรรมเคมี..........ลายมือชื่ออาจารย์ที่ปรึกษา.................

ปีการศึกษา..........2550..........

4870397521: MAJOR CHEMICAL ENGINEERING

KEYWORDS: LIQUID-PHASE SELECTIVE HYDROGENATION/ TITANIA SUPPORTED PALLADIUM CATALYSTS/SMSI

PATCHARAPORN WEERACHAWANASAK: LIQUID-PHASE SELECTIVE HYDROGENATION OF PHENYLACETYLENE ON MICRON AND NANO-SIZED TiO_2 SUPPORTED Pd CATALYSTS THESIS ADVISOR: ASST. PROF. JOONGJAI PANPRANOT Ph.D., 106 pp.

The characteristics and catalytic properties of Pd catalysts supported on micron and nano-sized TiO_2 were investigated in the liquid-phase selective hydrogenation of phenylacetylene to styrene. Moreover, the effect of reducing temperature on the strong metal-support interaction has been studied. All of Pd/TiO_2 catalysts were prepared by incipient wetness impregnation method. The TiO_2-micron-sized was obtained commercially from Aldrich whereas the TiO_2-nano-sized was derived by solvothermal method. It was found that when supported on the nano-sized TiO_2, the Pd/TiO_2 catalyst that reduced in H_2 at $500^{\circ}C$ exhibited strong metal-support interaction (SMSI) and much improved catalyst performance in liquid-phase selective hydrogenation of phenylacetylene. However, as revealed by CO pulse chemisorption, X-ray photoelectron spectroscopy (XPS), transmission electron microscopy (TEM), and CO-temperature program desorption results, the SMSI effect was not detected for the micron-sized TiO_2 supported ones. It is suggested that during high temperature reduction, the inner Ti^{3+} in large crystallite size TiO_2 was more difficult to diffuse to the Pd surface than the surface Ti^{3+} in the smaller crystallite size ones. Sintering of Pd^0 metal was observed instead. Furthermore, a series of nanocrystalline TiO_2 supported Pd catalysts with various TiO_2 crystallite sizes in the range of 9-23 nm were investigated. Higher Pd dispersion and smaller Pd particles were obtained on the catalysts with smaller TiO_2 crystallite size. However, such catalysts exhibited lower hydrogenation activities. For most cases, styrene selectivity at 100% phenylacetylene conversion was improved when the catalysts were reduced at $500^{\circ}C$ due probably to the strong metal-support interaction effect. The SMSI effect, however, was more pronounced for the Pd catalysts supported on smaller crystallite size TiO_2 as shown by the different catalyst behaviors when reduced at 40 and $500^{\circ}C$.

Department ....Chemical Engineering........... Student's signature .Patcharaporn Weerachawanasa

Field of Study...........Chemical Engineering........... Advisor's signature ...J. Pan...........

Academic year ....2007...............

ACKNOWLEDGEMENTS

CONTENTS

CHAPTER

CHAPTER

CHAPTER

LIST OF TABLES

LIST OF FIGURES

FIGURE   Page

CHAPTER I

INTRODUCTION

1.1 Rationale

Hydrogenation of carbon-carbon triple bonds, particularly to the olefinic bonds, has been the subject of numerous investigations since the very early stage of the study on catalytic hydrogenation, not only in terms of its synthetic utility but also with respect to the selectivity of catalytic metal for the selective hydrogenation.

The selective hydrogenation of alkynes to alkenes has fundamental importance in the fine chemicals production and industrial polymerization processes. In general, the selective hydrogenation reactions are carried out both in gas phase and liquid phase but a large number of these reactions are carried out in liquid phase using batch type slurry processes. The noble metal or transition metals group VIII are mostly catalyzed in the hydrogenation reactions because they adsorb hydrogen with dissociation and the bonding is not too strong. The major advantages of noble metal catalysts are their relatively high activity, mild process conditions, easy separation, and better handling properties. The noble metals which have an effective in hydrogenation process are Pd, Pt, Rh, and Ru. However, palladium is one of the most frequently used metals in such processes since it has the unique ability to selectively hydrogenation. (Guczi, L. et al., 1998)

The performance of noble metal catalysts in liquid-phase hydrogenation has been found to be dependent on several factors such as liquid composition (substrate structure, solvent effect, etc), catalyst nature (elemental composition, morphology, support effects, modifiers, etc) and reaction conditions (temperature, pressure, etc) The deactivation of catalyst is an important problem in catalytic liquid phase hydrogenation because activity and selectivity of the reaction is decrease after several runs. There are several factors affecting the catalyst deactivation in liquid phase

hydrogenation such as sintering of metal particles and coalescence, leaching of active phases and supports and poisoning of strongly adsorbed molecules.

The catalyst supports must present a good stability to high temperature and a sufficiently large surface area. Various supports have been used in preparation of supported palladium catalyst for selective hydrogenation in liquid phase such as silica, alumina, carbon, and titania.

Titania is of particular interest as a support for Pd catalysts in hydrogenation reactions because it exhibits a strong metal-support interaction (SMSI). It was found that noble metal supported on reduced oxides such as titania exhibits differences in catalytic activity and selectivity in hydrogenation reaction when reduced at high temperature, compared with the one reduced at lower temperature or the corresponding noble metal supported on un-reducible supports (without SMSI). For example, Li et $al.$ (2004) studied SMSI for anatase and rutile titania supported palladium catalysts and showed that pre-reduced by H_2 at lower temperature results in SMSI for anatase titania supported palladium catalyst, but not for rutile titania supported palladium catalyst. The Pd/TiO_2 catalysts with SMSI were found to exhibit higher selectivities for anatase titnia supported palladium catalyst than rutile titania supported palladium catalyst.

However, to our knowledge the effect of TiO_2 crystallite size on the SMSI has not been studied very often especially for the nanocrystalline ones, therefore, it is the focuses of this thesis to investigate the characteristics and catalytic properties for palladium supported on micron and nano-sized titania in liquid-phase selective hydrogenation of phenylacetylene to styrene. In this investigation, the nano-TiO_2 was synthesized by the solvothermal method. Commercially available micron-sized TiO_2 was also used for comparison purposes. Moreover, the effect of reducing temperature on the SMSI effect on supported palladium catalysts was investigated.

1.2 Research Objectives

1. To investigate the characteristics and catalytic properties of palladium catalysts supported on micron-and nano-sized TiO_2 in liquid-phase selective hydrogenation.

2. To investigate the effect of reducing temperature on the strong metal support interaction on the micron and nano-sized TiO_2 supported Pd catalysts.

3. To investigate the effect of various nanocrystallite size of TiO_2 supported Pd catalysts on the strong metal support interaction and catalytic properties in liquid-phase selective hydrogenation.

1.3 Research Scopes

Part I

1. Preparation of nano-sized TiO_2 using solvothermal method in 1,4-butanediol and the micron-sized TiO_2 was obtained commercially from Aldrich.

2. Preparation of TiO_2-supported palladium catalysts (Pd/TiO_2) with 1% wt palladium loading using incipient wetness impregnation method.

3. Characterization of the titania-supported palladium catalysts using several techniques such as, X-ray diffraction (XRD), N_2 physisorption, Scanning electron microscopy (SEM), Transmission electron microscopy (TEM), CO pulse chemisorption, CO-temperature program desorption, Electron spin resonance (ESR), X-ray photoelectron spectroscopy (XPS) and Atomic absorption spectroscopy (AAS).

4. Reaction study of the micron and nano-sized TiO_2-supported palladium catalysts in liquid-phase selective hydrogenation of phenylacetylene using stirring batch reactor (stainless steel autoclave 50 ml).

Part II

1. Preparation the series of nanocrystallite size TiO_2 supports by solvothermal method. The amount of TNB, reaction temperature, and holding time were adjusted to obtain various nanocrystallite size of TiO_2 in the range of 9-23 nm.

2. Preparation of $1\%Pd/TiO_2$ catalysts using incipient wetness impregnation method.

3. Characterization of the catalysts using several techniques such as, X-ray diffraction (XRD), N_2 physisorption, Scanning electron microscopy (SEM), Transmission electron microscopy (TEM), CO pulse chemisorption and Atomic absorption spectroscopy (AAS).

4. Reaction study in liquid phase selective hydrogenation of phenylacetylene on various nanocrystallite size of TiO_2 supported palladium catalysts using stirring bath reactor.

1.4 Research Methodology

```
┌─────────────────────┐
│  Literature reviews │
└─────────────────────┘
```

┌─────────────────────────────┐   ┌─────────────────────────────┐
│ The micron-sized TiO_2 obtain │   │ Synthesis of nano-sized-TiO_2 with various │
│ commercially from Aldrich   │   │ crystallite sizes by solvothemal method │
└─────────────────────────────┘   └─────────────────────────────┘

┌───┐
│ Preparations of TiO_2 supported Pd (1 % wt Pd) catalysts │
│ using the incipient wetness impregnation method. │
└───┘

┌───┐
│ Catalysts characterization using, XRD, BET, SEM, TEM, │
│ XPS, ESR, AAS, pulse CO-chemisorption, and CO-TPD │
└───┘

┌───┐
│ Reduction of all catalysts by H_2 at different │
│ various reducing temperature ($40^{o}C$ and $500^{o}C$) │
└───┘

┌───┐
│ Reaction study in liquid phase selective │
│ hydrogenation of phenylacetylene │
└───┘

┌─────────────────────┐
│   Data analysis   │
└─────────────────────┘

CHAPTER II

THEORY

2.1 Hydrogenation

Catalytic hydrogenation reaction is a well known versatile reaction widely used in organic syntheses. Many functional groups contained in organic substrates can be hydrogenated to produce several useful compounds which has been used for wide applications such as monomers for production of various polymers, fats and oil for producing edible and no edible products, and intermediates used in pharmaceutical industry. Hydrogenation processes are often carried out in a small scale in batch reactor. Batch processes are usually most cost effective since the equipment need not to be dedicated to a single reaction. Typically the catalyst is powdered and slurried with reactant; a solvent is usually present to influence product selectivity and to adsorb the reaction heat liberated by the reaction. Since most hydrogenations are highly exothermic, careful temperature control is required to achieve the desired selectivity and to prevent temperature runaway.

Selective hydrogenation of alkynes is an addition of hydrogen to a carbon-carbon triple bond in order to produce only alkenes product. The overall effect of such an addition is the reductive removal of the triple bond functional group. The simplest source of two hydrogen atoms is molecular hydrogen (H_2), but mixing alkynes with hydrogen does not result in any discernable reaction. However, careful hydrogenation of an alkynes proceeds exclusively to the alkenes until the former is consumed, at which point the product alkenes is very rapidly hydrogenated to an alkanes. Although the overall hydrogenation reaction is exothermic, a high activation energy prevents it from taking place under normal conditions. This restriction may be circumvented by the use of a catalyst, as shown in the following diagram.
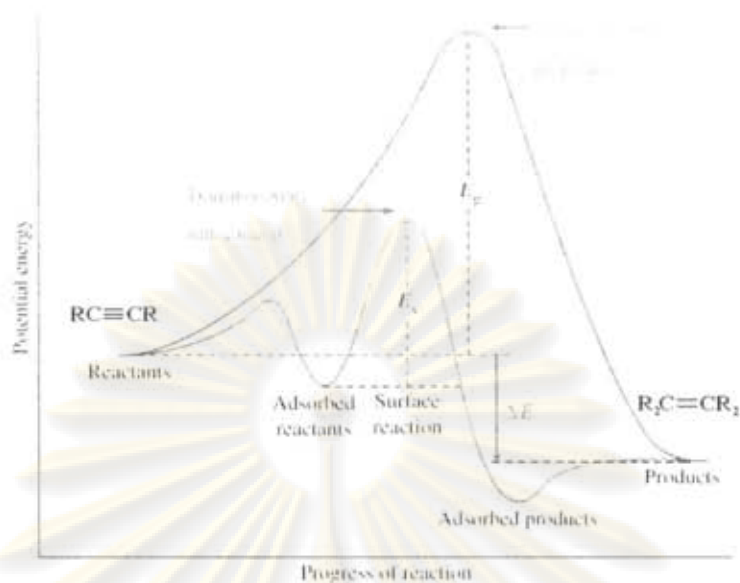
Catalysts are substances that change the rate (velocity) of a chemical reaction without being consumed or appearing as part of the product. Catalysts act by lowering the activation energy of reactions, but they do not change the relative potential energy of the reactants and products. Finely divided metals, such as platinum, palladium and nickel, are among the most widely used hydrogenation catalysts.

Selective hydrogenation of alkyne to alkene is the reaction which takes place on the surface of the metal catalyst. The mechanism of the reaction can be described in four steps:

Step 1: Hydrogen molecules react with the metal atoms at the catalyst surface. The relatively strong H-H sigma bond is broken and replaced with two weak metal-H bonds.
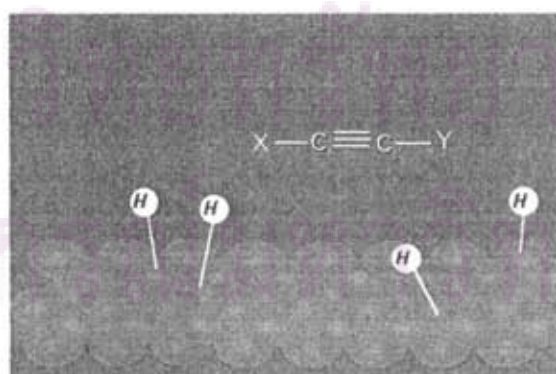
Step 2: The pi bond of the alkyne interacts with the metal catalyst weakening the bond. A hydrogen atom is transferred from the catalyst surface to one of the carbons of the triple bond.
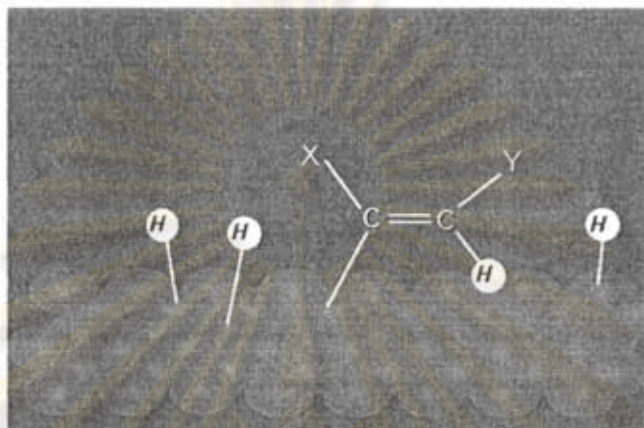
Step 3: The pi bond of the alkyne interacts with the metal catalyst weakening the bond. A second hydrogen atom is transferred from the catalyst surface forming the alkene.
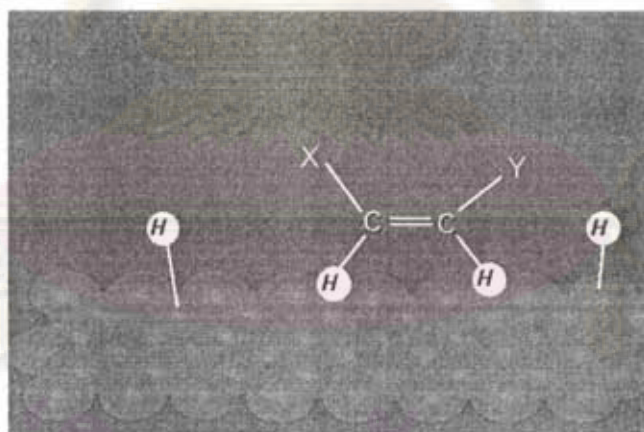
Step 4: The alkene is released from the catalyst's surface allowing the catalyst to accept additional hydrogen and alkene molecules.
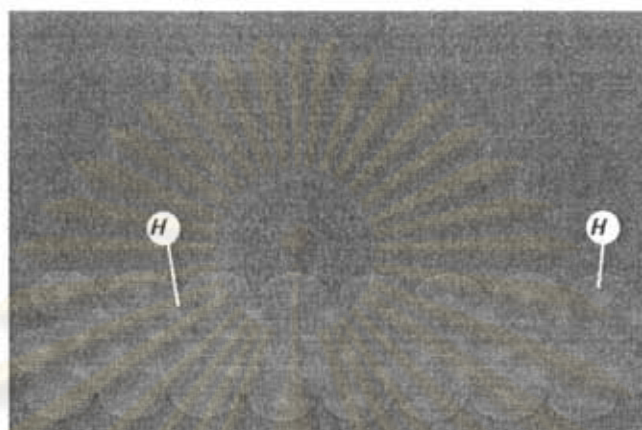
Phenylacetylene hydrogenation scheme (see in **Figure2.1**) consists of two consecutive steps in parallel with a single step directly to the final hydrogenation product.
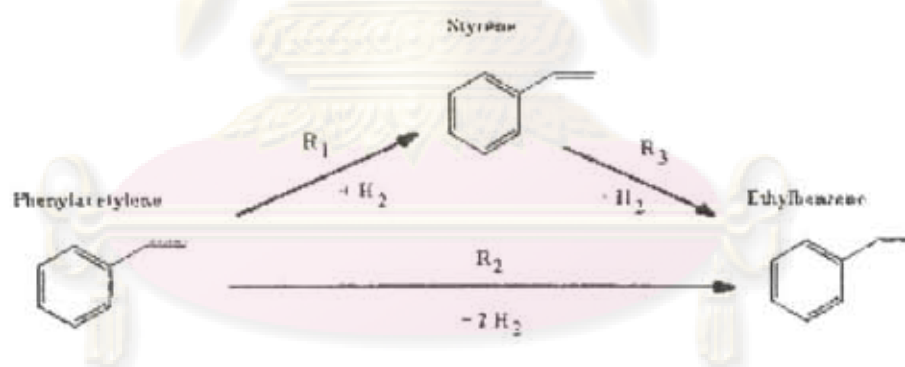
Figure2.1 Scheme of Phenylacetylene hydrogenation (X. Huang *et al.*, 2003)

2.2 Palladium-Based Catalysts

Palladium, the preferred metal of choice for alkyne selective hydrogenation, is normally used as a supported heterogeneous catalyst and frequently in presence of some form of additive to promote selectivity. For heterogeneous system in particular catalyst performance is strongly influenced by, firstly, the ability to get reactants to the active sites, then to establish the optimum hydrogen-to-hydrocarbon surface coverage, and, finally, the rapid removal of the hydrogenated products. These constitute the 'mass transfer limitations' and can have on overriding impact on the ability to achieve selective hydrogenation. In this respect, the nature of the support (inertness, surface area, pore size distribution) controls molecular access to the active sites and can also participate in unwanted side reaction through so-called 'spillover' effects.

2.3 Titanium (IV) oxide

2.3.1 Physical and chemical properties

Titanium (IV) oxide occurs naturally in three crystalline forms :

1. Rutile, which tends to more stable at high temperatures. The application of almost rutile type is used in industrial products such as paints, cosmetics foodstuffs and sometimes found in igneous rocks.

2. Anatase, which tends to be more stable at lower temperatures. This type generally shows a higher activity in hydrogenation and photo catalytic than other types of titanium dioxide.

3. Brookite, which is usually found only in minerals and has a structure belonging to orthorhombic crystal system.

A summary of the crystallographic properties of the three varieties is given in **Table 2.1**

Table 2.1 Crystallographic properties of anatase, brookite, and rutile.

Properties	Anatase	Brookite	Rutile
Crystal structure	Tetragonal	Orthorhombic	Tetragonal
Optical	Uniaxial, negative	Biaxial, positive	Uniaxial, negative
Density, g/cm^3	3.9	4.0	4.23
Harness, Mohs scale	$5^1/_2 - 6$	$5^1/_2 - 6$	$7 - 7^1/_2$
Unit cell	$D_4a^{19}.4TiO_2$	$D_2h^{15}.8TiO_2$	$D_4h^{12}.3TiO_2$
Dimension, nm			
a	0.3758	0.9166	0.4584
b		0.5436	
c	0.9514	0.5135	2.953

Both of rutile and anatase type have a structure belonging to tetragonal crystal system but they are not isomorphous (**Figure 2.2**). The two tetragonal crystal types are more common because they are easy to make. Anatase occurs usually in near-regular octahedral, and rutile forms slender prismatic crystal, which are frequently twinned. Rutile is the thermally stable form and is one of the two most important ores of titanium.

The three allotropic forms of titanium dioxide have been prepared artificially but only rutile, the thermally stable form, has been obtained in the form of transparent large single crystal. The transformation form anatase to rutile is accompanied by the evolution of ca. 12.6 kJ/mol (3.01 kcal/mol), but the rate of transformation is greatly affected by temperature and by the presence of other substance which may either catalyze of inhibit the reaction. The lowest temperature at which conversion of anatase to rutile takes place at a measurable rate is ca. 700°C, but this is not a transition temperature. The change is not reversible; ΔG for the change from anatase to rutile is always negative.
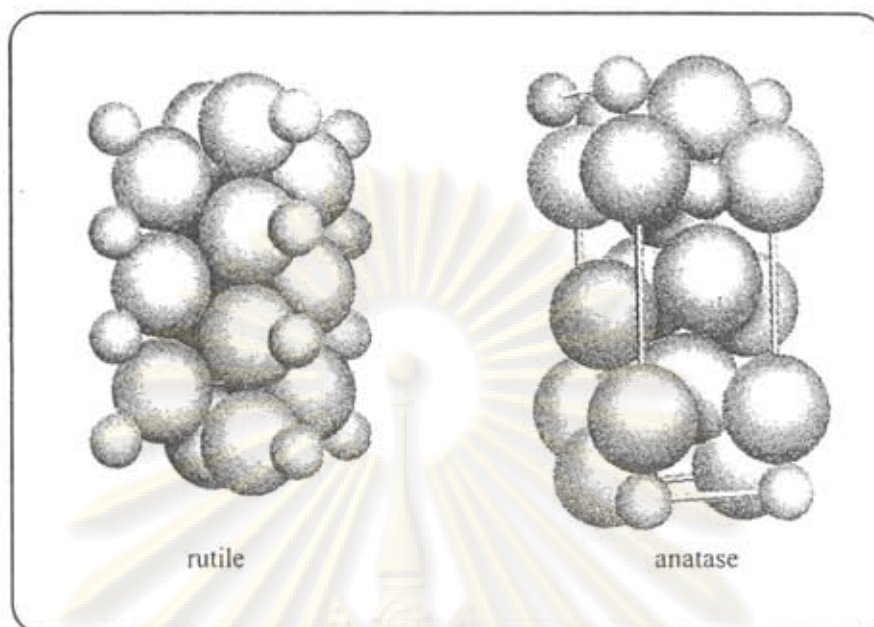
Figure 2.2 Crystal structure of TiO_2. (Fujishima *et al.*, 1999)

Brookite has been produced by heating amorphous titanium (IV) oxide, prepared from an alkyl titanates of sodium titanate with sodium or potassium hydroxide in an autoclave at 200 to 600°C for several days. The important commercial forms of titanium (IV) oxide are anatase and rutile, and these can readily be distinguished by X-ray diffraction spectrometry.

Since both anatase and rutile are tetragonal, they are both anisotropic, and their physical properties, e.g. refractive index, vary according to the direction relative to the crystal axes. In most applications of these substances, the distinction between crystallographic direction is lost because of the random orientation of large numbers of small particles, and it is mean value of the property that is significant.

Measurement of physical properties, in which the crystallographic directions are taken into account, may be made of both natural and synthetic rutile, natural anatase crystals, and natural brookite crystals. Measurements of the refractive index of titanium dioxide must be made by using a crystal that is suitably orientated with respect to the crystallographic axis as a prism in a spectrometer. Crystals of suitable

size of all three modifications occur naturally and have been studied. However, rutile is the only form that can be obtained in large artificial crystals from melts. The refractive index of rutile is 2.75. The dielectric constant of rutile varies with direction in the crystal and with any variation from the stoichiometric formula, TiO_2; an average value for rutile in powder from is 114. The dielectric constant of anatase powder is 48.

Titanium dioxide is thermally stable (mp 1855°C) and very resistant to chemical attack. When it is heated strongly under vacuum, there is a slight loss of oxygen corresponding to a change in composition to $TiO_{1.97}$. The product is dark blue but reverts to the original white color when it is heated in air.

Hydrogen and carbon monoxide reduce it only partially at high temperatures, yielding lower oxides or mixtures of carbide and lower oxides. At ca. 2000°C and under vacuum, carbon reduces it to titanium carbide. Reduction by metal, e.g., Na, K, Ca, and Mg, is not complete. Chlorination is only possible if a reducing agent is present; the position of equilibrium in the system is The reactivity of titanium dioxide towards acids is very dependent on the temperature to which it has been heated. For example, titanium dioxide that has been prepared by precipitation from a titanium (IV) solution and gently heated to remove water is soluble in concentrated hydrochloric acid. If the titanium dioxide is heated to ca. 900°C, then its solubility in acids is considerably reduced. It is slowly dissolved by hot concentrate sulfuric acid, the rate of salvation being increased by the addition of ammonium sulfate, which raises the boiling point of the acid. The only other acid in which it is soluble is hydrofluoric acid, which is used extensively in the analysis of titanium dioxide for trace elements. Aqueous alkalies have virtually no effect, but molten sodium and potassium hydroxides, carbonates, and borates dissolve titanium dioxide readily. An equimolar molten mixture of sodium carbonate and sodium borate is particularly effective as is molten potassium pyrosulfate.

$$TiO_2 + 2Cl_2 \rightleftharpoons TiCl_4 + O_2$$

The reactivity of titanium dioxide towards acids is very dependent on the temperature to which it has been heated. For example, titanium dioxide that has been prepared by precipitation from a titanium (IV) solution and gently heated to remove water is soluble in concentrated hydrochloric acid. If the titanium dioxide is heated to ca. 900°C, then its solubility in acids is considerably reduced. It is slowly dissolved by hot concentrate sulfuric acid, the rate of salvation being increased by the addition of ammonium sulfate, which raises the boiling point of the acid. The only other acid in which it is soluble is hydrofluoric acid, which is used extensively in the analysis of titanium dioxide for trace elements. Aqueous alkalies have virtually no effect, but molten sodium and potassium hydroxides, carbonates, and borates dissolve titanium dioxide readily. An equimolar molten mixture of sodium carbonate and sodium borate is particularly effective as is molten potassium pyrosulfate.

2.4 Strong Metal Support Interaction (SMSI)

Strong metal support interaction (SMSI) was found by S.J.Tauster et al in 1978. (Tauster, Fung and Garten. 1978) SMSI is the loss of the metal's ability to chemisorb molecules which normally react without difficulty at metal surfaces: hydrogen and carbon monoxide. (Bond, G.C.1983) Generally, the SMSI account for the changes in catalytic activity when the group VIII metals Fe, Ni, Rh, Pt, Pd, and Ir, supported on reducible oxides (TiO_2, TaO_5, CeO_2, NbO, etc.), are reduced at elevated temperature. Furthermore, the effect of high reduction in hydrogen at high temperature is not to cause particle growth by sintering, so the loss of chemisorption capacity cannot be attributed to this. However transmission electron microscopy has revealed suggestions of alteration in the morphology of metal particles. Another notable feature of SMSI is that it is reversed by oxidising conditions. Oxygen chemisorption is not suppressed, and any explanation of the effect must take account of this.

2.5 Solvothermal Method

Solvothermal method have been developed for synthesis of metal oxide and binary metal oxide with large surface area, high crystallinity and high thermal stability (Payakgul *et al.*, 2005) by using solvent as the reaction medium. The solvothermal method is similar to the hydrothermal method except that organic solvents are used instead of water. This method can effectively prevent the products from oxidizing. The solvothermal treatment could be used to control grain size, particle morphology, crystalline phase and surface chemistry by regulating sol composition, reaction temperature, pressure, nature of solvent, additives, and aging time. In particular, the particles prepared by the solvothermal method were reported to have larger surface area, smaller particle size, and were more stable than those obtained by other methods such as the sol–gel one. (Kang *et al.*, 2004)

Titanium precursor such as titanium alkoxide, was used as starting material for titania synthesis. Titanium precursor was first suspended in organic solvent in a test tube of autoclave. The crystalline titania was formed at temperature in the rang of 200-340°C in autoclave. Autogeneous pressure during the reaction gradually increased as the temperature was raised. It has been reported that physiochemical properties of the synthesized titania depend on the reaction conditions as well as the calcination temperature.

CHAPTER III

LITERATURE REVIEW

3.1 Synthesis of nanocrystalline TiO$_2$ by solvothemal method

M. Kang *et al.* (2001) synthesized TiO$_2$ photocatalysts by using the sol–gel and solvothermal methods in order to study renders a reliable synthesis procedure of the TiO$_2$ photocatalyst having the anatase structure of nano size. After that, physical properties and catalytic performances of two kinds TiO$_2$ photocatalysts were compared. The TiO$_2$ powder (Cat.2) obtained by the solvothermal method at 300°C exhibited a pure anatase structure without any further treatment, while the TiO$_2$ powder (Cat.1) prepared by the sol–gel method was transformed to the anatase structure after thermal treatment at 500°C for 3 h. Cat.2 had higher surface area (121m^2/g) and surface charge (+24.1 mV) than Cat.1 (51m^2/g, +16.4 mV).

M. Kang *et al.* (2003) synthesized TiO$_2$ and Fe/TiO$_2$ nonoparticles in 1,4 butanediol with solvothermal method. The TiO$_2$ and Fe/TiO$_2$ particles exhibited an uniform anatase structure with particle size below 50 nm after synthesis at 300°C for 1 h without any treatments. Attained Fe/TiO$_2$ particles had a higher hydrophilic property compared with TiO$_2$. The anatase structure was stable in 10-mol% H$_2$O addition as a reactant, but it was transferred into rutile structure with an increase of added H$_2$O.

C.S. Kim *et al.* (2003) synthesized TiO$_2$ nanoparticles in toluene solutions with titanium isopropoxide (TIP) as precursor by a solvothermal synthetic method. After synthesis at 250°C for 3 h with solutions at the weight ratios 10/100, 20/100 and 30/100 nanocrystalline TiO$_2$ particles are formed and they have a uniform anatase structure with average particle size below 20 nm. Average size of the nanocrystalline particle increases as increasing the amount of TIP precursor in this composition range. For the products obtained from the solution of 5/100 and 40/100, crystalline particles cannot be obtained. The 5/100 of TIP in the mixture may be too small amount to

synthesize TiO_2 nanoparticles at $250^{\circ}C$ and longer time is also needed to obtain adequate size of the particle. In the mixture of 40/100 TIP the synthetic process of TiO_2 particles may be hindered by agglomeration of the reactants due to surplus of precursor.

W. Payakgul et al. (2005) synthesized titania using thermal decomposition of titanium (IV) n-butoxide (TNB) in organic solvents yields nanosized anatase titania without the contamination of other phases. The formation of anatase titania crystals and their phase transformation are investigated by using X-ray diffraction (XRD), SEM, BET techniques. It is suggested that anatase titania synthesized in 1,4 butanediol is the result from direct crystallization while titania synthesized in toluene is transformed from precipitated amorphous intermediate. Thermal stability of products investigated by calcination at various temperatures and photocatalytic activity evaluated from ethylene decomposition reaction suggest that amount of defect structures in titania synthesized depends upon the solvent used.

W. Kongsuebchart et al. (2006) synthesized nano-TiO_2 powder by solvothermal method under various reaction conditions in order to obtain average crystallite sizes of 9–15 nm. Increasing of TNB concentrations, the reaction temperatures, and the holding times resulted in an increase in the average crystallite size of TiO_2. The amounts of surface defect of TiO_2 were measured by means of temperature-programmed desorption of CO_2 and electron spin resonance spectroscopy. It was found that the ratios of surface defect/specific surface area increased significantly with increasing TiO_2 crystallite size. Moreover, the TiO_2 with higher amounts of surface defects exhibited much higher photocatalytic activity for ethylene decomposition.

C.S. Kim et al. (2007) synthesized nanocrystalline TiO_2 powders of anatase phase by the solvothermal route from the $Ti(OR)_4$ precursor precipitated in toluene under different concentrations and studied the particle size effect on the phase transformation of nanocrystalline TiO_2. The results illustrated that the particle size of TiO_2 powder increases with the composition of TTIP. Average particle size is about

10 nm and 20 nm for contents of precursor below 10 mol% and above 50 mol%, respectively. When the composition of precursor is 20 mol%, the extent of increase is very high. After annealing at 700 °C for 3 h, diffraction peaks of rutile phase appears in the powder of size 11 nm. On the other hand, diffraction peaks of rutile phase appear slightly at 750 °C and anatase phase almost disappear after annealing at 800 °C in the powder of size 21 nm. Consequently, difference of coarsening mechanism between powder A (11 nm) and powder B (21 nm) exists and coarsening rate of the grains is higher in powder A than powder B.

3.2 Supported Pd catalyst in liquid-phase hydrogenation

S.D. Jackson *et al.* (1995) studied hydrogenation of phenylacetylene and styrene over a palladium/carbon catalyst. The kinetics of the reactions were investigated and activation energies of 26 ± 2 kJ mol^{-1} 41 ± 8 kJ mol^{-1} were obtained for phenylacetylene hydrogenation and styrene hydrogenation, respectively. Both reactions were found to be zero order concerning the alkyne or alkene. However the order in phenylacetylene changed from zero order to first order at approximately 60% conversion. This change was due to the effect of styrene co-adsorption and not the concentration of phenylacetylene. Competitive hydrogenation between the alkene and alkyne resulted in a dramatically reduced rate of hydrogenation for both species. This reduced rate was explained by a reduction in the amount of surface hydrogen as well as the altered bonding of the phenylacetylene.

F. Arena *et al.* (1996) investigated the catalytic behavior of palladium supported on oligomeric aramides in the liquid phase selective hydrogenation of phenylacetylene to styrene, by comparison with conventional Pd-supported systems, such as Pd/oligo-p-phenylenterephthalamide (OPTA), Pd/carbon, Pd/Al$_2$O$_3$ and Pd/SiO$_2$. The influences of the reduction temperature and metal loading on the activity/selectivity of the title reaction are explained in terms of different reducibility patterns of the catalysts, as well as in the light of a peculiar support effect of the organic matrix on Pd particles.

J. Panpranot *et al.* (2004) studied the differences between Pd/SiO_2 and Pd/MCM-41 catalysts in liquid-phase hydrogenation. SiO_2-small pore, SiO_2-large pore, MCM-41-small pore and MCM-41-large pore were used as supports. The catalysts were prepared by incipient wetness impregnation. The reaction was carried out at 25^oC and 1 atm in a stainless steel Parr autoclave. The results showed that the characteristics and catalytic properties of the silica supported Pd catalysts in liquid-phase hydrogenation were affected by type of silica, pore size and pore structure. The catalyst activities were found to be merely dependent on the Pd dispersion, which as itself a function of the support pore structure. Among the four types of the supported Pd catalysts used in this study, Pd/MCM-41-large pore showed the highest Pd dispersion and the highest hydrogenation rate with the lowest amount of metal loss.

J. Panpranot *et al.* (2006) studied liquid-phase hydrogenation of cyclohexene under mild conditions on Pd/SiO_2 in different organic solvents (benzene, heptanol, and NMP), under pressurized carbon dioxide, and under solvent less condition were investigated and compared. In the cases of using organic solvents, the hydrogenation rates depended on polarity of the solvents in which the reaction rates in high polar solvents such as heptanol and NMP were lower than that in a non-polar solvent. Hydrogenation rates were much higher when the reactions were performed under high-pressure CO_2 or under solvent less condition. The use of high-pressure CO_2 can probably enhance H_2 solubility in the substrate resulting in a higher hydrogenation activity. However, metal sintering and leaching in the presence of high-pressure CO_2 were comparable to those in organic solvents.

N. Marin-Astorga *et al.* (2005) studied competitive hydrogenation reactions between phenyl alkyl acetylenes over Pd/MCM-41 and Pd/SiO_2 catalysts have been studied. The catalysts were prepared by impregnation MCM-41 and SiO_2 with $Pd(acac)_2$ precursor, with metal content close to 1 wt.%. All the supports were characterised by nitrogen adsorption–desorption isotherms at 77 K, XRD, TGA measurements. The catalysts were characterized by H_2 and CO chemisorption, XPS and TEM measurements. Three competitive reaction systems 1-phenyl-1-pentyne/1-phenyl-1-propyne, 1-phenyl-1-pentyne/1-phenyl-1-butyne, 1-phenyl-1-butyne/1-

phenyl-1-propyne have been examined. The results show that the competitive reaction results in an increase of the hydrogenation rate for phenyl alkyl acetylene with minor alkyl chain size in all studied systems. However, the 1-phenyl-1-pentyne/1-phenyl-1-propyne couple revealed a rate enhancement for 1-phenyl-1-propyne, but 1-pheny-l-pentyne single activity is higher than 1-phenyl-1-pentyne mixture, being the hydrogenation of 1-phenyl-1-propyne more favored. Kinetic analysis of the reactions revealed that often the hydrogenation of the phenyl alkyl acetylenes is a zero order in a competitive environment. 1-Phenyl-1-propyne was very sensitive to the presence of the second phenyl alkyl acetylene. Competitive hydrogenation also increases the selectivity to the respective alkenes as can be expected from the competition for active sites.

M. G. Musolino et $al.$ (2007) studied the effect of metal particle size and supports of palladium catalysts in selective liquid phase conversion of cis-2-butene-1,4-diol affording also, when hydrogenated, 2-hydroxytetrahydrofuran.. Palladium catalysts on different supports (SiO_2, Al_2O_3, TiO_2, ZrO_2, MgO and ZnO) have been tested. The metal particle size was determined by TEM. The acidic properties of the catalysts were studied by FT-IR spectroscopy using pyridine as probe molecule. The influence of some preparative variables, such as the particle size, the support, the partial hydrogen pressure, on the catalytic behavior of palladium catalysts has been investigated. TEM measurements indicated that Pd particles diameter observed was in the range 2.5–10 nm. No significant variation of TOF and selectivity values with the metal particle size was observed in this range. Moreover, the activity and the selectivity towards reaction products were found to be strongly dependent on the acid–base characteristics of the support. The acid systems have been found more active and selective to isomerisation and hydrogenolysis products than the basic ones. No hydrogenolysis reaction was observed on basic supports. Among the examined catalysts, Pd/TiO_2 resulted the most selective to 2-hydroxytetrahydrofuran.A maximum yield to this compound of about 74% was, in fact, obtained at 0.01 MPa of H_2 pressure.

3.3 Role of TiO$_2$ in selective hydrogenation.

A. Dandekar and M.A.Vannice (1999) studied crotonaldehyde hydrogenation on Pt/TiO$_2$ and Ni/TiO$_2$ SMSI catalysts. A kinetic and DRIFTS (diffuse reflectance FTIR) investigation of crotonaldehyde adsorption and hydrogenation was conducted over TiO$_2$-supported Pt and Ni with the intent of gaining insight into the adsorption modes of molecules with carbonyl groups on these catalysts in the SMSI and non-SMSI states. Significant enhancement in selectivity toward crotyl alcohol was observed with each catalyst after reduction at 773 K. DRIFT spectra under reaction conditions identified crotonaldehyde species strongly adsorbed through the C=C bond and weakly coordinated through both the C=C and the C=O bonds on these catalysts after reduction at 573 K, which gave a peak at 1693 cm^{-1}. After reduction at 773 K, an additional adsorbed species with a strong band at 1660 cm^{-1}, indicating a significant interaction between the carbonyl group and the surface, was observed, which is presumed to be stabilized at interfacial Pt–TiO$_x$ and Ni–TiO$_x$ sites. A decrease in the surface coverage of this species paralleled a drop in selectivity to crotyl alcohol with time on stream. After reduction at 573 K, decarbonylation occurred during the initial few minutes on stream to create adsorbed CO on Pt/TiO$_2$ in addition to carbon deposition, but these reactions were significantly suppressed after reduction at 773 K, presumably due to a TiO$_x$ overlayer which covers part of the Pt surface and breaks up the ensembles of Pt atoms required for these reactions

M.G. Musolino *et al.* (2003) studied liquid phase hydrogenation and isomerization of some α,β-unsaturated primary and secondary alcohols have been investigated in tetrahydrofuran over a 2.5% TiO$_2$ supported palladium catalyst at 303 K and 0.01 MPa partial hydrogen pressure. The double bond isomerization reaction of these substrates leads also to formation of the corresponding saturated aldehydes or ketones. Catalytic activity and selectivity were found to depend strongly on the steric and electronic effects of the substituents on the double bond of the alcohol.

D. C. Lee *et al.* (2003) studied the selective hydrogenation of 1,3-butadiene on TiO$_2$-modified Pd/SiO$_2$ catalysts. The properties of Pd/SiO$_2$ catalysts modified with

titanium oxide were examined by determining their activity with respect to the partial hydrogenation of 1,3-butadiene included in an excess amount of butenes and by characterizing their surfaces using infrared (IR) spectroscopy, X-ray photoelectron spectroscopy (XPS), H_2 chemisorption, and temperature-programmed desorption (TPD). The results indicated that TiO_2-modified catalysts had an improved selectivity for the conversion of 1,3-butadiene to 1-butene, particularly when the catalysts were reduced at high temperatures,e.g.,$500^{\circ}C$. IR and chemisorption results suggest that, when the catalyst is reduced at $500^{\circ}C$, the Pd surface is decorated with partially-reduced TiO_x similar to the case of TiO_2-supported catalysts, which show strong metal-support interaction (SMSI). XPS and TPD results indicate that Pd surface is also modified electronically, in that the charge is transferred from the Ti species to Pd and the adsorption of 1-butene to the Pd surface becomes weaker. It can be concluded that the strong interaction between the Pd surface and partially reduced TiO_2 is responsible for the improved selectivity of the catalyst for the conversion of 1,3-butadiene to 1-butene.

Y. Li *et al.* (2004) investigated in situ EPR and IR by using CO as probe molecules show that even pre-reduced by H_2 at lower temperature results in SMSI for anatase titania supported palladium catalyst, but not for rutile titania supported palladium catalyst, which is attributed that the Ti^{3+} ions produced by reduction of Ti^{4+} are fixed in the surface lattice of TiO_2, as rutile titania is more thermodynamically and structurally stable than anatase titania so that the Ti^{3+} ions fixed in the surface lattice of anatase TiO_2 is easier to diffuse to surface of palladium particle than one in the surface lattice of rutile TiO_2. The reason why the pre-reduction of both anatase and rutile supported palladium catalyst at higher temperature results in SMSI between Ti^{3+} and Pd is attributed that the thermal diffusion of produced Ti^{3+} ion at higher temperature is much easier than at lower temperature so that it could overcome the binding of surface lattice of both anatase and rutile titania to move to the surface or surrounding of palladium particle.

P. Reyes *et al.* (2004) investigated the hydrogenation of citral over a series of supported iridium catalysts. The nature of the support (TiO_2 and SiO_2), the effect of

additives (Fe and Ge), and the influence of the reduction temperature on catalyst performance have been examined. It was found that the presence of ionic species, such as, promoters or species generated upon reduction at high temperature of the reducible TiO_2 support, i.e. TiO_x moieties, leads to catalysts active and highly selective to the hydrogenation of the carbonyl bond. This is explained in terms of the presence of positively charged (Fe^{3+}, Ge^{4+}) species in intimate contact with Ir, which are responsible for the polarisation of the C=O bond.

J. Xu *et al.* (2005) studied liquid phase selective hydrogenation of maleic anhydride (MA) to butyric acid (BA) used Pd/TiO_2 catalyst which prepared by difference method, sol-gel, impregnation and deposition-precipitation method. It was clearly seen that Pd/TiO_2 catalyst prepared by sol-gel is an excellent catalyst for selective hydrogenation of MA in liquid phase to BA. The high conversion (100%) of MA and high yield towards BA were attributed to the strong adsorption of MA or succinic anhydride (SAH) species via the C=O bond in di-σ mode on interfacial Pd-TiO_x site which was induced by the high temperature reduction step. Meanwhile, the reaction temperature and the interaction between metal and support has an obvious influence on the yield of BA.

3.4 Comment on the previous works

From the previous studies, Pd is the one of the most useful catalysts used in liquid-phase hydrogenation reaction. Furthermore types of solvent and support show the important roles in catalytic activity. TiO_2 is one of the most interesting supports because it has a large surface areas and it exhibits a strong metal-support interaction (SMSI). Y. Li *et al.* (2004) investigated effect of reducing temperature with the strong metal support interaction of anatase and rutile titania supported palladium catalyst. However, the effect of TiO_2 crystallite size on TiO_2 supported palladium catalysts in catalytic liquid-phase hydrogenation has not been well studied so far. Thus it is the aim of this study to investigate the catalytic behavious of palladium supported on micron-and nano-sized titania in the liquid phase selective hydrogenation.

CHAPTER IV

EXPERIMENTAL

This chapter describes the experimental procedure used in this research which can be divided into four sections. The preparation of TiO_2 supports are shown in section 4.1. Details of catalyst preparation are explained in section 4.2. The reaction study in phenylacetylene hydrogenation is given in section 4.3. Finally, Properties of the catalyst characterized by various techniques are discussed in section 4.4

4.1 Preparation of TiO_2 supports

There are two type of TiO_2 supports used in this research the first type is micron sized TiO_2 and the second type is nano-sized TiO_2. The micron-sized anatase TiO_2 was obtained commercially from Aldrich and the nano-sized anatase TiO_2 used in this experimental were prepared by solvothermal method.

4.1.1 Preparation of TiO_2 supports using the solvothermal method

The chemicals used for TiO_2 supports preparation are shown in table 4.1.

Table 4.1 Chemicals used in the preparation of TiO_2

Chemical	Supplier
Titanium (IV) tert-butoxide (97%TNB, $Ti[O(CH_2)_3CH_3]_4$	Aldrich
1,4-butanediol (1,4-BG, $HO(CH_2)_4OH$)	Aldrich
Methyl alcohol	Aldrich

The solvothermal-derived nano-TiO$_2$ supports were prepared by using specific amount of TNB as shown in Table 4.2. The starting material was suspended in 100 ml of 1,4-butanediol in a test tube and put into the bigger test tube. In the gap between two test tubes, 30 ml of 1,4-butanediol was added. Then setup both tubes into an autoclave. After the autoclave was completely purged with nitrogen, the autoclave was heated to desired temperature (see Table 4.2) at the rate of 2.5°C-min^{-1}. When the temperature was reached the autoclave was held at that temperature for a specific time duration as shown in Table 4.2. The reaction performed inside autoclave during heat up and hold at constant temperature. When the desired holding time was achieved the reactor was cooled down to room temperature. The resulting powders were collected after repeated washing with methanol by centrifugation. They were then dried by air at room temperature. The schematic drawing of equipments used for TiO$_2$ support preparation are shown in Figure 4.1

Table 4.2 The condition used for the preparation of TiO$_2$

Conditions	Amount of TNB (g)	Solvent (1.4 Butanediol) (ml)	Temperature (°C)	Holding time (hr)
1	15	100	300	0.5
2	25	100	300	2
3	25	100	320	6
4	25	100	340	12
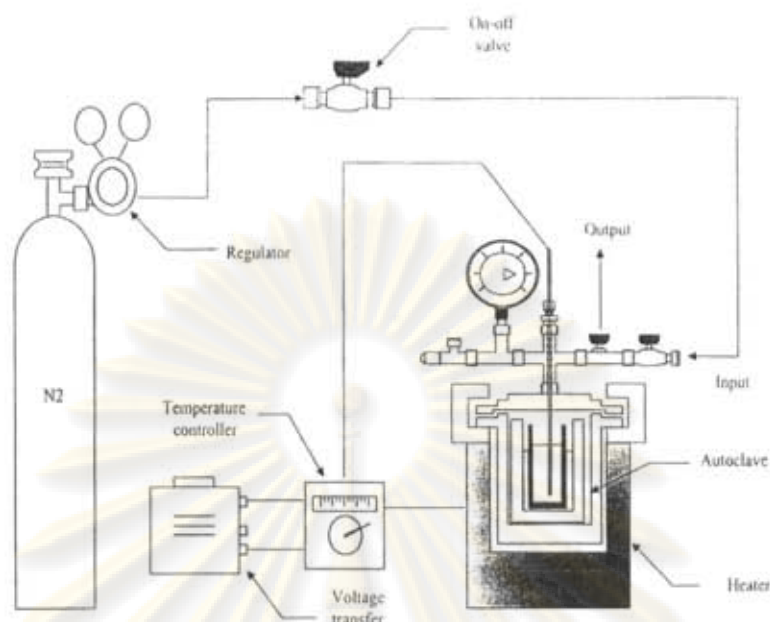
Figure 4.1 The schematic drawing of equipments used for the preparation of TiO$_2$.

4.2 Catalyst Preparation

4.2.1 Palladium Loading

In this experimental, the incipient wetness impregnation method had been used for palladium loading. Pd(NO$_3$)$_2$.6H$_2$O was used as precursor in this methods. The incipient wetness impregnation procedure was as following:

1. Palladium nitrate hydrate (1% loading) was dissolved in deionized water which its volume equals to pore volume of catalyst.

2. TiO$_2$ support was impregnated with aqueous solution of palladium by the incipient wetness technique. The palladium solution was dropped slowly to the TiO$_2$ support.

3. The impregnated support was left to stand at room temperature for 6 hours to assure adequate distribution of metal complex. After that the catalyst was dried in the oven at 110 °C overnight.

4. The catalyst was calcined in air at 450 °C for 3 h.

4.3 The Reaction Study in Liquid-Phase Hydrogenation

The liquid phase selective hydrogenation of phenylacetylene was performed in order to investigate all research objectives. Ethanol was used as reaction medium. The reactions were carrier out in bath type autoclave reactor.

4.3.1 Chemicals and Reagents

The chemicals and reagents used in the reactions are shown in Table 4.3

Table 4.3 The chemicals and reagents used in the reaction

The chemicals and reagents	Supplier
High purity grade Hydrogen (99.99vol. %)	Thai Industrial Gases Limited
Absolute ethyl alcohol (99.99vol. %)	Aldrich
Phenylacetylene	Fluka

4.3.2 Instruments and Apparatus

The schematic diagram of liquid-phase hydrogenation shows in Figure 4.2. The main instruments and apparatus in the reaction study are explained as follow:

The autoclave reactor

The 50 ml stainless steel autoclave was used as reactor. Hot plate stirrer with magnetic bar was used to heat up the reactant and to ensure that the reactant and the catalyst are well mixed.

Gas chromatography

A gas chromatography equipped with flame ionization detector (FID) with GS-alumina capillary column will be used to analyze the composition of feed and products.

Table 4.4 Operating conditions for the gas chromatograph

Gas Chromatograph	Shimadzu GC-14A
Detector	FID
Capillary column	GS-alumina (length =30 m, I.D. = 0.53 mm)
Carrier gas	Helium (99.99vol. %)
Make-up Gas	Nitrogen (99.99vol. %)
Flow rate of carrier gas	25 cc/min
Flow rate of make-up gas	45 cc/min
Column temperature	200°C
Detector temperature	250°C
Injector temperature	280°C

4.3.3   Liquid-Phase Hydrogenation Procedure

The reaction study section was divided into two parts. The first part phenylacetylene hydrogenation was performed in ethanol solvent under mild condition which various H_2-pressure. In the second part, phenylacetylene hydrogenation was carrier out with H_2 pressure 5 bar at room temperature for 60 min. The reactions in both parts were carried out in two steps. The first step was catalyst preparation and the second step was hydrogenation study.

1. Reduction step

Approximately 0.2 gram of supported Pd catalyst was placed into the U-tube of Micromeritic. After that, the catalyst was reduced by the hydrogen gas at the volumetric flow rate of 50 ml/min at 40°C and 500 °C   for 2 h.

2. Reactant preparation and hydrogenation step

0.5 ml of phenylacetylene and 4.5 ml of ethanol was mixed in the volumetric flask. Then 0.05 g of catalyst and the mixture were introduced into the autoclave reactor. After that the reactor was filled with hydrogen. The liquid phase

hydrogenation was carried out at $30^{\circ}C$ for desire reaction time. After the reaction the vent valve was slowly opened to prevent the loss of product. Then the product mixture was analyzed by gas chromatography with flame ionization detector (FID) and the catalyst was characterized by several techniques.
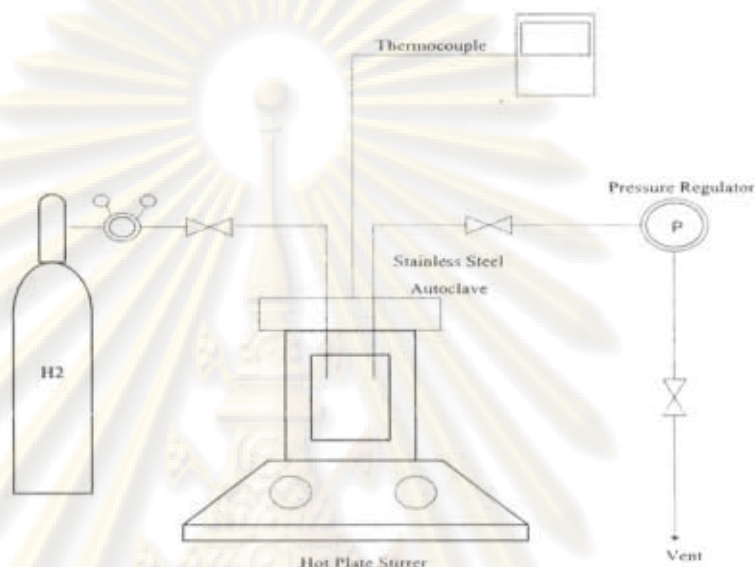
Figure 4.2 The schematic diagram of liquid-phase hydrogenation

4.4 Catalyst Characterization

The fresh catalyst will be characterized by several techniques such as

4.4.1 X-ray Diffraction (XRD)

The bulk crystal structure and chemical phase composition were determined by diffraction of an X-ray beam as a function of the angle of the incident beam. The XRD spectrum of the catalyst was measured by using a SIEMENS D5000 X-ray diffractometer and CuK_{α} radiation with Ni filter in the 2θ range of 10-80 degrees resolution 0.04°. The crystallite size was calculated from Scherrer's equation.

4.4.2 N₂ Physisorption

The BET surface area of sample, average pore size diameters and pore size distribution were determined by physisorption of nitrogen (N_2) using Micromeritics ASAP 2020 (surface area and porosity analyzer). Each sample was degassed under vacuum pressure <10 μm Hg in the Micromeritics system at 150°C for 4 h prior to N_2 physisorption.

4.4.3 CO-Pulse Chemisorption

The metal active sites and the relative percentages dispersion of palladium supported catalysts were determined by CO-pulse chemisorption technique using Micromeritics ChemiSorb 2750 (pulse chemisorption system). The known amount of CO was pulsed into the catalyst bed at room temperature. Carbon monoxide that was not adsorbed was measured using thermal conductivity detector. Pulsing was continued until catalyst surface was saturated with CO. The number of metal active sites was calculated in the basic assumption that only one CO molecule adsorbed on one metal active site (Anderson *et al.*, 1995, Ali *et al.*, 1998 and Mahata *et al.*, 2000).

Approximately 0.2 g of catalyst was filled in a u-tube, incorporated in a temperature-controlled oven and connected to a thermal conductivity detector (TCD). He was introduced into the reactor at the flow rate of 30 ml/min in order to remove remaining air. Prior to chemisorption, the samples were reduced in a H_2 flow rate at 50 ml/min with heated at an increasing rate of 10 °C/min from room temperature to 40°C or 500°C and held at this temperature for 2 h. After that cooled down to ambient temperature in a He flow, then CO was plus into the catalyst bed at room temperature. Carbon monoxide that was not adsorbed was measured using thermal conductivity detector. Pulsing was continued until no further carbon monoxide adsorption was observed. Calculation details of %metal dispersion are given in Appendix C.

4.4.4 Transmission Electron Microscopy (TEM)

The palladium oxide particle size and distribution of palladium on titanium supported catalysts were observed using AJEM-200CX transmission electron microscope operated at 160 kV at the Scientific and Technological Research Equipment Center (STREC), Chulalongkorn University.

4.4.5 Scanning Electron Microscopy (SEM)

Catalysts granule morphology and elemental distribution were obtained using a JEOL JSM-35F scanning electron microscope. The SEM was operated using the back scattering electron (BSE) mode at 20 kV at the Scienctific and Technological Researh Equipment Center, Chulalongkorn University (STREC)

4.4.6 X-ray Photoelectron Spectroscopy (XPS)

The XPS spectra, the binding energy and the composition on the surface layer of the catalysts were determined by using a Kratos Amicus X-ray photoelectron spectroscopy. The analyses were carried out with these following conditions: Mg Ka X-ray source at current of 20 mA and 12 kV, 0.1 eV/step of resolution, and pass energy 75 eV and the operating pressure was approximately 1×10^{-6} Pa

4.4.7 Electron Spin Resonance (ESR)

ESR will be performed to determine the defect of surface catalysts by JEOL JAPAN. The ESR using model JES-RE2X at the Scienctific and Technological Researh Equipment Center, Chulalongkorn University (STREC)

4.4.8 Temperature Programmed Desorption (TPD)

Temperature programmed desorption of CO has been carried out in order to elucidate the influences of TiO_2 crystallite size, Pd dispersion, and reduction temperature on the strength and mechanism of CO adsorption on TiO_2 supported Pd

catalysts. Temperature programmed desorption (TPD) study was performed in a Micromeritic ChemiSorb 2750 automated system attached with ChemiSoft TPx software. The amount of CO adsorbed on the surface was determined by TPD with a temperature range from 30 to 800 °C. The thermal conductivity detector was used to measure the amount of CO.

Approximately 0.2 g of a calcined catalyst was placed in a quartz tube in a temperature-controlled oven and reduced by hydrogen flowing over catalyst at the rate of 50 ml/min for 1 h at 40°C or 500°C using a ramp rate of 10°C and cooled down to the room temperature by helium flow. The catalyst surface was adsorped with CO by applying a high purity grade CO at 50 ml/min for 1 h ensuring the saturated catalyst. Then the samples were flushed with helium at flow rate of 30 ml/min down to room temperature for about 1 h. The temperature-programmed desorption was performed with a constant heating rate of ca. 10°C/min from 30°C to 800°C. The amount of desorbed ethylene or CO was measured by analyzing the effluent gas with a thermal conductivity detector.

CHAPTER V

RESULTS AND DISCUSSIONS

The results and discussions in this chapter are divided into two parts. In the first part the characteristic and catalytic properties of catalysts, 1%Pd/TiO$_2$-micron (prepared from micron-sized TiO$_2$) and 1%Pd/TiO$_2$-nano (prepared from nano-sized TiO$_2$), were investigated in the liquid phase selective hydrogenation of phenylacetylene. The reaction was carried out at 30°C and various H$_2$-pressures in autoclave reactor. Several analytical techniques were used for characterization of the catalysts such as, XRD, N$_2$-physisorption, CO-pulse chemisorption, SEM, TEM, XPS, and CO-temperature program desorption. Furthermore, the effect of reducing temperature on the strong metal support interaction (SMSI) on supported palladium catalysts was investigated. The second part, liquid-phase selective hydrogenation of phenylacetylene under mild conditions has been investigated on a series of nanocrystalline TiO$_2$ supported Pd catalysts with various TiO$_2$ crystallite sizes in the range of 9-23 nm. The several techniques were used for characterization all catalysts in the same as first part. Moreover, the effect of TiO$_2$ crystallite sizes to the SMSI effect was investigated.

5.1 Comparative study of Pd supported on micron and nano-sized TiO$_2$ catalysts

5.1.1 Characterization of TiO$_2$ supports and Pd/TiO$_2$ catalysts

5.1.1.1 X-Ray Diffraction (XRD)

Bulk crystal structure and chemical phase composition of a crystalline material having crystal domains of greater than 3-5 nm can be detected by diffraction of an X-ray beam as a function of the angle of the incident beam. The measurements were carried out at the diffraction angles (2θ) between 10° and 80°. Broadening of the diffraction peaks were used to estimate crystallite diameter from Scherrer Equation.

The TiO₂ supports which used in preparation of catalysts sample (1%Pd/TiO₂-micron and 1%Pd/TiO₂-nano) were characterized by X-ray diffraction technique. The XRD patterns of the micron-and nano-sized TiO₂ are shown in the **Figure5.1**. Both samples exhibited the characteristic peaks of the anatase TiO₂ at $2\theta = 25^\circ$ (major), 37°, 48°, 55°, 56°, 62°, 71°, and 75°. The average crystallite sizes of the TiO₂-micron and TiO₂-nano calculated from the full width at half maximum of the XRD peak at $2\theta = 25^\circ$ using Scherrer equation were 100 nm ($\sim 0.1\ \mu m$) and 14 nm, respectively. The average crystallite size of TiO₂-micron in this study was found to be much larger than many commercially available TiO₂ widely used in the industry such as P-25 (Degussa), PC-500 and AT-1 (Millennium Chemicals), and Hombikat UV-100 (Sachtleben Chemie) in which the TiO₂ crystallite sizes are in the range of 10-30 nm. (Panagiotopoulou et al. 2006)
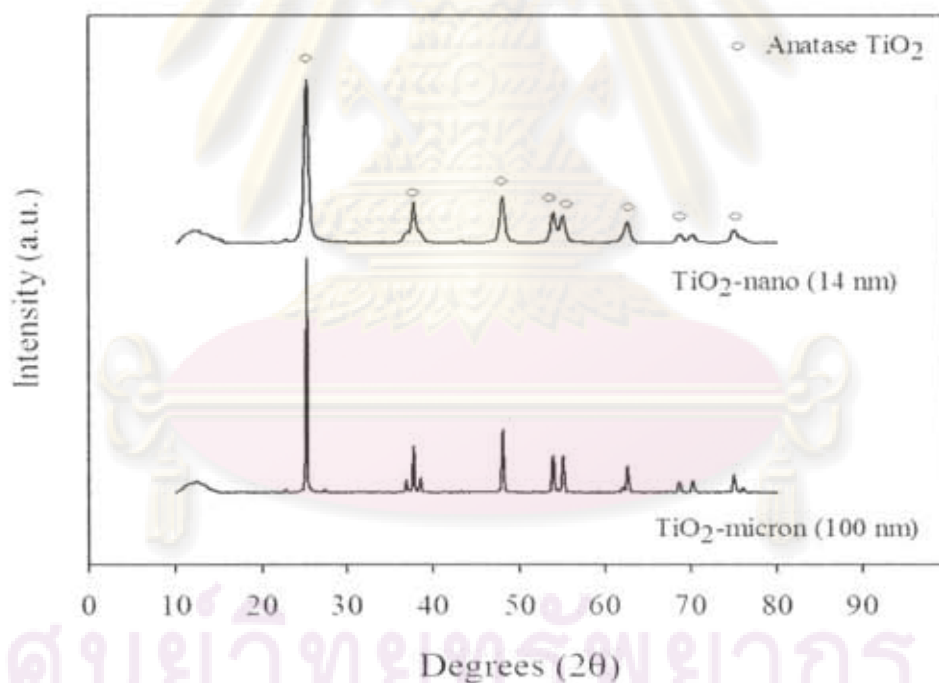
Figure 5.1 The XRD patterns of the micron-and nano-sized TiO₂

The XRD patterns of 1%Pd-TiO₂-micron and 1%Pd/TiO₂-nano, which prepared by impregnation method, in the calcined state are shown in **Figure5.2**. The XRD characteristic peaks for PdO at 2θ of ca. 33.8° were observed in both samples after calcinations step because PdO occurred during in the calcinations step in air.

However, the XRD characteristic peaks corresponding to Pd^{o} metal ($2\theta = 40.2^{o}$ and 46.7^{o}) were not observed after reduced at $40^{o}C$ and $500^{o}C$ due probably to the low amount of Pd present or it was in a highly dispersed form (see in **Figure5.3** and **Figure5.4**.)

Furthermore, the average crystallite sizes of 1%Pd/TiO$_2$ catalysts were calculated from the Scherrer equation (see in **Table5.1**). For1%Pd/TiO$_2$-micron when reduced at $40^{o}C$ and $500^{o}C$, the crystallite sizes of TiO$_2$ were 96 and 94 nm, respectively. While 1%Pd/TiO$_2$-nano after reduction at $40^{o}C$ and $500^{o}C$, the crystallite sizes of TiO$_2$ were 16 and 17 nm, respectively. It was found that reduction with H$_2$ either $40^{o}C$ or $500^{o}C$ did not result in significant changes of the TiO$_2$ crystallite sizes for both type of TiO$_2$ supports. But a slight increased in TiO$_2$ crystallite sizes of TiO$_2$-nano from 14 to 17 nm was probably caused by high temperature calcinations and reduction of catalysts at $500^{o}C$.

Table 5.1 The crystallite sizes of TiO$_2$ support and 1%Pd/TiO$_2$ catalysts

Samples	Crystallite sizes of TiO$_2$ (nm)
TiO$_2$-micron	100
TiO$_2$-nano	14
1%Pd/TiO$_2$-micron-R40	96
1%Pd/TiO$_2$-micron-R500	94
1%Pd/TiO$_2$-nano-R40	16
1%Pd/TiO$_2$-nano-R500	17

Figure 5.2 The XRD patterns of 1%Pd/TiO₂-micron and 1%Pd/TiO₂-nano after calcinations step
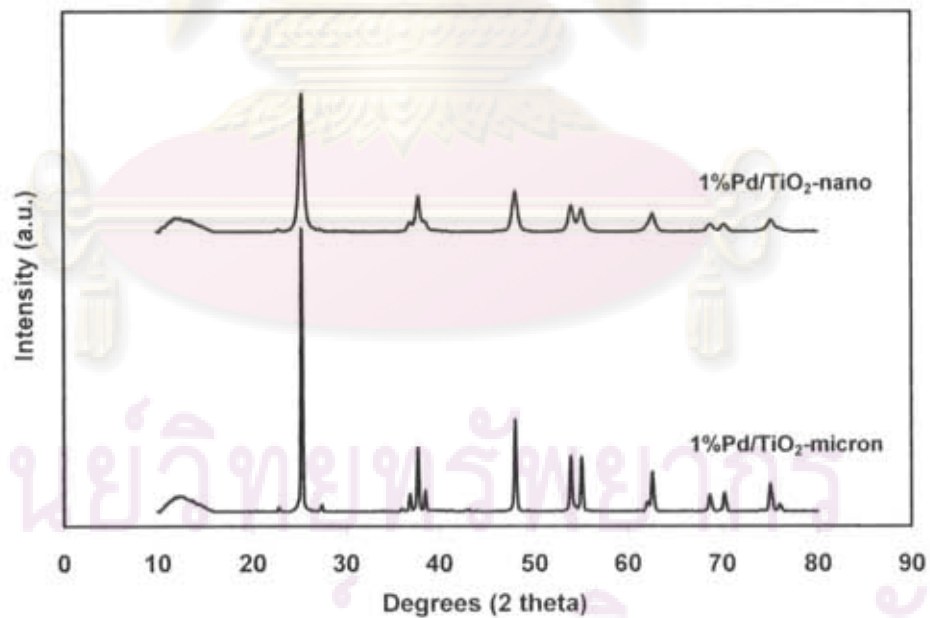
Figure 5.3 The XRD patterns of 1%Pd/TiO₂-micron and 1%Pd/TiO₂-nano when reduced at 40°C

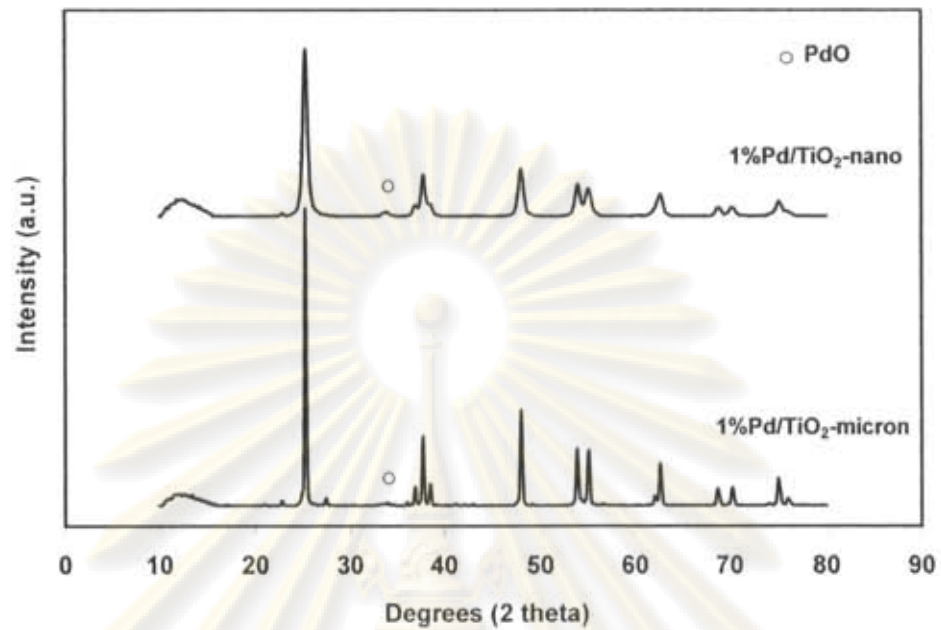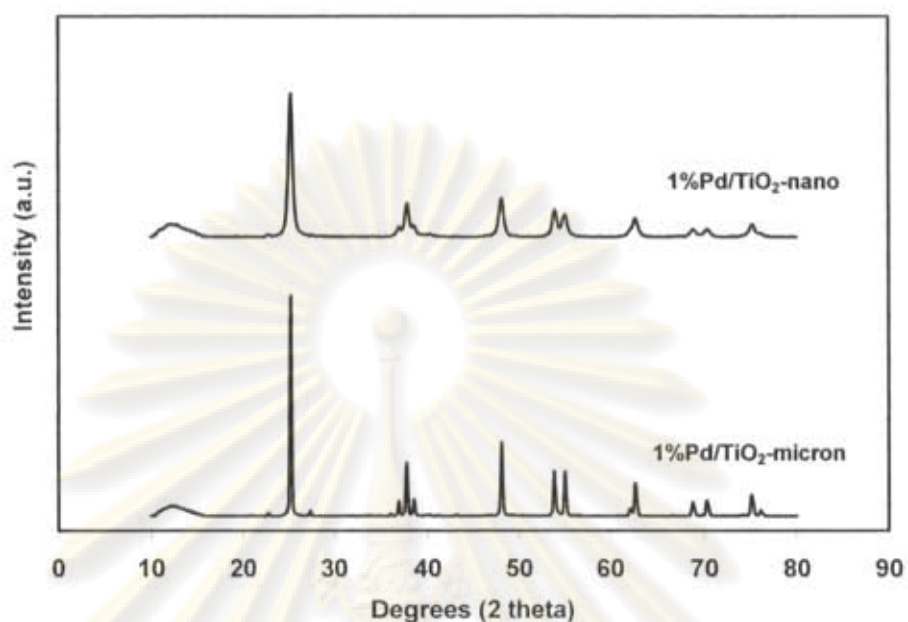**Figure 5.4** The XRD patterns of 1%Pd/TiO$_2$-micron and 1%Pd/TiO$_2$-nano when reduced at 500°C

5.1.1.2 N$_2$ Physisorption

BET surface area, pore volume and pore diameter of the TiO$_2$ and the Pd supported on TiO$_2$ catalysts which determined by N$_2$ physisorption technique are summarized in **Table 5.2**. The N$_2$ adsorption-desorption isotherms of the TiO$_2$-micron and TiO$_2$-nano are shown in **Figure 5.5** and **5.6**, respectively. It was clearly seen that that both of TiO$_2$ supports contained meso pore but very little pore volume was found for the TiO$_2$-micron. The pore volumes of TiO$_2$-micron and TiO$_2$-nano were 0.02 and 0.40 cm^3/g, respectively. The BET surface area of TiO$_2$-micron and TiO$_2$-nano were 10 and 79 m^2/g, respectively. Because TiO$_2$-nano is nanocrystalline, its BET surface area was much higher than that of TiO$_2$-micron.

The BET surface area of the 1%Pd/TiO$_2$-micron, which was reduced at 40 and 500°C were 9 and 11 m^2/g, respectively. There were no significantly differences between the BET surface area of the 1%Pd/TiO$_2$-micron and the original TiO$_2$-micron support suggesting that most of the palladium were deposited on the external surface of the support. In contrast, the BET surface areas of the 1%Pd/TiO$_2$-nano, which was reduced at 40 and 500 $^{\circ}$C were 73 and 68 m^2/g, respectively. It was found that, the BET surface areas of the 1%Pd/TiO$_2$-nano decreased after Pd loading indicating that Pd was deposited in some of the pores of the TiO$_2$ support. These results corresponded to the decrease of TiO$_2$ pore volume for 1%Pd/TiO$_2$-nano-R40 and 1%Pd/TiO$_2$-nano-R500 from 0.40 to 0.31 and 0.28 cm^3/g, respectively.

ศูนย์วิทยทรัพยากร
จุฬาลงกรณ์มหาวิทยาลัย

Table 5.2 N₂ physisorption properties of TiO₂ supports and Pd supported on
TiO₂ catalysts

Samples	BET surface area (m^2/g)	Pore volume (cm^3/g)	Pore diameter (nm)
TiO₂-micron	10	0.02	7.6
TiO₂-nano	79	0.40	14.9
1%Pd/TiO₂-micron-R40	9	0.03	1.3
1%Pd/TiO₂-micron-R500	11	0.03	1.2
1%Pd/TiO₂-nano-R40	73	0.31	0.6
1%Pd/TiO₂-nano-R500	68	0.28	0.8
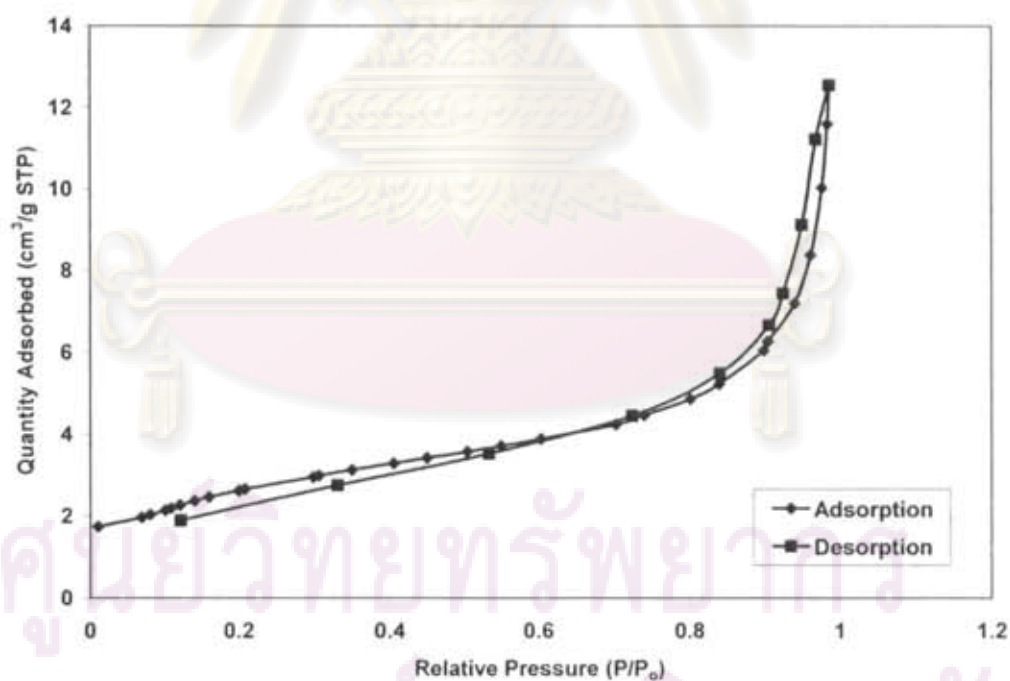
Figure 5.5 N₂ adsorption-desorption isotherms of TiO₂-micron
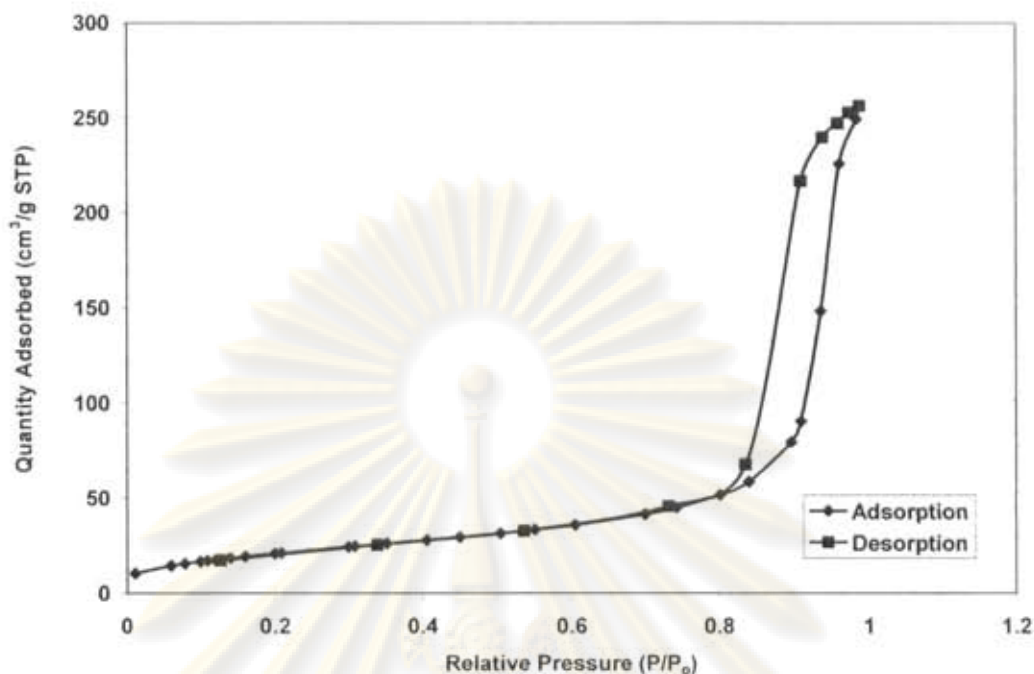
Figure 5.6 N$_2$ adsorption-desorption isotherms of TiO$_2$-nano

5.1.1.3 Atomic Absorption Spectroscopy (AAS)

Atomic absorption spectroscopy is a very common technique for quantitative measurement of atomic composition based on photon absorption of a vaporized aqueous solution prepared from the starting material.

In this study, the percentage of palladium loading was determined by atomic absorption spectroscopy (AAS) to confirm the actual amount of palladium loading in the fresh catalysts. **Table5.3** shows the actual amount of palladium loading in the fresh catalysts (1%Pd/TiO$_2$-micron and 1%Pd/TiO$_2$-nano). The AAS results were used to calculate % palladium dispersion and palladium particle size from CO-chemisorption technique.

Table 5.3 The actual amounts of palladium loading in fresh catalysts by AAS

Catalysts	Actual amount of Pd loading (%)
1%Pd/TiO$_2$-micron	1.3
1%Pd/TiO$_2$-nano	1.1

5.1.1.4 Metal active sites

The metal active sites measurement is based on chemisorption technique. Chemisorption is relatively strong, selective adsorption of chemically reactive gases on available metal sites or metal oxide surfaces at relatively higher temperatures (i.e. 25-400°C); the adsorbate-adsorbent interaction involves formation of chemical bonds and heats of chemisorption in the order of 50-300 kJ mol^{-1}.

Since H$_2$ chemisorption on Pd bridge bonding may occur so there is no precise ratio of atom to Pd metal surface. H/Pd stiochiometry may be varied from 1, 1/2 or 1/3. However, for CO chemisorption, CO/Pd stiochiometry is normally equal to 1. Exposed active surface areas of Pd of the catalysts were calculated from the irreversible pulse CO chemisorption technique based on the assumption that one CO molecule adsorbs on one palladium site (Anderson *et al.*, 1985, Ali and Goodwin, 1998 , Sales *et al.*, 1999 and Mahata *et al.*, 2000). The amounts of CO chemisorption on the catalysts reduced at 40°C and 500°C, the percentages of palladium dispersion, and average Pd^0 particle size are given in **Table 5.4**. The amounts of CO chemisorption of 1%Pd/TiO$_2$-micron were 8.30x10^{18} and 1.60x10^{18} site/g.catalyst for 1%Pd/TiO$_2$-micron-R40 and 1%Pd/TiO$_2$-micron-R500, respectively. While the amounts of CO chemisorption of 1%Pd/TiO$_2$-nano were 8.56x10^{18} and 1.89x10^{18} site/g.catalyst for 1%Pd/TiO$_2$-nano-R40 and 1%Pd/TiO$_2$-nano-R500, respectively. These results show the low CO chemisorption as catalysts reduced at 500°C due probably to sintering of Pd metal at high reduction temperature or the SMSI effect on

these catalysts. It was corresponded with decreasing of %Pd dispersion when the catalysts were reduced at 500°C for both TiO_2-micron and TiO_2-nano-supported Pd catalysts. Furthermore, %Pd dispersion for 1%Pd/TiO_2-micron decreased by 86 % while that of 1%Pd/TiO_2-nano decreased by 83.3%. The corresponding Pd^0 particle sizes calculated based on CO chemsiorption were varied from 6.7 to 48.7 nm.

Table5.4 Results from CO chemisorption of Pd supported on TiO_2 catalysts

Catalysts	CO chemisorption ($*10^{-18}$ site/g.cat)	%Pd dispersion	d_p Pd^0 (nm)
1%Pd/TiO_2-micron-R40	8.30	16.4	6.9
1%Pd/TiO_2-micron-R500	1.60	2.3	48.7
1%Pd/TiO_2-nano-R40	8.56	16.8	6.7
1%Pd/TiO_2-nano-R500	1.89	2.8	40.6

5.1.1.5 Scanning Electron Microscopy (SEM)

Scanning electron microscopy (SEM) is a powerful tool for observing directly surface texture and morphology of catalyst materials. In the backscattering scanning mode, the electron beam focused on the sample is scanned by a set of deflection coils. Backscattered electrons or secondary electrons emitted from the sample are detected.

The SEM micrographs of TiO_2 and 1%Pd/TiO_2 catalysts reduced at 40 and 500°C are shown in **Figure5.7**. The TiO_2-micron had a uniform particle size of 0.1-0.2 μm while the TiO_2-nano consisted of irregular shape of very fine particles agglomerated. Morphologies of the reduced 1%Pd/TiO_2 catalysts were not significantly different from the corresponding TiO_2 supports suggesting high thermal stability of the TiO_2.
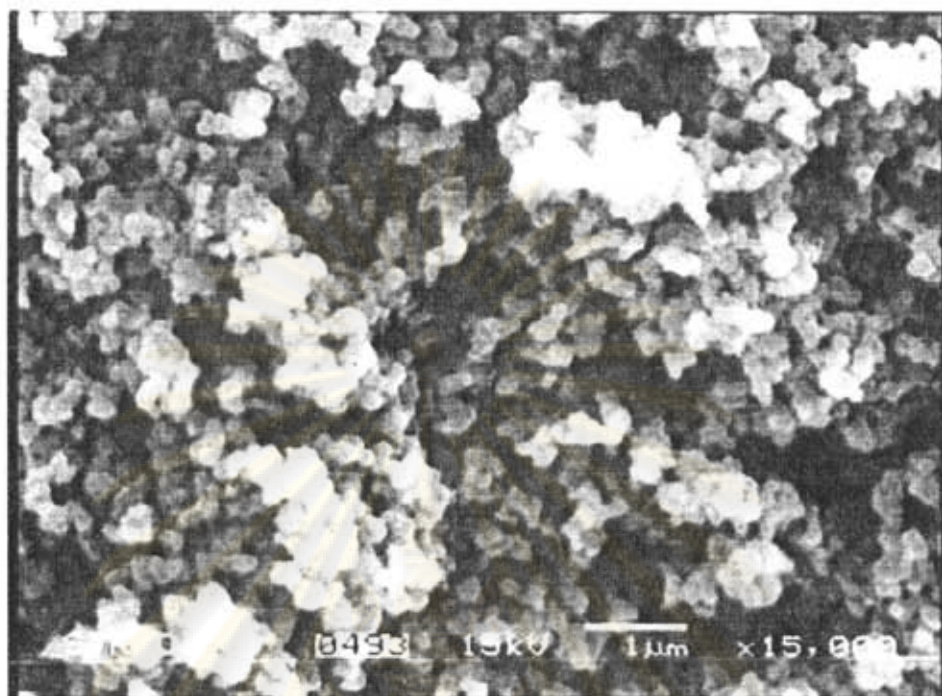
(A) TiO$_2$-micron
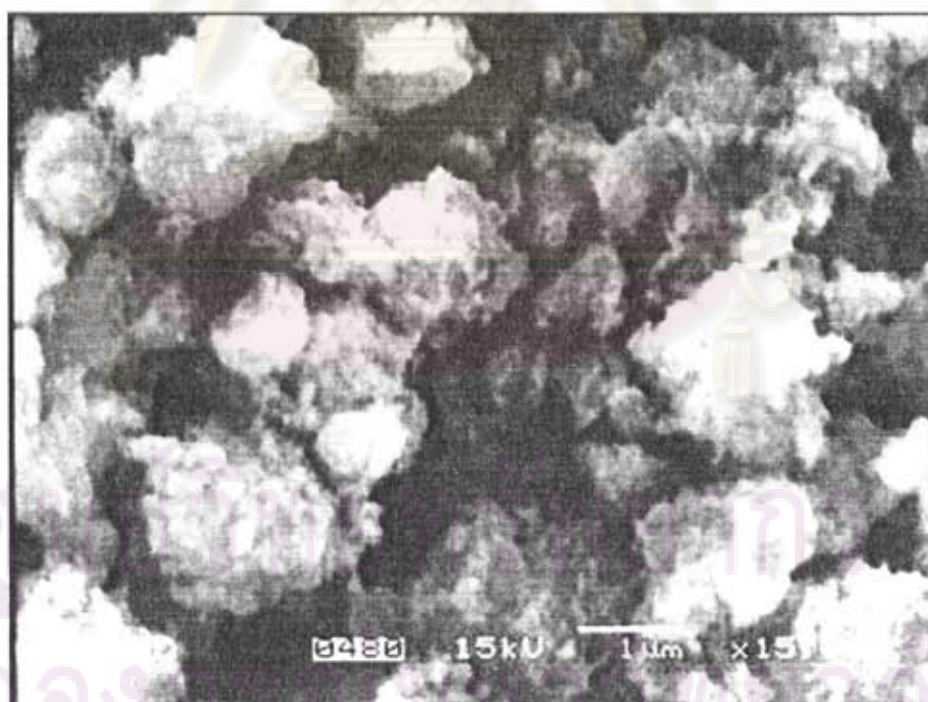
(B) TiO$_2$-nano
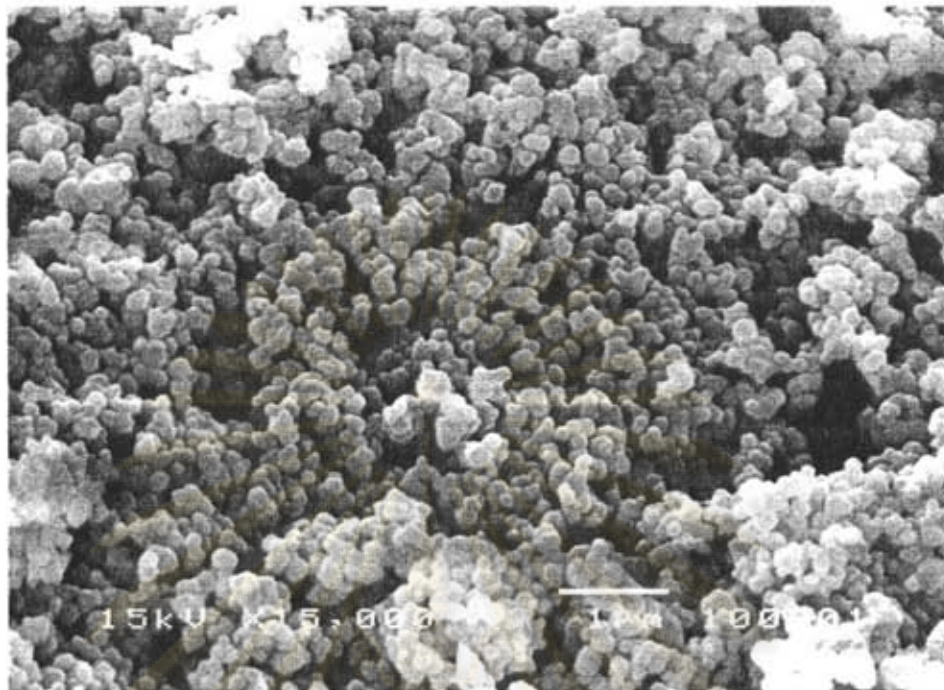
(C) 1%Pd/TiO$_2$-micron-R40
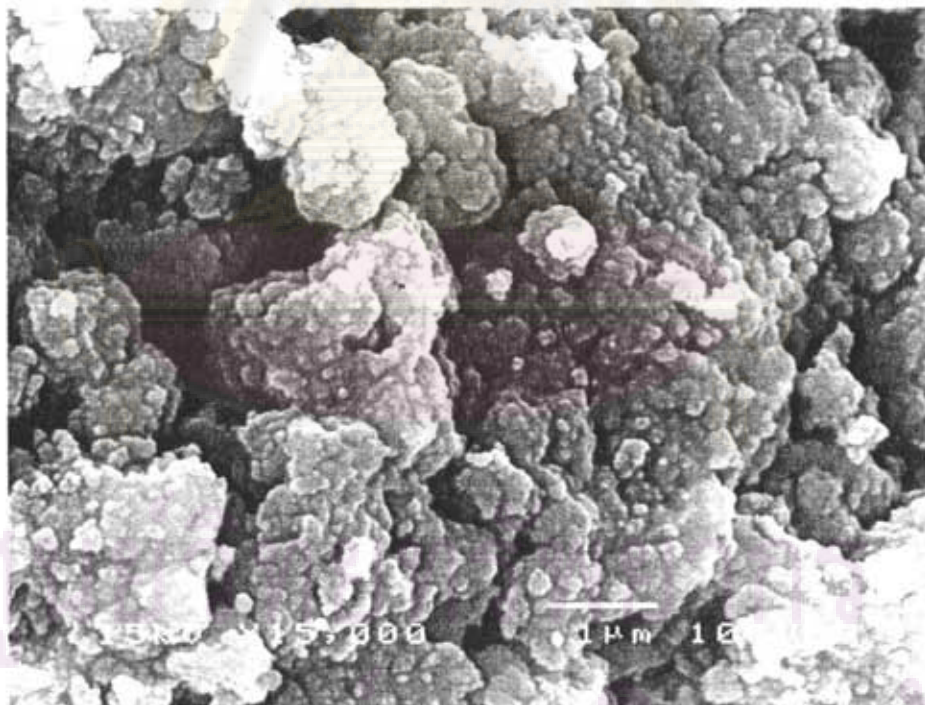
(D) 1%Pd/TiO$_2$-micron-R500
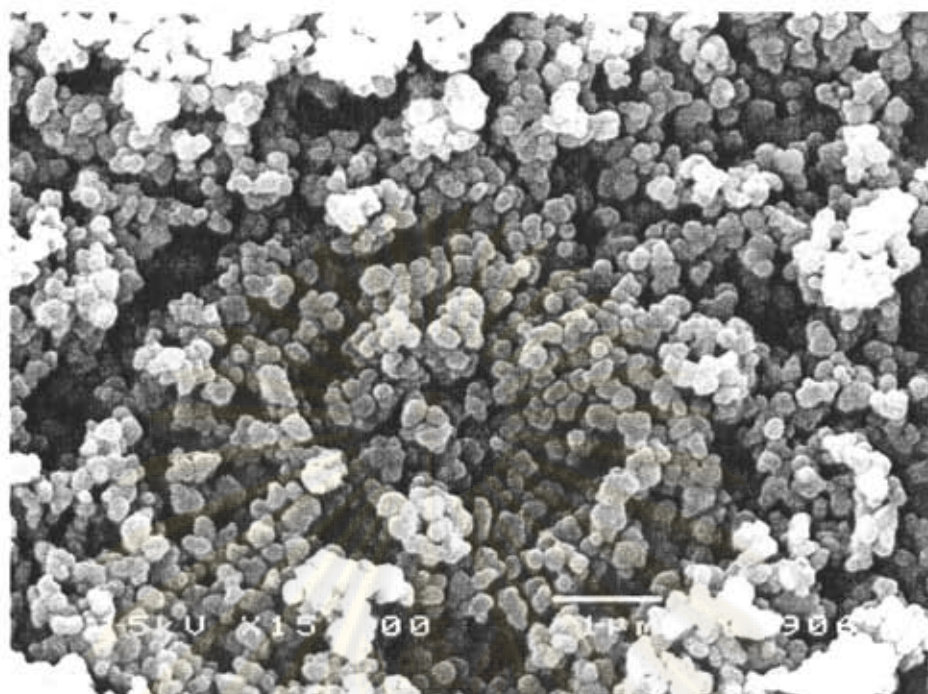
(E) 1%Pd/TiO$_2$-nano-R40
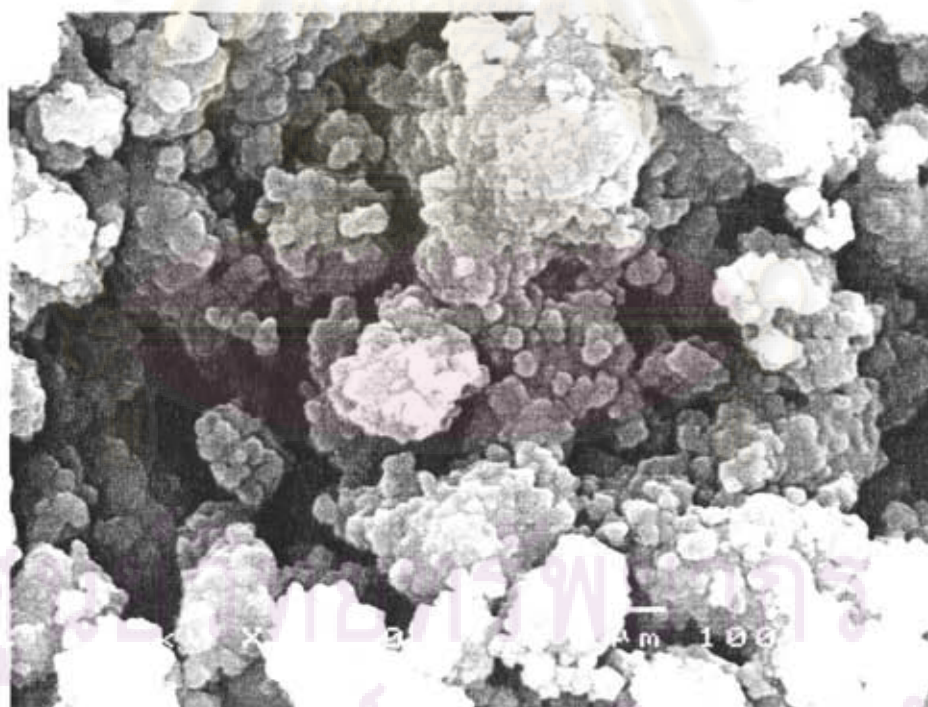
(F) 1%Pd/TiO$_2$-nano-R500

Figure 5.7 SEM micrographs of TiO$_2$ supports and Pd supported on TiO$_2$ catalysts

5.1.1.6 Transmission Electron Microscopy (TEM)

TEM is a useful tool for determining crystallite size and size distribution of supported metals. It allows determination of the micro-texture and microstructure of electron transparent samples by transmission of a focused parallel electron beam to a fluorescent screen with a resolution presently better than 0.2 nm.

TEM analysis has been carried out in order to physically measure the Pd^0 particle sizes on the various TiO_2 supports and the results are shown in **Figure 5.8**. The particle sizes of various TiO_2 supports were consistent to those obtained from XRD results. It is clearly seen that on the TiO_2-micron, Pd^0 metal particle sizes increased when the catalysts were reduced at 500^oC whereas those on the TiO_2-nano were essentially the same to those reduced at 40^oC. Such results indicate that sintering of Pd^0 metal occurred on the 1%Pd/TiO_2-micron catalyst during high temperature reduction. This could also result in the lower amount of CO chemsiorption observed. For the 1%Pd/TiO_2-nano reduced at 500^oC, the low CO chemisorption and an over estimation of the Pd^0 metal particle sizes indicate that the catalyst exhibited strong metal-support interaction under high temperature reduction since no change in the Pd^0 particle size was observed.
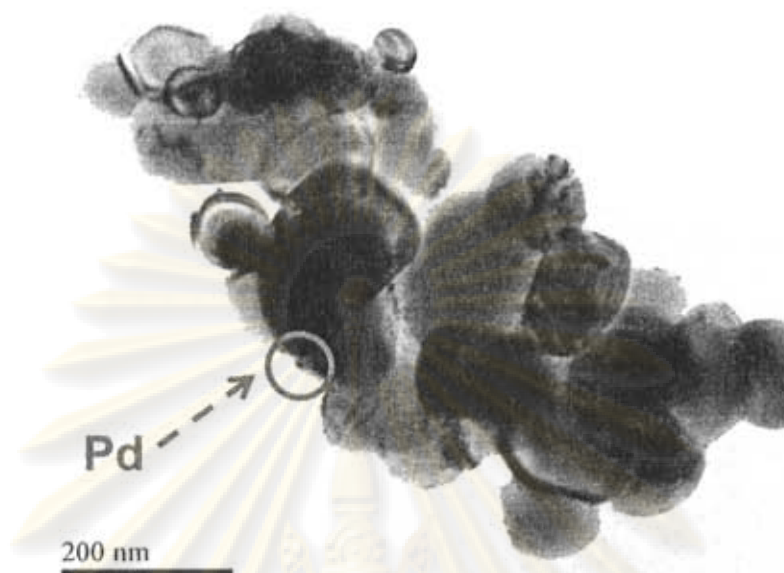
(A) 1%Pd/TiO$_2$-micron-R40

(B) 1%Pd/TiO$_2$-micron-R500
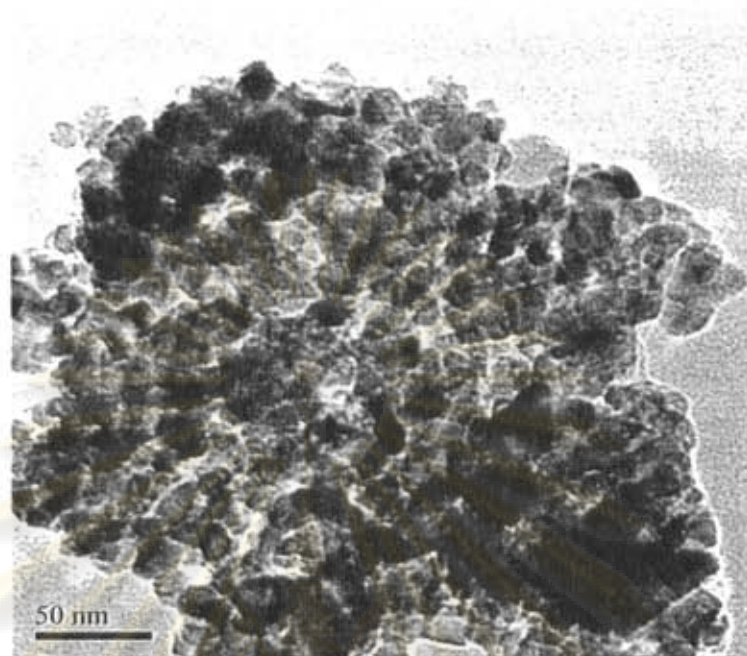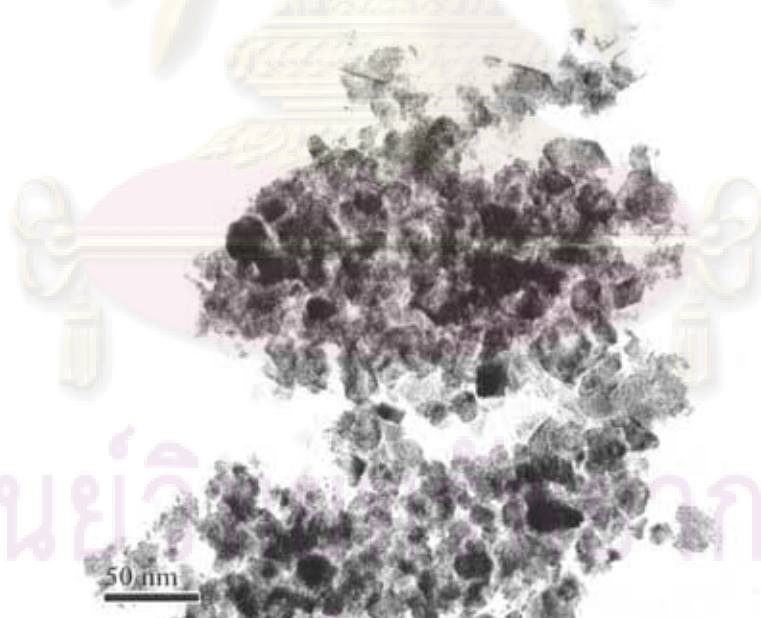
(C) 1%Pd/TiO$_2$-nano-R40

(D) 1%Pd/TiO$_2$-nano-R500

Figure 5.8 TEM micrographs of Pd supported on TiO$_2$ catalysts various
reducing temperature

5.1.1.7 Strong Metal Support Interaction Test (SMSI Test)

The SMSI effect on these catalysts was confirmed by measuring the amounts of CO chemisorption of the re-calcined (at $450^{\circ}C$) and re-reduced (at $40^{\circ}C$) catalysts after they were subjected to reduction at $500^{\circ}C$. If the catalyst has the SMSI effect, the metal active site can be totally recovered after SMSI test. Because of notable feature of SMSI is that it is reversed by oxidizing conditions.

The results are illustrated in **Figure5.9**. It was found that the amount of CO chemisorption of the re-calcined and re-reduced $1\%Pd/TiO_2$-micron was less than that reduced at $40^{\circ}C$ suggesting that sintering of Pd^0 occurred during high temperature reduction while the amount of CO chemisorption of the re-calcined and re-reduced $1\%Pd/TiO_2$-nano can be totally recovered. It is generally known that strong metal-support interaction in TiO_2 supported Pd catalysts occurred after a high temperature reduction $\geq 500^{\circ}C$. It is thus surprising that such interaction was not detected on our $1\%Pd/TiO_2$-micron. However, it should be noticed that the TiO_2 crystallite sizes used for preparation of Pd/TiO_2 catalysts in most studies in the literature were in nanometer range (usually less than 50 nm) (Li *et al.*, 2004, Musolino *et al.*, 2007). Panagiotopoulou et al (Panagiotopoulou *et al.*, 2006) also reported that formation of substoichiometric TiO_x species started at lower temperature and was more facile over Pt/TiO_2 for small TiO_2 particle sizes (10-35 nm). On the other hand, a very recent study by Musolino et al. (Musolino *et al.*, 2004) on the selective liquid-phase hydrogenation of cis-2-butene-1,4-diol to 2-hydroxy tetrahydrofuran on various supported Pd catalysts revealed the absence of SMSI effect for the Pd/TiO_2 catalyst reduced at high temperature. The interpretation of the observed behavior has not been given by such authors. However, the TiO_2 support used in their study was also anatase phase TiO_2 from Aldrich with the specific surface area of ~9 m^2/g which similar to the micron-sized TiO_2 reported in this study.

Figure 5.9 The results of SMSI test on 1%Pd/TiO$_2$-micron and 1%Pd/TiO$_2$-nano

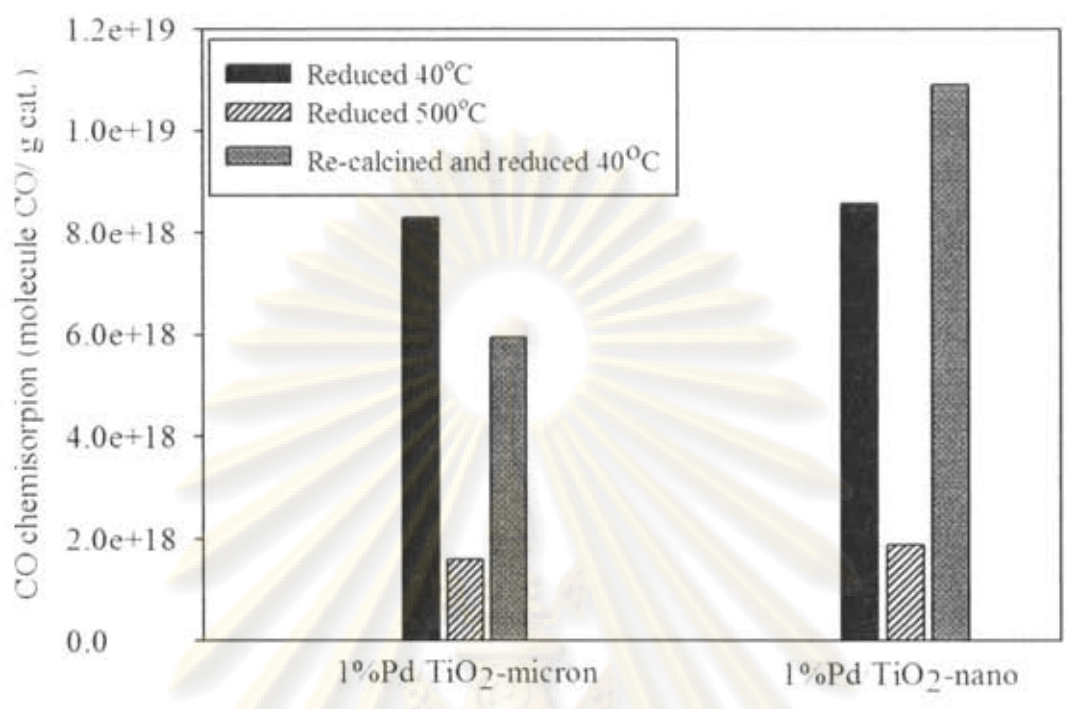### 5.1.1.8 X-ray Photoelectron Spectroscopy (XPS)

Surface compositions of the catalysts were analyzed using a Kratos Amicus X-ray photoelectron spectroscopy. The XPS analysis were carried out with following conditions: Mg Ka X-ray source at current of 20 mA and 12 keV, resolution 0.1 eV/step, and pass energy 75 eV. The operating pressure is approximately 1×10^{-6} Pa.

A survey scan was performed in order to determine the elements on the catalyst surface. The elemental scan was carried out in the next step for C 1s, O 1s, Ti 2p and Pd 3d. Binding energies of each element was calibrated internally with carbon C 1s at 285.0 eV. Photoemission peak areas are determined by using a linear routine. Deconvolution of complex spectra are done by fitting with Gaussian (70%)–Lorentzian (30%) shapes using VISION2 software equipped with the XPS system.

The surface compositions of the catalysts as well as the interaction between Pd and the TiO_2 supports were confirmed by XPS analysis. The binding energies, and full width of half maximum (FWHM) are shown in **Table 5.5.** The atomic concentrations of Ti 2p, O 1s, and Pd 3d on various Pd/TiO_2 catalysts are given in **Table 5.6**. The intense peaks at binding energies 458.5 eV indicate only the presence of Ti^{4+} in the TiO_2 samples. (Liqiang, J. *et al.*, 2003) The O 1s and C 1s peak were identified at binding energy 530 and 285 eV (J. Guillot *et al.*, 2001), respectively. There was no peak at binding energy of 461.2 ($Ti\ 2p^{1/2}$) and 456.5 eV ($Ti\ 2p^{3/2}$) which represent Ti^{3+} species in TiO_2 samples. (Liqiang, J. *et al.*, 2003 and Kumar, P. *et al.*, 2000)

From table 5.5, the atomic concentration ratios of Ti/O for TiO_2-micron and TiO_2-nano were significantly different that is 0.028 and 0.204, respectively. It was clearly seen that, the Ti/O atomic ratio were found to be much higher for the TiO_2-nano than the TiO_2-micron suggesting that the solvothermal-derived TiO_2 possessed more oxygen vacancies (or so-called Ti^{3+} defective sites) on the TiO_2 surface than the TiO_2-micron. However, there was also probably an oxygen-rich layer near the surface of the TiO_2 particles, which is formed by oxygen adsorption and easy oxidation of titanium surface. (Zhang et al. 1997)

The atomic concentration ratios of Pd/Ti for 1%Pd/TiO$_2$-micron and 1%Pd/TiO$_2$-nano dramatically decreased when reducing temperature was 500°C. For Pd/Ti ratios of 1%Pd/TiO$_2$-micron catalysts were found to be 0.073 and 0.062 when reducing temperature were 40 to 500°C, respectively. Whereas Pd/Ti surface concentration ratio of 1%Pd/TiO$_2$-nano were 0.009 to 0.004 after reduce at 40 and 500°C, respectively. The results indicate that when reduced at 500°C, the Pd/Ti surface concentration decreased by 15 and 55% for 1%Pd/TiO$_2$-micron and 1%Pd/TiO$_2$-nano, respectively. A slight decrease of Pd/Ti surface concentration for 1%Pd/TiO$_2$-micron may be due to larger Pd^0 particle size formed by sintering as shown by TEM, while a large decrease of Pd/Ti on the 1%Pd/TiO$_2$-nano would be due to decoration of Pd^0 metal surface by the reducible TiO$_2$ supports. The binding energies of Pd 3d$_{5/2}$ (335.0-335.2 eV) and the FWHM less than 2 revealed that palladium was in the form of Pd^0 metal for both cases (Wagner, C. D. *et al.*, 1978).

Table 5.5 The binding energies and FWHM of Ti 2p, O 1s, and Pd 3d in samples from XPS results

Samples	Ti 2p		O 1s		Pd 3d	
	B.E.(eV)	FWHM	B.E.(eV)	FWHM	B.E.(eV)	FWHM
TiO$_2$-micron	458.6	1.259	532.3	2.362	-	-
TiO$_2$-nano	458.7	1.308	530.0	1.675	-	-
1%Pd/TiO$_2$-micron-R40	458.7	1.516	530.2	2.324	335.0	1.704
1%Pd/TiO$_2$-micron-R500	458.7	1.846	530.2	1.846	335.2	1.849
1%Pd/TiO$_2$-nano-R40	458.7	1.292	530.0	1.596	335.0	1.570
1%Pd/TiO$_2$-nano-R500	458.6	1.319	529.9	1.681	n/d	n/d

n/d = not determined

Table 5.6 Atomic concentration ratio of Ti/O and Pd/Ti in the samples from XPS results

Samples	% Atomic Concentration			Ti/O	Pd/Ti
	Ti 2p	O 1s	Pd 3d		
TiO_2-micron	2.684	97.316	-	0.028	-
TiO_2-nano	16.854	83.146	-	0.203	-
1%Pd/TiO_2-micron-R40	10.891	88.311	0.798	0.123	0.073
1%Pd/TiO_2-micron-R500	14.941	84.134	0.926	0.178	0.062
1%Pd/TiO_2-nano-R40	17.317	82.533	0.150	0.210	0.009
1%Pd/TiO_2-nano-R500	15.986	83.956	0.058	0.190	0.004

5.1.1.9 Electron Spin Resonance Spectroscopy (ESR)

Electron spin resonance technique is a technique for studying chemical species that have one or more unpaired electrons, such as organic and inorganic free radicals or inorganic complexes possessing a transition metal ion.

The presence of Ti^{3+} in both TiO_2-micron and TiO_2-nano supports was revealed by electron spin resonance spectroscopy technique. The ESR results are shown in **Figure 5.10.** The Ti^{3+} species are produced by trapping of electrons at defective sites of TiO_2 and the amount of accumulated electrons may therefore reflect the number of defective sites. (Ikeda et al., 2003) The signal of g value less than 2 was assigned to Ti^{3+} ($3d^1$). (Howe, R.F. et al., 1985) Nakaoka et al.(Nakaoka and Nosaka 1997) reported six signals of ESR measurement occurring on the surface of titania: (i) $Ti^{4+}O^-Ti^{4+}OH^-$, (ii) surface Ti^{3+}, (iii) adsorbed oxygen (O^{2-}), (iv) $Ti^{4+}O^{2-}Ti^{4+}O^{2-}$, (v) inner Ti^{3+}, and (vi) adsorbed water. In this study, it is clearly seen that the solvothermal-derived TiO_2 exhibited only one strong ESR signal at g value of 1.997 which can be attributed to Ti^{3+} at the surface. Many Ti^{3+} ESR signals were observed for the TiO_2-micron indicating that more than one type of Ti^{3+} defects were presented

in the sample i.e., surface Ti^{3+} and inner Ti^{3+}. Moreover, less amount of surface Ti^{3+} was present on the micron-sized TiO_2. Literature data reported that the presence of Ti^{3+} promotes strong metal-support interaction in Pd/TiO_2 catalysts since Ti^{3+} can easily diffuse from the lattice of TiO_2 to surface of Pd particles (Li et al., 2004). The results in this study, however, have shown that probably only the surface Ti^{3+} has high mobility, the other Ti^{3+} species may not be able to diffuse easily to Pd^0 surface so that Pd catalyst supported on the TiO_2-micron with significant amount of Ti^{3+} did not exhibited the strong metal-support interaction.
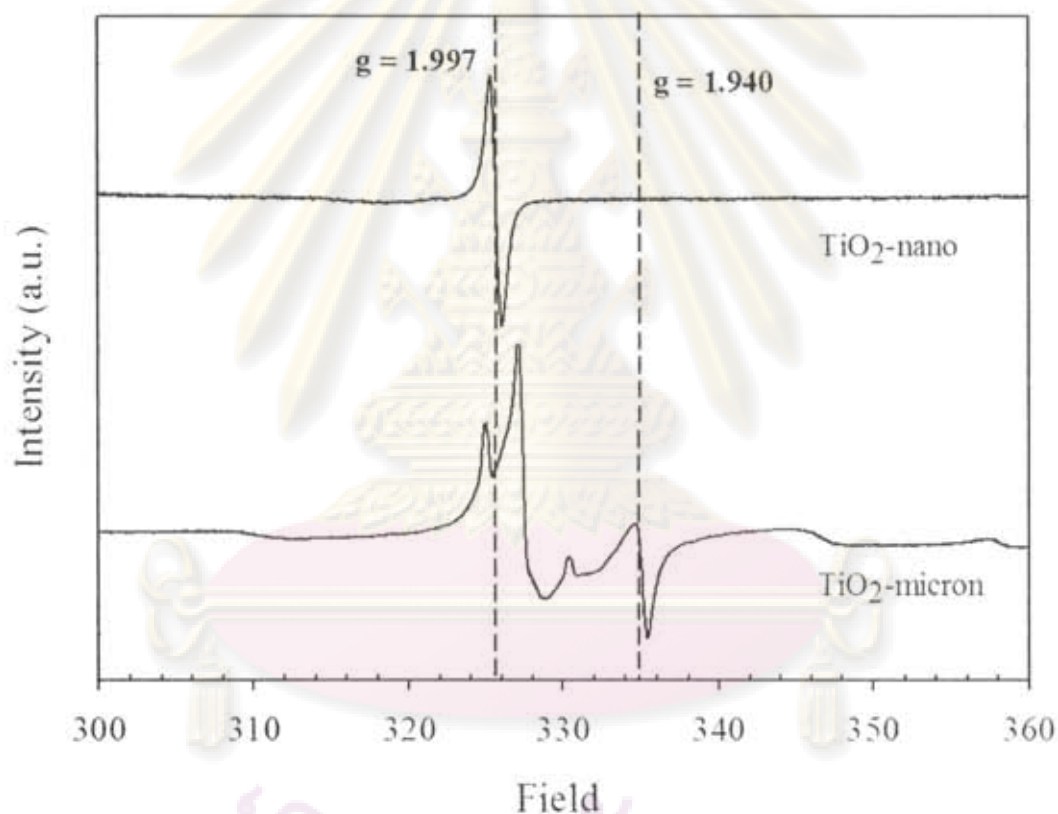

Figure 5.10 ESR spectra of TiO_2-micron and TiO_2-nano

5.1.1.10 CO Temperature Programmed Desorption (CO-TPD)

Temperature program desorption of CO has been carried out in order to elucidate the influences of TiO_2 crystallite size, Pd dispersion, and reduction temperature on the strength and mechanism of CO adsorption on TiO_2 supported Pd catalysts. The amount of CO adsorbed on the surface was determined by temperature programmed desorption using a thermal conductivity detector and the Micromeritics Chemisorb 2750 analyzer. The profiled of CO temperature programmed desorption of the catalysts are shown in **Figure 5.11 and 5.12**.

Figure 5.11 shows the profiled of CO temperature programmed desorption of 1%Pd/TiO$_2$-micron reduced at 40 and 500°C. For 1%Pd/TiO$_2$-micron reduced at 40°C, two main desorption peaks were obserbed at ca.340 and 640°C which may be attributed to CO adsorbed on different adsorption sites probably Pd^0 with different particle sizes and/or adsorption on Ti^{3+} sites. (Benvenutti, E. V. *et al.*, 1999) But for 1%Pd/TiO$_2$-micron reduced at 500°C, both peaks were slightly shifted to higher temperature. However, the amounts of CO desorption were not significant different for 1%Pd/TiO$_2$-micron reduced at 40°C or 500°C indicating that CO adsorption strength was not much different for the catalysts reduced at low or high temperature.

Furthermore, the 1%Pd/TiO$_2$-nano catalysts reduced at 40 and 500°C are shown in **Figure 5.12**. In contrast, 1%Pd/TiO$_2$-nano reduced at 40°C exhibited several desorption peaks at 100-800°C indicating various adsorption sites on the catalyst surface. However, the peaks become almost flat when the catalyst was reduced at 500°C indicating negligible CO adsorption under such conditions. In other words, CO was weakly adsorbed under high temperature reduction conditions due to the strong metal-support interaction effect.
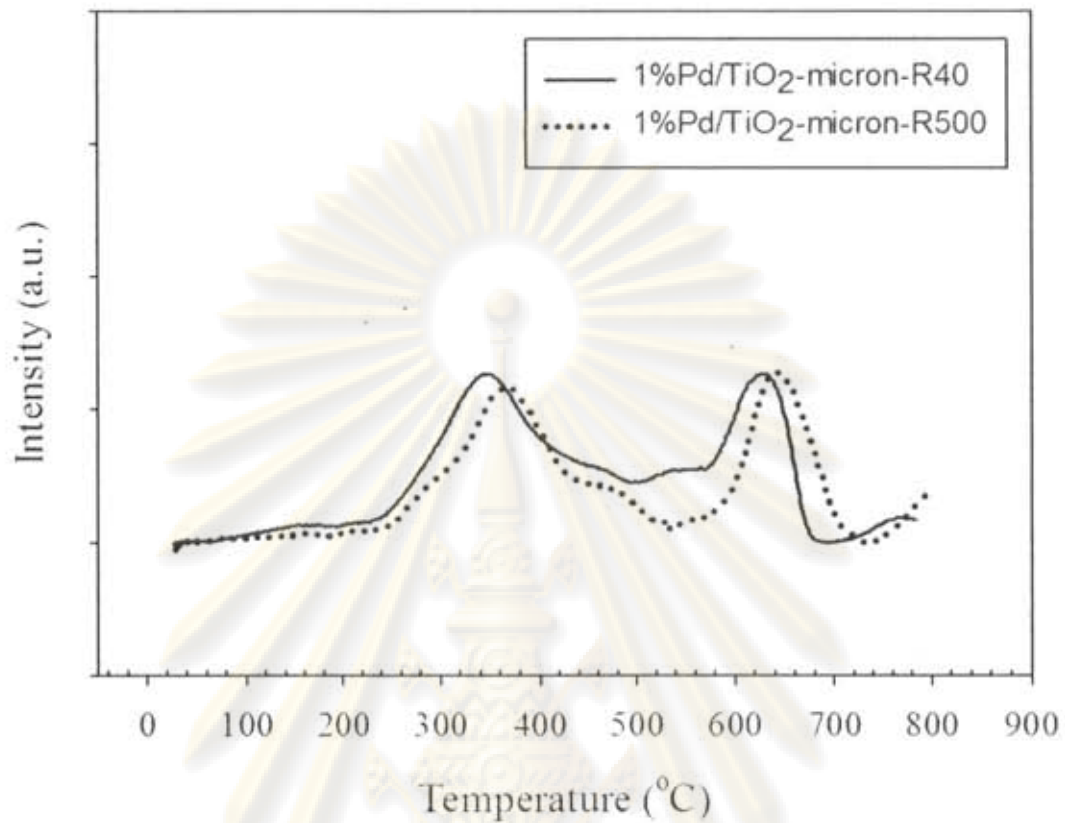
Figure 5.11 Profile of CO temperature programmed desorption of 1%Pd/TiO$_2$-micron
reduced at 40 and 500°C
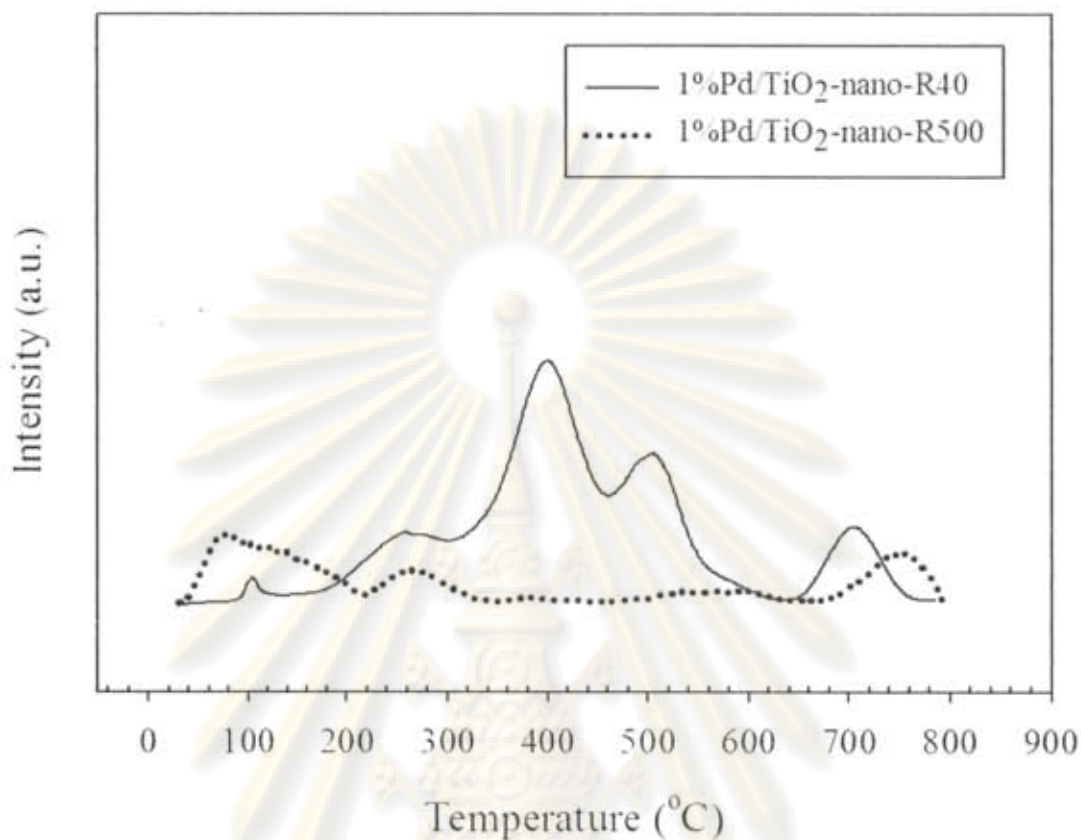
Figure 5.12 Profile of CO temperature programmed desorption of 1%Pd/TiO$_2$-nano reduced at 40 and 500°C

5.1.2 The Catalytic Performance of 1%Pd/TiO₂-micron and 1%Pd/TiO₂-nano Catalysts in Liquid Phase Selective Hydrogenation of Phenylacetylene.

The performance of the catalysts in liquid phase selective hydrogenation of phenylacetylene was determined in terms of phenylacetylene conversion and selectivity towards styrene. Phenylacetylene conversion is defined as moles of phenylacetylene consumed with respect to phentlacetylene in the feed. Selectivity is the ratio of the mole of styrene (desired product) was obtained to total mole of products (Styrene and Ethylbenzene). Ideally, there should be one phenylacetylene molecule converted to styrene for every hydrogen molecule consumed, or 100% selectivity, since all of the phenylacetylene is converted into styrene. In actual practice, some hydrogen will always be consumed in the side reaction of styrene conversion to ethylbenzene.

In this study, the reaction was carried out in ethanol solvent at 30°C and various H_2 pressures from 1-3 bars. The substrate: ethanol ratio was 1: 9. The products are analyzed by gas chromatography with flame ionization (GC-FID) using GS-alumina column. The performance of the 1%Pd/TiO₂-micron and 1%Pd/TiO₂-nano catalysts in liquid-phase selective hydrogenation of phenylacetylene under mild conditions are shown in **Figure 5.13**.The x-axis showed phenylacetylene conversions and the y-axis showed the styrene selectivities. It was clearly seen that when phenylacetylene conversions less than 80%. Both catalysts exhibited high styrene selectivities ($\geq$ 95%). The selectivity for styrene significantly dropped to 72-81% when conversion of phenylacetylene reached 100% for all the catalysts except 1%Pd/TiO₂-nano reduced at 500°C that retained its high styrene selectivity > 90%. Such results suggest that the strong metal-support interaction on 1%Pd/TiO₂-nano catalyst produced great beneficial effect on the catalyst performance. The presence of SMSI effect may result in an inhibition of the adsorption of the product styrene on the 1%Pd/TiO₂-nano hence high styrene selectivity was obtained. Nevertheless, high temperature reduction had shown to slightly improve the catalyst performance of 1%Pd/TiO₂-micron catalyst. It has been reported that specific activity (turnover frequencies) of Pd^{0} also increases with increasing Pd^{0} particle size. The results in this study thus follow the well-established trend in the literature about the dependence of

liquid-phase hydrogenation activity on Pd^0 particle size. (Carturan, G. *et al.*, 1982, Sarkany, A. *et al.*, 1986, Angel and Benitez, 1994, Duca, D. *et al.*, 1995, Albers, P. *et al.*, 1999, Molnar, A. *et al.*, 2001, Marin-Astroga, N. *et al.*, 2005) However, it should be emphasized that our results support the importance of the strong metal-support interaction effect in order to obtain high catalytic performance of the TiO_2 supported Pd catalysts in liquid-phase selective hydrogenation.
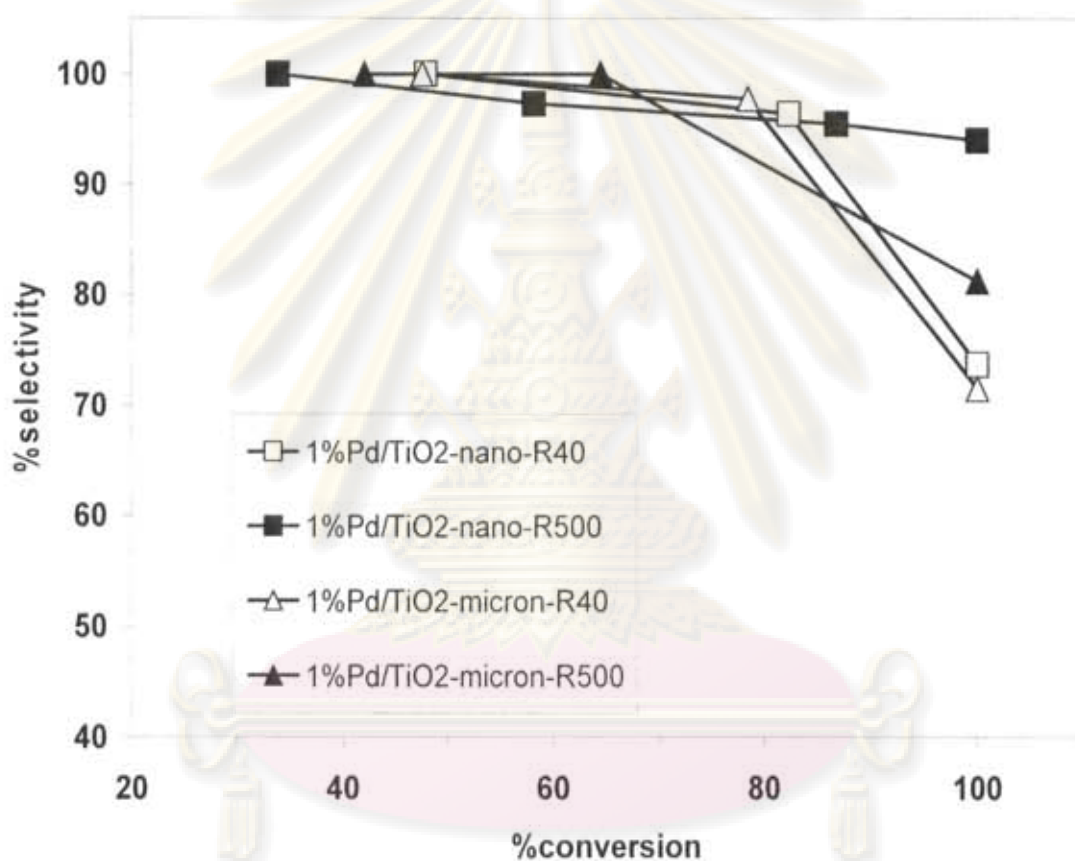

Figure 5.13 The Performance curve of 1%Pd/TiO_2-micron and 1%Pd/TiO_2-nano in Liquid Phase Selective Hydrogenation of Phenylacetylene

5.2 Comparative study of Pd supported on the series of nanocrystalline TiO$_2$ catalysts

In the second part the effect of various nanocrystallite sizes of TiO$_2$ in liquid phase selective hydrogenation of phenylacetylene was investigated. In this part, the nanocrystallite sizes of TiO$_2$ supports were prepared by solvothermal method and characterized by XRD, N$_2$ physisorption techniques and scanning electron microscopy (SEM). Moreover, the palladium supported on TiO$_2$ catalysts was characterized by several techniques to investigate the SMSI effect on the performance of this reaction.

5.2.1 Characterization of TiO$_2$ supports

5.2.1.1 X-ray Diffraction (XRD)

The XRD-patterns of TiO$_2$-derived solvothermal method are shown in **Figure 5.14.** The characteristic peak of pure anatase phase TiO$_2$ were observed at $2\theta = 25^\circ$ (major), 37°, 48°, 55°, 56°, 62°, 71°, and 75° without contamination of other phase such as rutile and bookite. The average crystallite sizes of TiO$_2$ were calculated from the full width at half maximum of the XRD peak at $2\theta = 25^\circ$ using Scherrer equation. The average crystallite sizes of TiO$_2$ were 9, 12, 17 and 23 nm, respectively. The synthesis conditions of TiO$_2$, reaction temperature, holding time and amount of substrates had effect to TiO$_2$ crystallite sizes (see in **Table5.7**).

Table5.7 The preparation conditions of nanocrystallite sizes of TiO$_2$ and average crystallite sizes from XRD results.

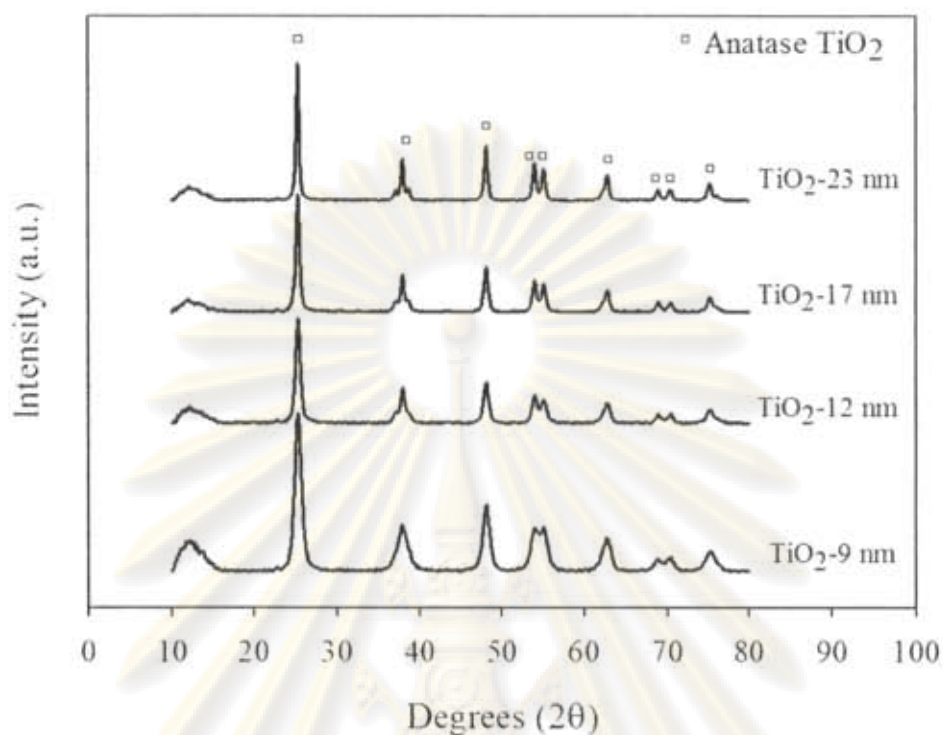| Samples	TNB(g)	Temp ($^\circ$C)	Holding Time (h)	XRD crystallite size of TiO$_2$ (nm)
TiO$_2$-9 nm	15	300	0.5	9
TiO$_2$-12 nm	25	300	2	12
TiO$_2$-17 nm	25	320	6	17
TiO$_2$-23 nm	25	340	12	23

Figure5.14 The XRD patterns of solvothermal derived-TiO$_2$ supports

5.2.1.2 N$_2$ Physisorption

BET surface area (S$_1$), pore volume, average pore diameter and specific surface area (S$_2$) of various crystallite sizes of TiO$_2$ supports were determined by N$_2$ physisorption technique and are shown in **Table5.8.** It was found that, the BET surface area decreased monotonically from 145 to 51 m^2/g when the crystallite sizes various from 9 to 23 nm, respectively. However, the specific surface area of TiO$_2$ samples was also calculated based on the correlation between surface area and crystallite size as follows:

$$S_2 = \frac{6}{d\rho}$$

where d is the average crystallite size and ρ is the density of TiO$_2$ (3.84 g.cm^{-3}) (Payakgul, W. *et al.*, 2005). This formula derived based on the assumption of spherical TiO$_2$ crystal. Spherical surface area and volume of spherical TiO$_2$ support

were used for calculated the specific surface area (S_2). Generally, specific surface area (S_2) is a material property of solids which measures the total surface area per unit of mass. It has a particular importance in case of adsorption, heterogeneous catalysis and reaction on surfaces. It is noticed that S_1 determined from N_2 physisorption was smaller than S_2 calculated based on the crystallite size for all the TiO_2 samples. This was probably the results of an amorphous-like phase contaminated in the TiO_2 particles (Kominami, H. *et al.*, 1999). Furthermore, the pore volume of TiO_2 supports were 0.42, 0.37, 0.38 and 0.32 cm^3/g when the crystallite size of TiO_2 increased from 9 to 23 nm, respectively. It was observed that, decreasing of BET surface area correspond to decreasing of pore volume from 0.42 to 0.32 cm^3/g. But the average pore diameter of TiO_2 supports increased from 8.1 to 20.2 nm when the BET surface area of TiO_2 decreased. The pore size distribution and N_2 physisorption adsorption-desorption isotherms of various crystallite sizes of TiO_2 supports are shown in **Figure5.15 to Figure5.19.** The results are indicated that the pores of all TiO_2 samples were meso pores.

Table5.8 BET surface area (S_1), pore volume, average pore diameter and specific surface area (S_2) of TiO_2 supports

Samples	BET surface area (S_1[a]) (m^2/g)	Pore Volume (cm^3/g)	Average Pore Diameter (nm)	Specific surface area (S_2[b]) (m^2/g)
TiO_2-9 nm	145	0.42	8.1	174
TiO_2-12 nm	88	0.37	12.5	130
TiO_2-17 nm	65	0.38	17.9	92
TiO_2-23 nm	51	0.32	20.2	68

[a] S_1 is specific surface area determined from N_2 physisorption results

[b] S_2 is specific surface area calculated based on the correlation between surface area and crystallite size of TiO_2

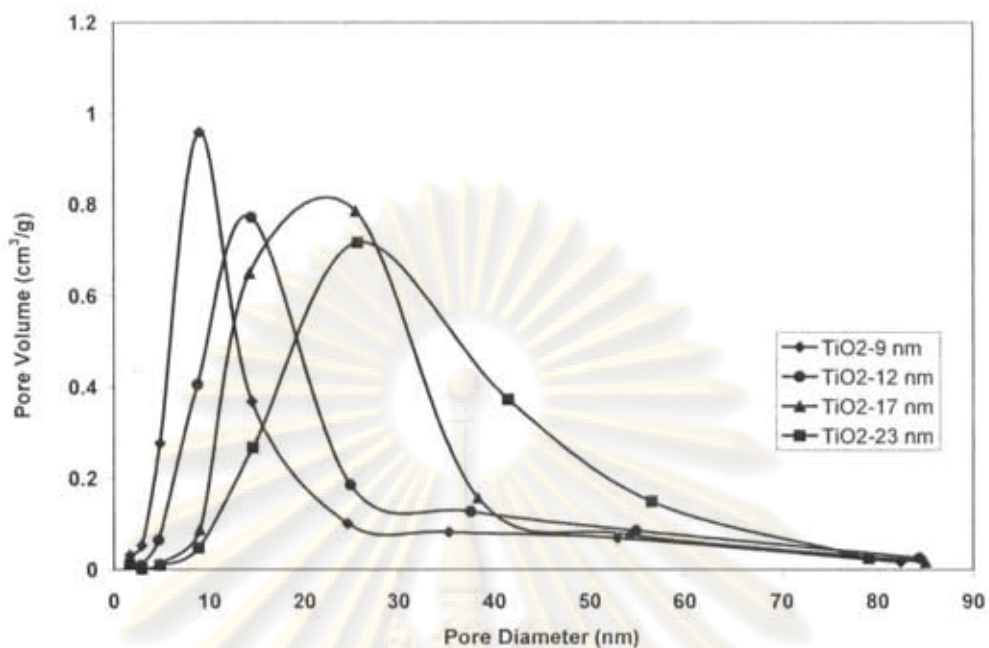**Figure5.15** Pore sizes distribution of TiO$_2$ samples
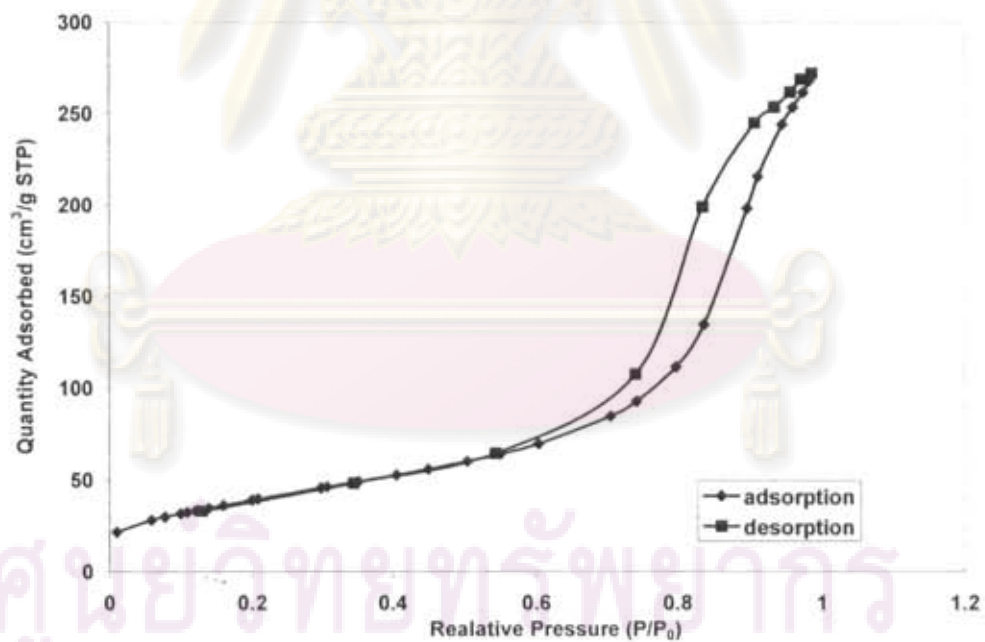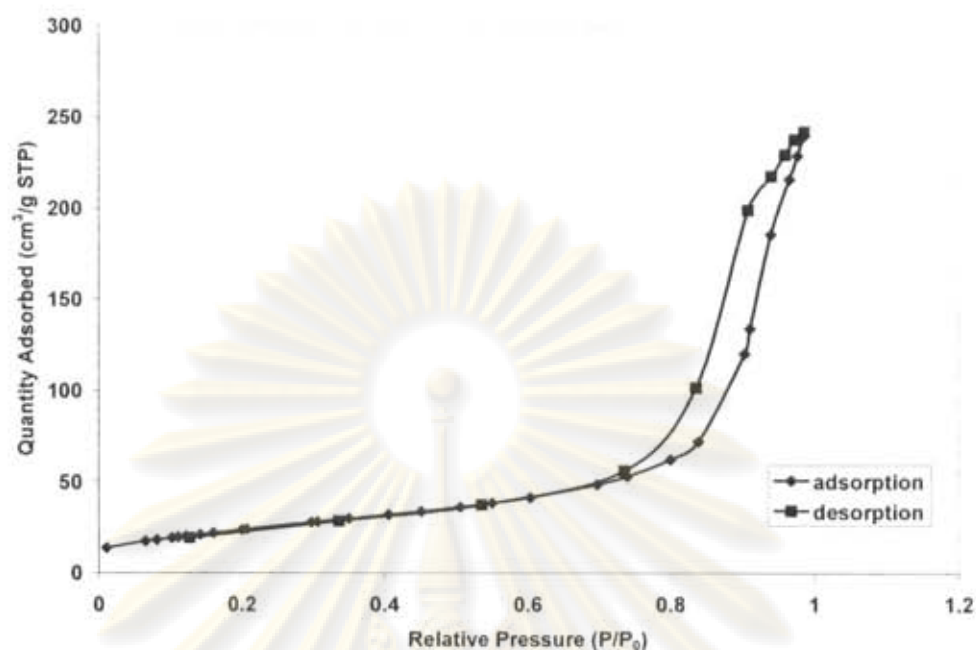

Figure5.16 N$_2$ adsorption-desorption isotherms of TiO$_2$-9 nm

Figure5.17 N_2 adsorption-desorption isotherms of TiO_2-12 nm
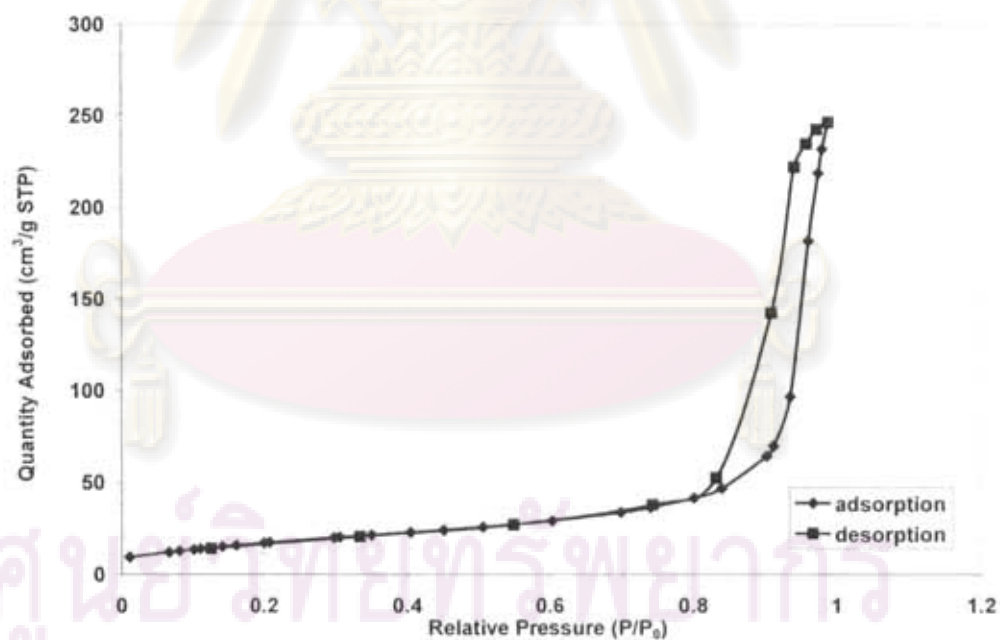
Figure5.18 N_2 adsorption-desorption isotherms of TiO_2-17 nm
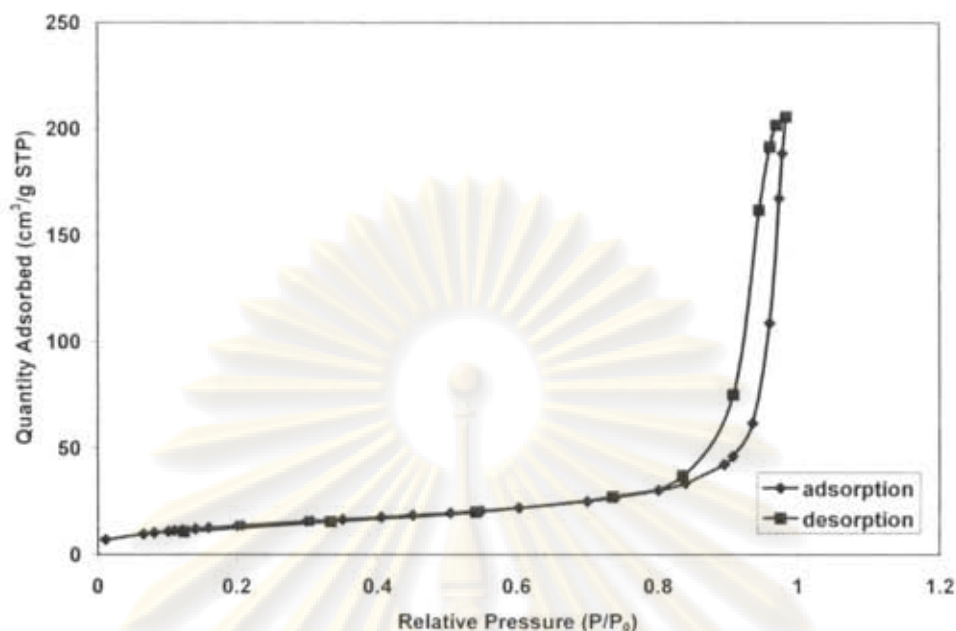
Figure5.19 N_2 adsorption-desorption isotherms of TiO_2-23 nm

5.2.1.3 Scanning Electron Microscopy (SEM)

The SEM micrograph of the various nanocrystallite sizes of TiO_2 supports are shown in **Figure5.20**. It revealed that the morphologies of all TiO_2-samples consisted of irregular shape of very fine particles agglomerated. There were not found the primary particle of TiO_2 supports and the crystallite sizes of all TiO_2 samples can be not observed because the SEM technique had the resolution in micron scale. However, the crystallite sizes of all TiO_2 samples were confirmed by TEM technique.
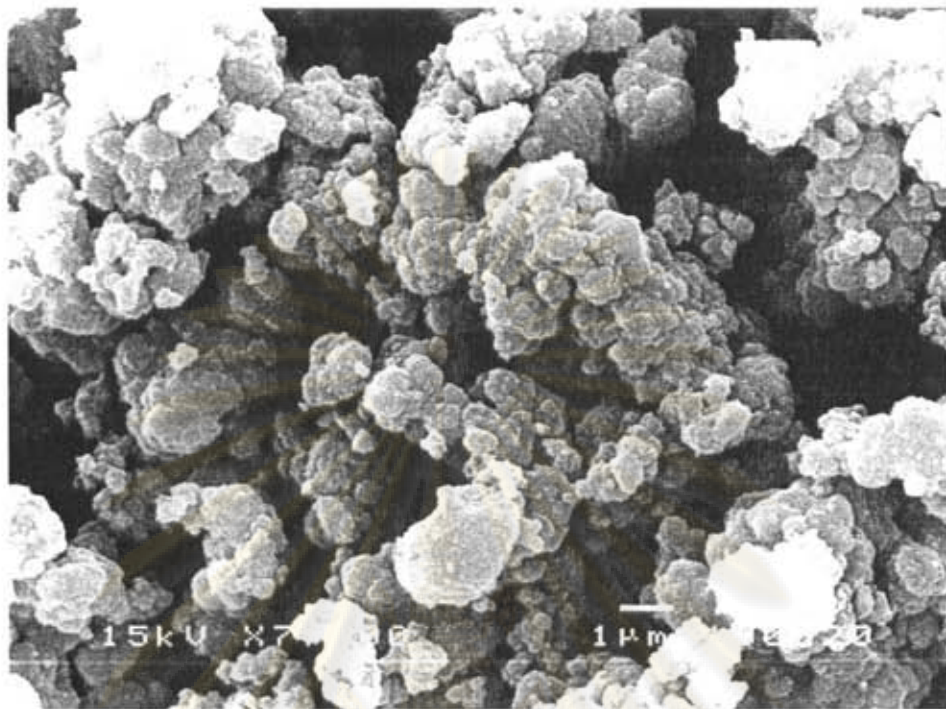
(A) TiO$_2$-9 nm
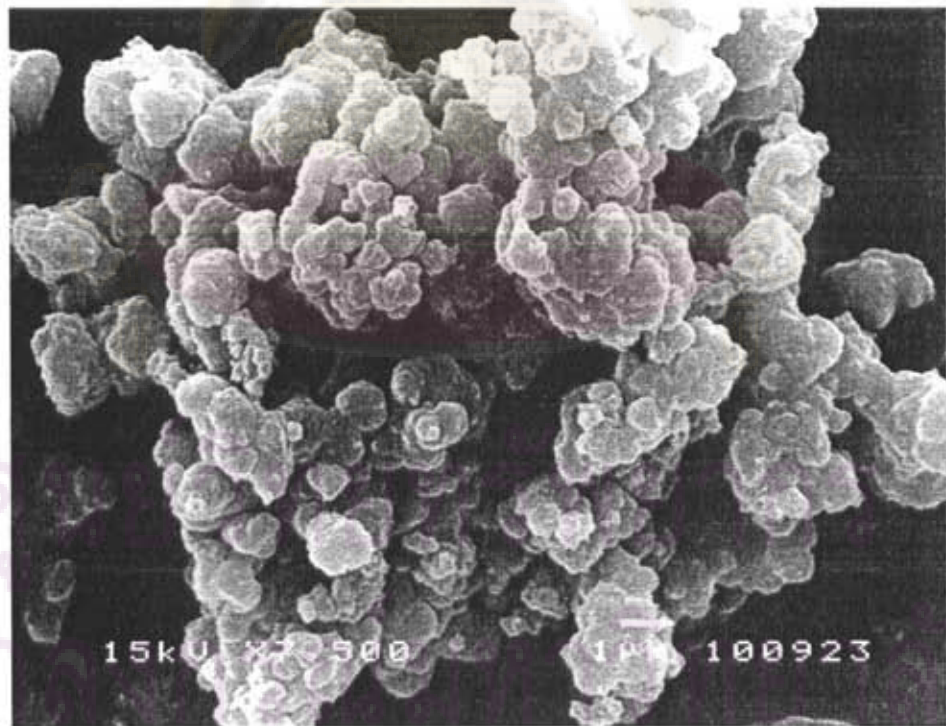
(B) TiO$_2$-12 nm

(C) TiO_2-17 nm

(D) TiO_2-23 nm

Figure5.20 SEM micrographs of various nanocrystallite sizes of TiO_2

5.2.2 Characterization of Pd supported on various crystallite size of TiO$_2$ catalysts

The palladium supported on various crystallite sizes of TiO$_2$ catalysts were preparation by incipient wetness impregnation method. 1%wt palladium was impregnated in all TiO$_2$ supports and the catalysts were characterized by several techniques.

5.2.2.1 X-ray Diffraction (XRD)

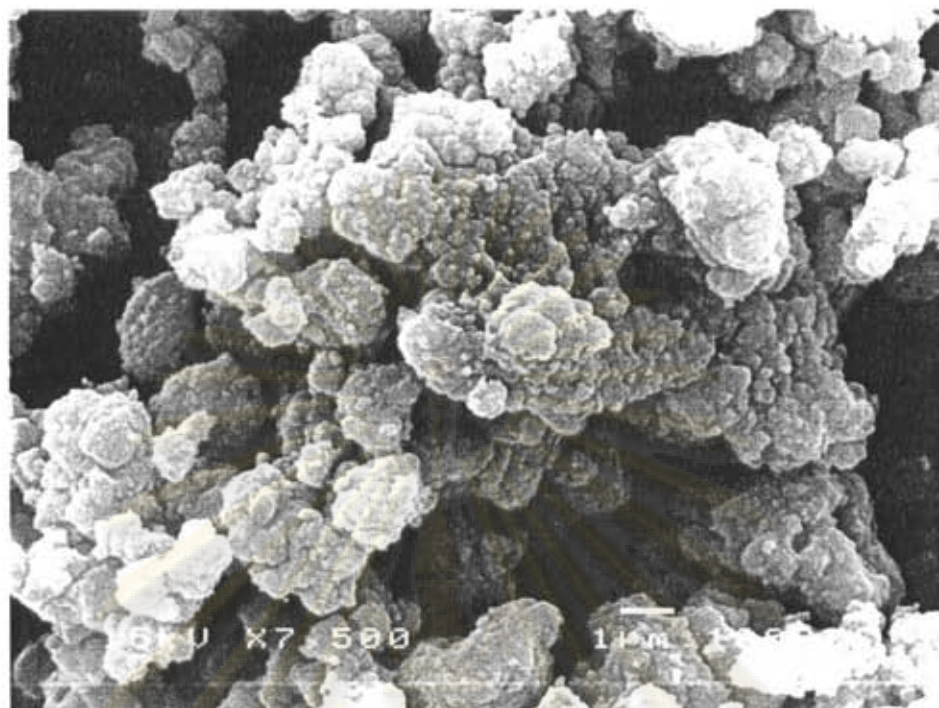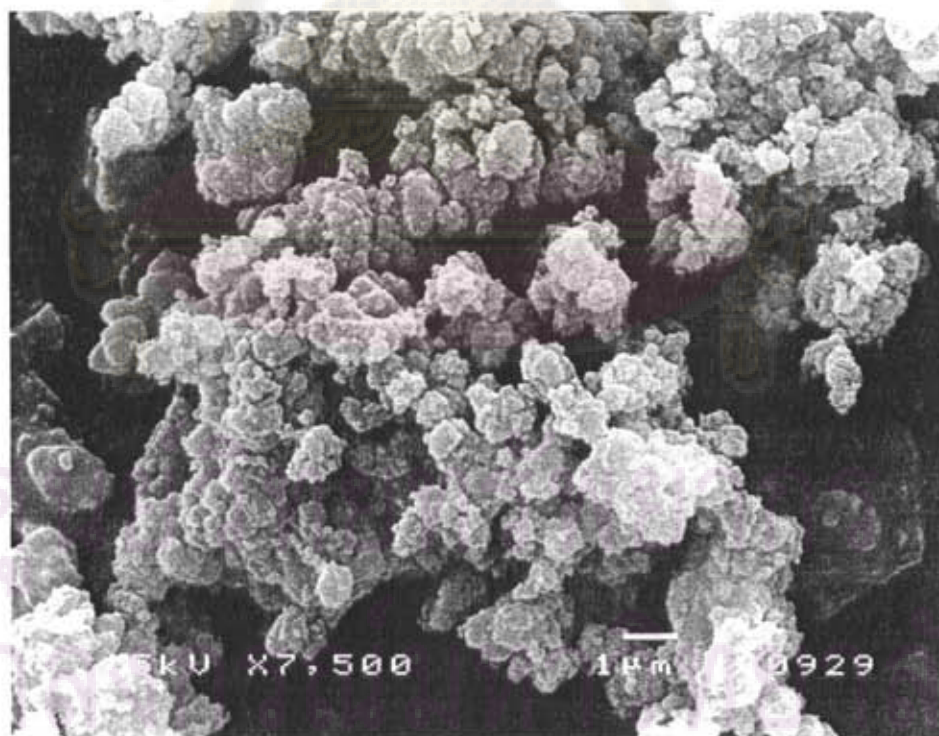The XRD patterns of 1%Pd-TiO$_2$ catalysts which various nanocrystallite sizes of TiO$_2$ supports, in the calcinations state are shown in **Figure5.21**. After impregnation and calcinations step, the XRD characteristic peaks corresponding to PdO were observed at $2\theta = $ ca.33.8° in every samples because the impregnated palladium was oxidized to metal oxide form after calcinations step. However, the PdO peaks for all catalysts were disappeared after reduction step at 40 and 500°C. Moreover, the XRD characteristic peaks of Pd$^\circ$ metal ($2\theta = $ 40.2°and 46.7°) were not observed after impregnation of Pd, calcinations, and reduction step suggesting that a highly dispersed form of Pd or the low amount of Pd loading.(see **Figure5.22** and **Figure5.23**)

After impregnated with approximately 1 wt% Pd, calcined, and reduced at 40 or 500°C, the crystallite sizes of all the TiO$_2$ samples as determined by XRD (show in **Table5.9**) were essentially unaltered except that of the smallest size TiO$_2$ (TiO$_2$-9 nm). The crystallite size of TiO$_2$-9 nm was found to be 11 nm after reduction at 500°C. A slight increase in the TiO$_2$ crystallite sizes of the TiO$_2$-9 nm from 9 to 11 nm suggests the lower stability of the smaller crystallite size TiO$_2$ compared to the larger size ones. It is generally found that the crystals of large crystallite size show higher thermal stability than the crystals of small crystallite size. (P. Praserthdam *et al.* 2003)

Table5.9 The crystallite sizes of TiO_2 support of 1%Pd/TiO_2 catalysts after calcinations and reduction at 40°C and 500°C

Samples	XRD crystallite sizes of TiO_2 (nm)		
	As-syn	Reduced[a] 40°C	Reduced[a] 500°C
1%Pd/TiO_2-9 nm	9	8	11
1%Pd/TiO_2-12 nm	12	12	13
1%Pd/TiO_2-17 nm	17	16	18
1%Pd/TiO_2-23 nm	23	23	23

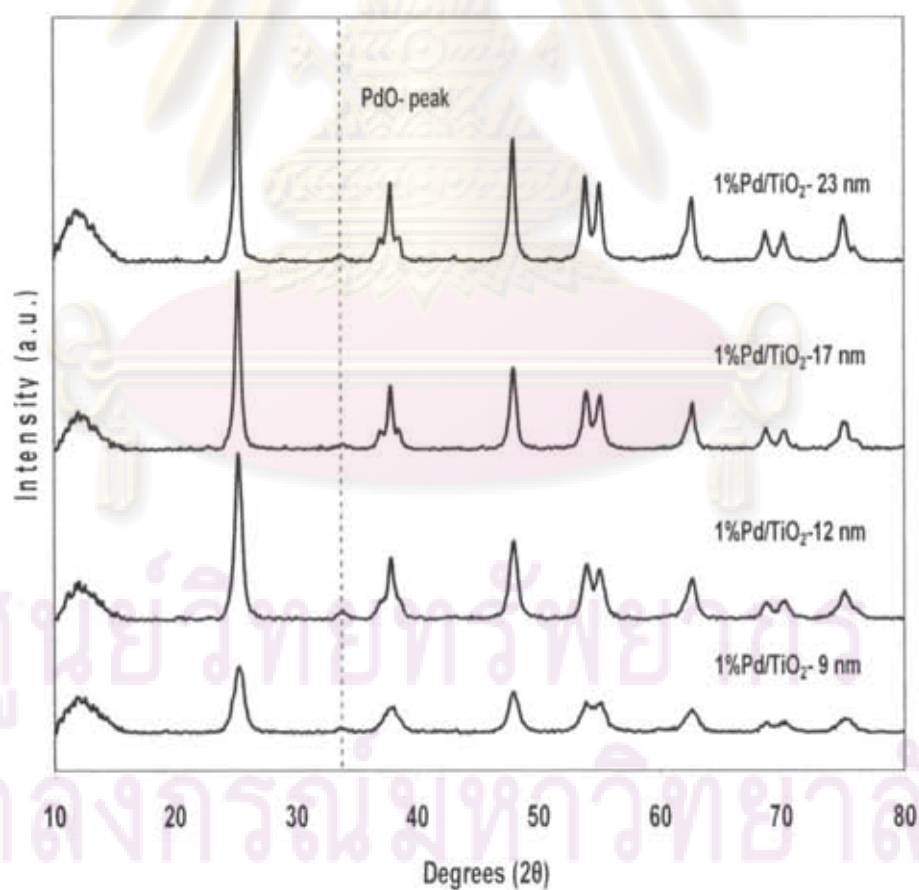a : after Pd was impregnated and calcined.

Figure5.21 The XRD patterns of 1%Pd/TiO_2 various crystallite sizes after calcinations step
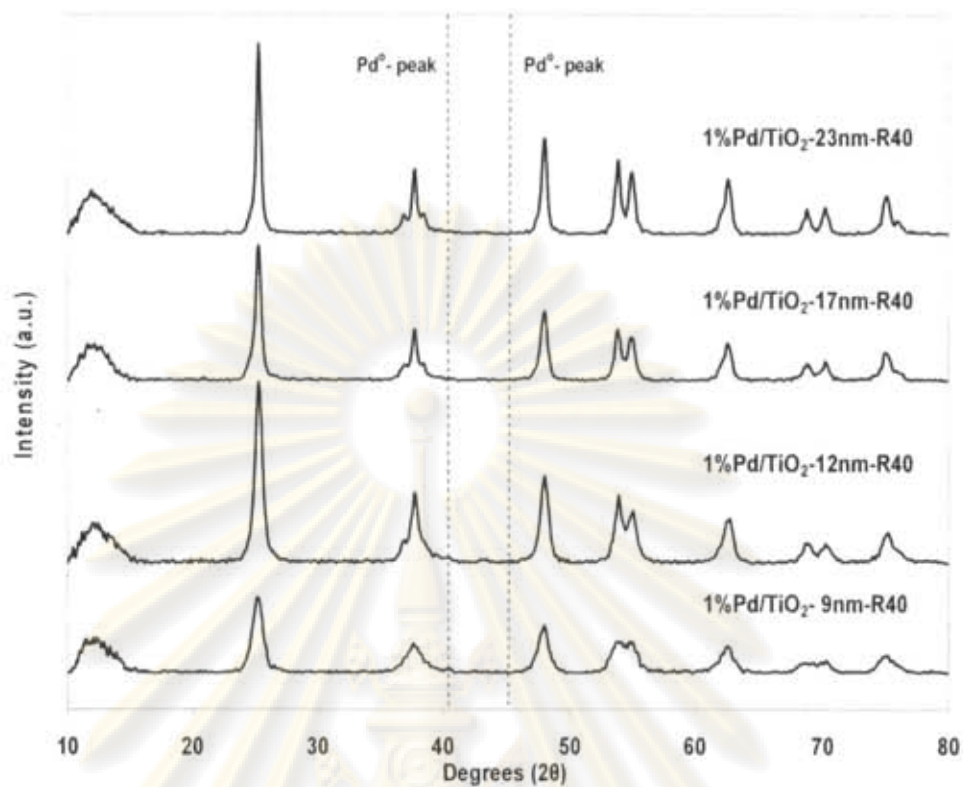
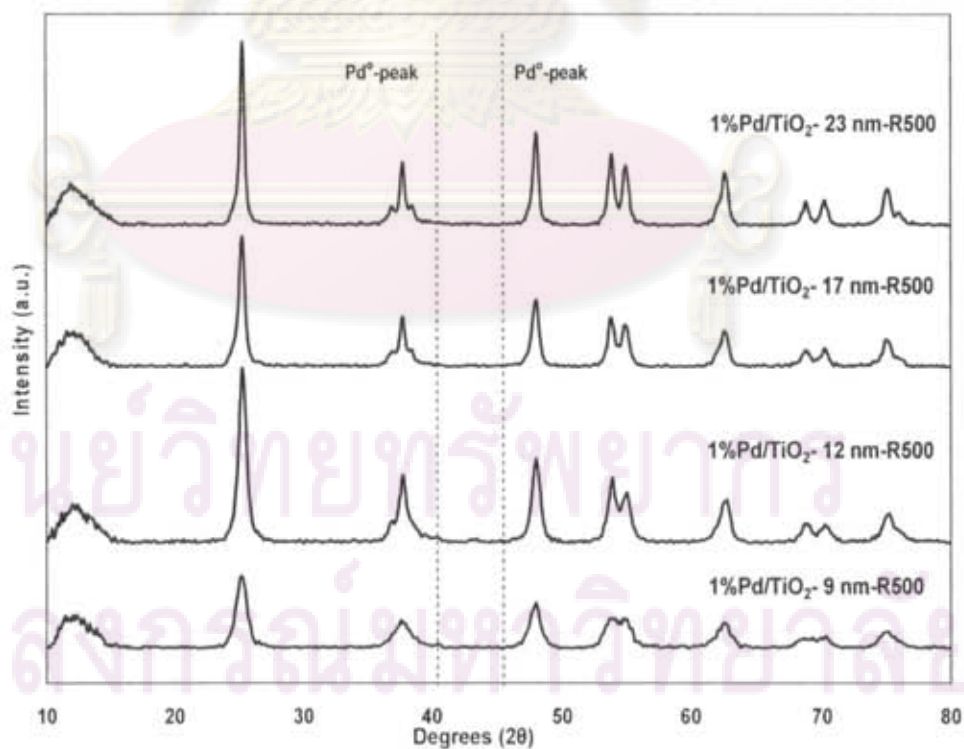**Figure5.22** The XRD patterns of 1%Pd/TiO$_2$ various crystallite sizes after reduction at 40°C

Figure5.23 The XRD patterns of 1%Pd/TiO$_2$ various crystallite sizes after reduction at 500°C

5.2.2.2 N_2 Physisorption

The BET surface area, pore volume and average pore diameter of the various TiO_2-supported Pd catalysts which reduced at 40 and 500°C was determined by N_2 physisorption techniques and are shown in **Table5.10**. From these results, the BET surface area of the Pd/TiO_2 catalysts were slightly decreased less than that of the original TiO_2 supports both of high and low reducing temperatures suggesting that palladium was deposited in some of the pores of TiO_2. Moreover, the results were consistent with pore volume of all catalysts which decreasing after palladium loading. It was found that, the average pore diameters of all Pd/TiO_2 catalysts were meso pore and smaller than the average pore diameters of original TiO_2 supports.

Table5.10 N_2 Physisorption results of Pd/TiO_2 catalysts

Catalysts	BET surface area (m^2/g)	Pore Volume (cm^3/g)	Average Pore Diameter (nm)
TiO_2-9 nm	145	0.420	8.1
1%Pd/TiO_2-9 nm-R40	135	0.300	6.3
1%Pd/TiO_2-9 nm-R500	89	0.202	6.2
TiO_2-12 nm	88	0.370	12.5
1%Pd/TiO_2-12 nm-R40	84	0.312	11.1
1%Pd/TiO_2-12 nm-R500	75	0.295	10.7
TiO_2-17 nm	65	0.380	17.9
1%Pd/TiO_2-17 nm-R40	62	0.296	14.3
1%Pd/TiO_2-17 nm-R500	60	0.304	14.2
TiO_2-23 nm	51	0.320	20.2
1%Pd/TiO_2-23 nm-R40	47	0.275	19.8
1%Pd/TiO_2-23 nm-R500	42	0.289	19.7

5.2.2.3 Scanning Electron Microscopy (SEM)

The morphologies of Pd/TiO$_2$ catalysts after reduced at 40 and 500°C were determined by Scanning Electron Microscopy (SEM) technique and are shown in **Figure5.24**. It was observed that, the morphologies of the 1%Pd/TiO$_2$ catalysts were not significantly different when reduction temperature changed from 40 to 500°C. Moreover, the morphologies of the 1%Pd/TiO$_2$ catalysts were not significantly different from the original TiO$_2$ supports. The particle size and shape of the catalyst particles also were not affected by impregnation of palladium (no changes in the particle size/shape).

(A) 1%Pd/TiO$_2$-9 nm-R40   (B) 1%Pd/TiO$_2$-9 nm-R500

(C) 1%Pd/TiO$_2$-12 nm-R40   (D) 1%Pd/TiO$_2$-12 nm-R500

(E)1%Pd/TiO$_2$-17 nm-R40   (F)1%Pd/TiO$_2$-17 nm-R500
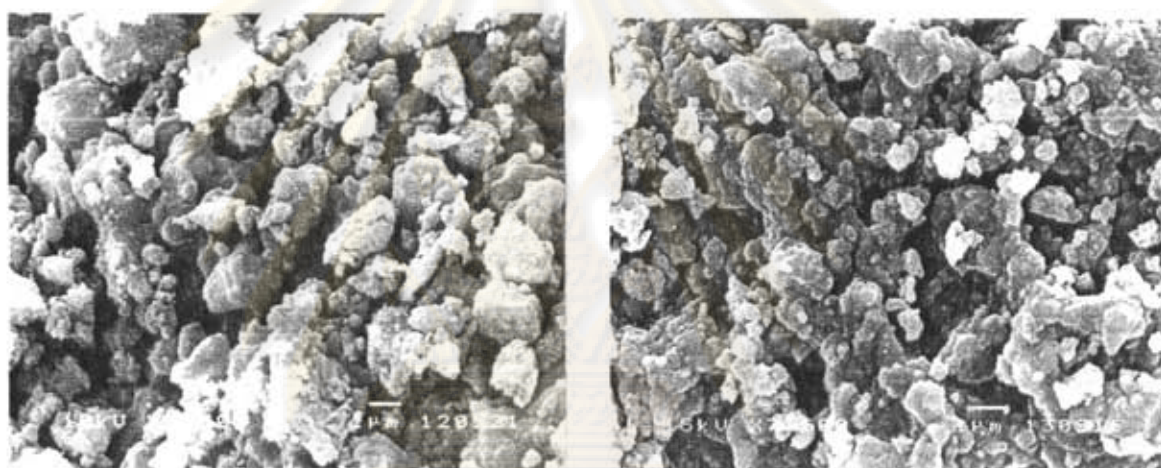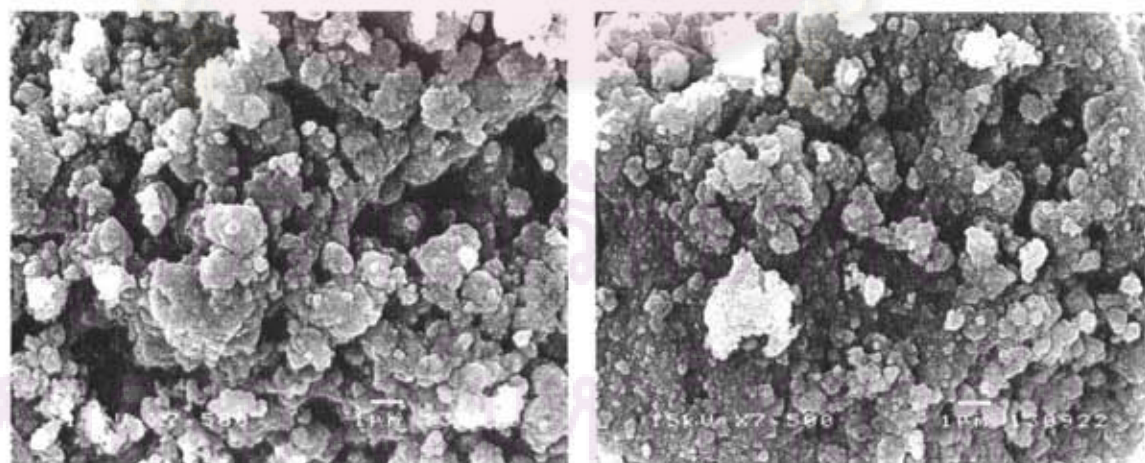
(G)1%Pd/TiO$_2$-23 nm-R40   (H)1%Pd/TiO$_2$-23 nm-R500
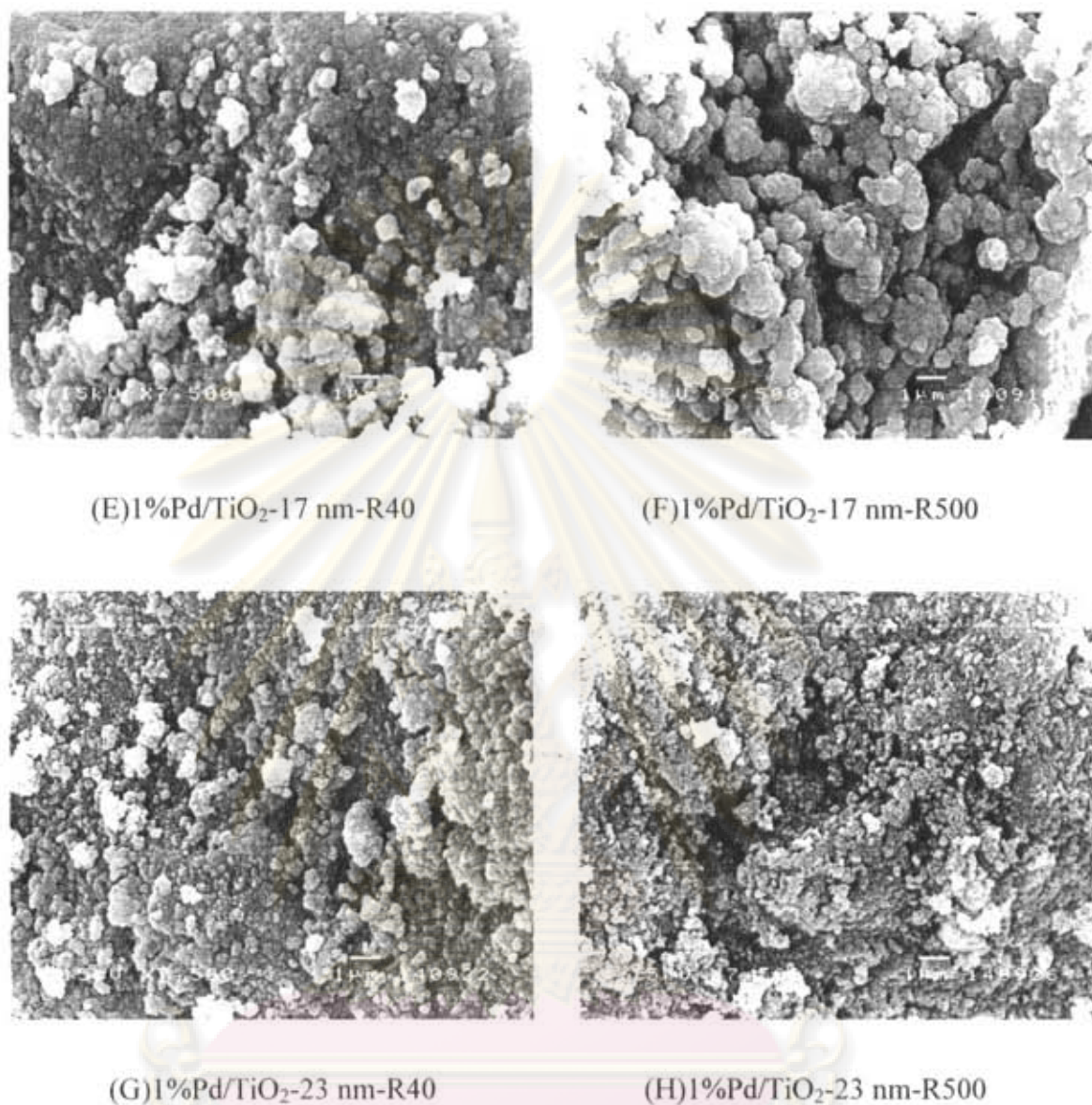
Figure5.24 SEM micrographs of 1%Pd/TiO$_2$ various crystallite sizes of TiO$_2$

5.2.2.4 Transmission Electron Microscopy (TEM)

TEM analysis has been carried out in order to physically measure the TiO$_2$ crystallite sizes as well as Pd particle/cluster sizes on the various Pd/TiO$_2$ catalysts. The TEM micrographs of palladium supported on various nanocrystallite sizes of TiO$_2$ catalysts with reduced at 40 and 500°C are shown in **Figure5.25.** It was observed that the crystallite sizes of TiO$_2$ supports were consistent to those obtained from XRD results. Reduction with H$_2$ either at 40 or 500°C did not result in

significant changes of the TiO_2 crystallite sizes. However, for the Pd/TiO_2-9 nm Pd/TiO_2-12 nm and Pd/TiO_2-17 nm after reduced at 40 and 500°C, the presence of Pd particles were not clearly seen whereas on the and Pd/TiO_2-23 nm, small Pd particles with average particle size around 5-6 nm were apparent. There was no significant difference on the Pd particle size observed for Pd/TiO_2-23 nm-R40 and Pd/TiO_2-23-R500 suggesting that Pd was not sintered after the catalyst was reduced at 500°C.
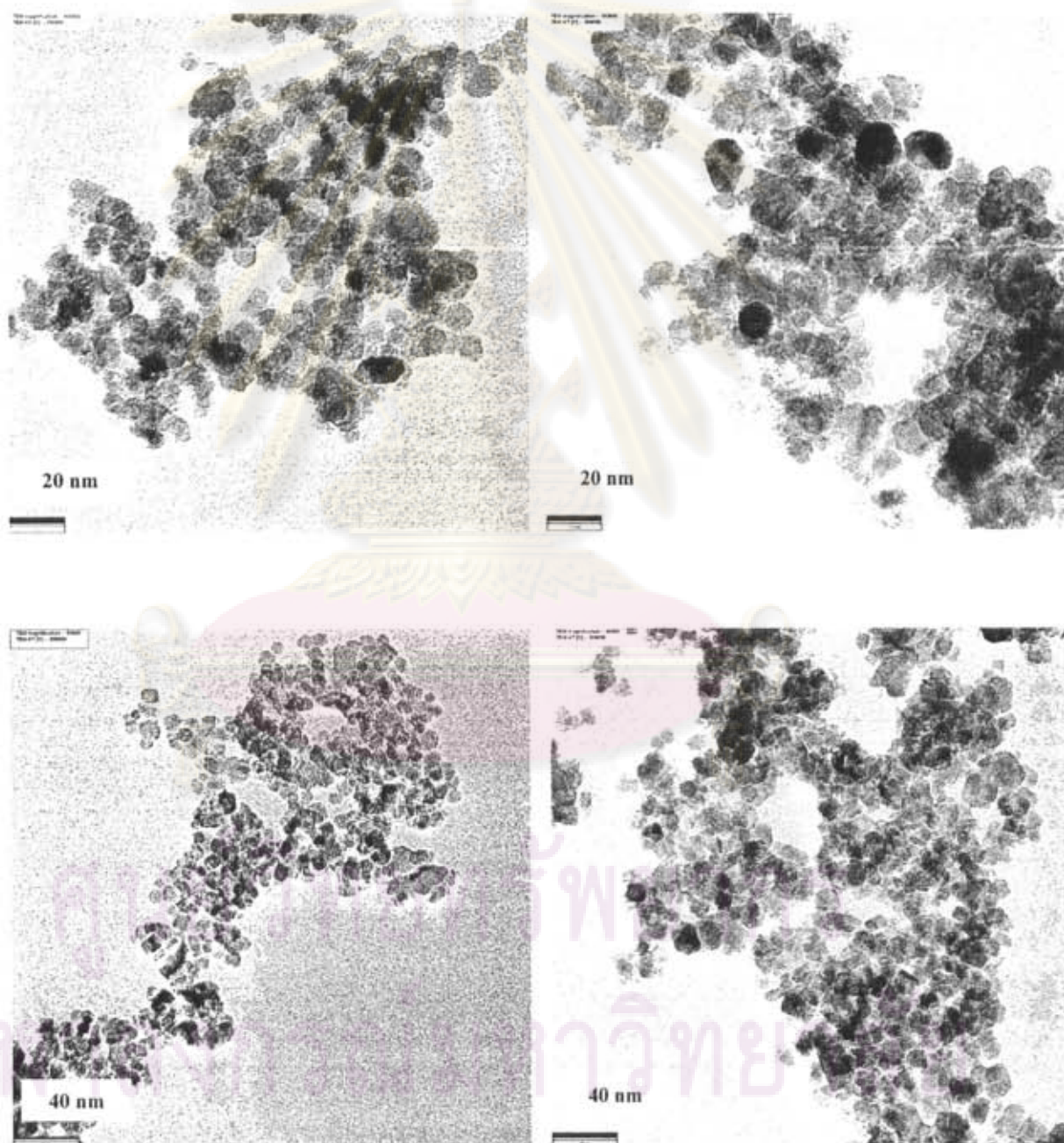
(A) 1%Pd/TiO_2-9 nm-R40   (B) 1%Pd/TiO_2-9 nm-R500
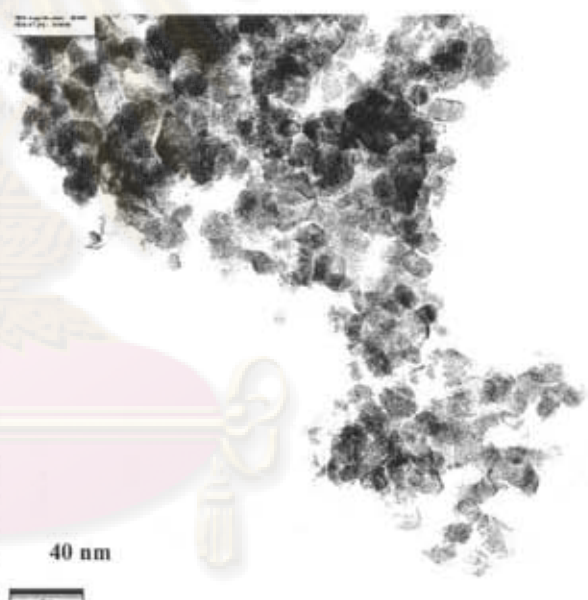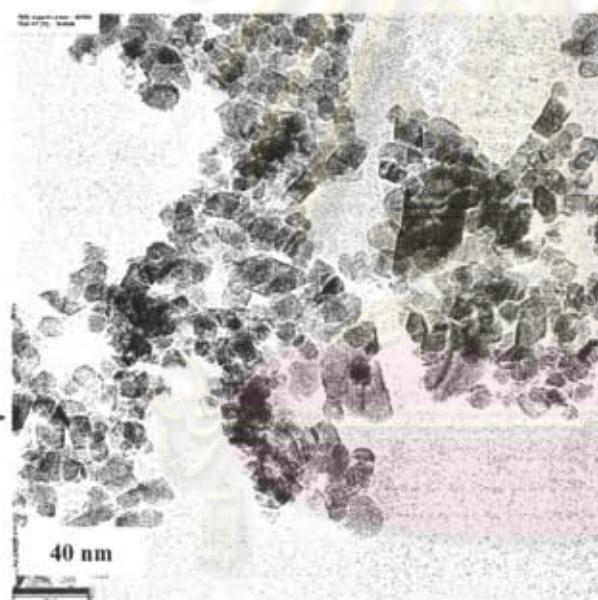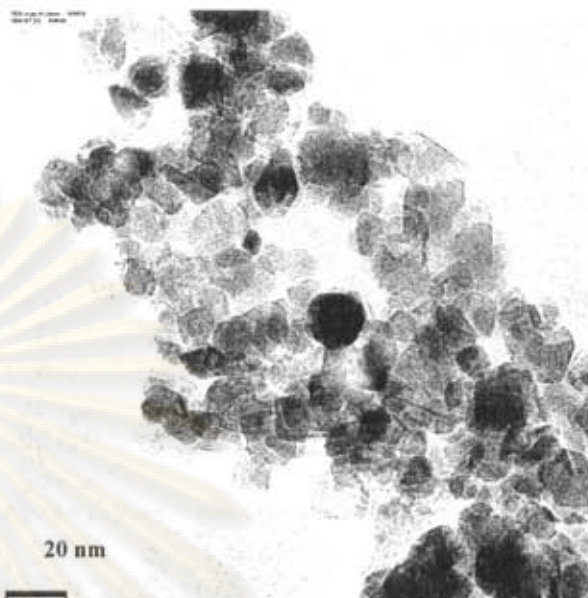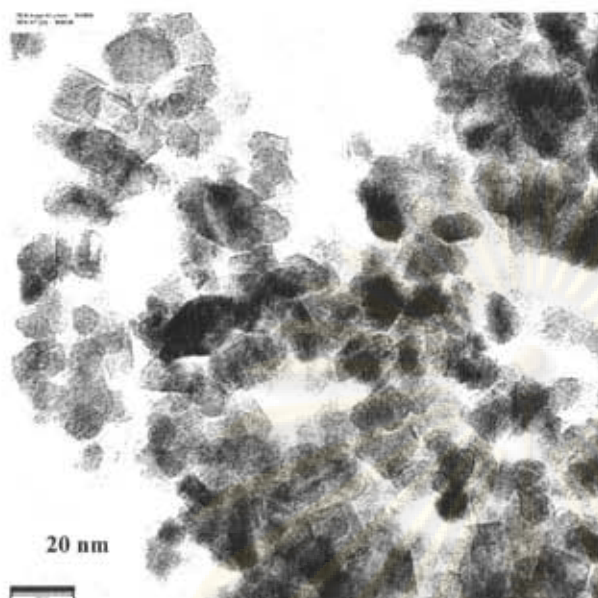
(C) 1%Pd/TiO$_2$-12 nm-R40   (D) 1%Pd/TiO$_2$-12 nm-R500
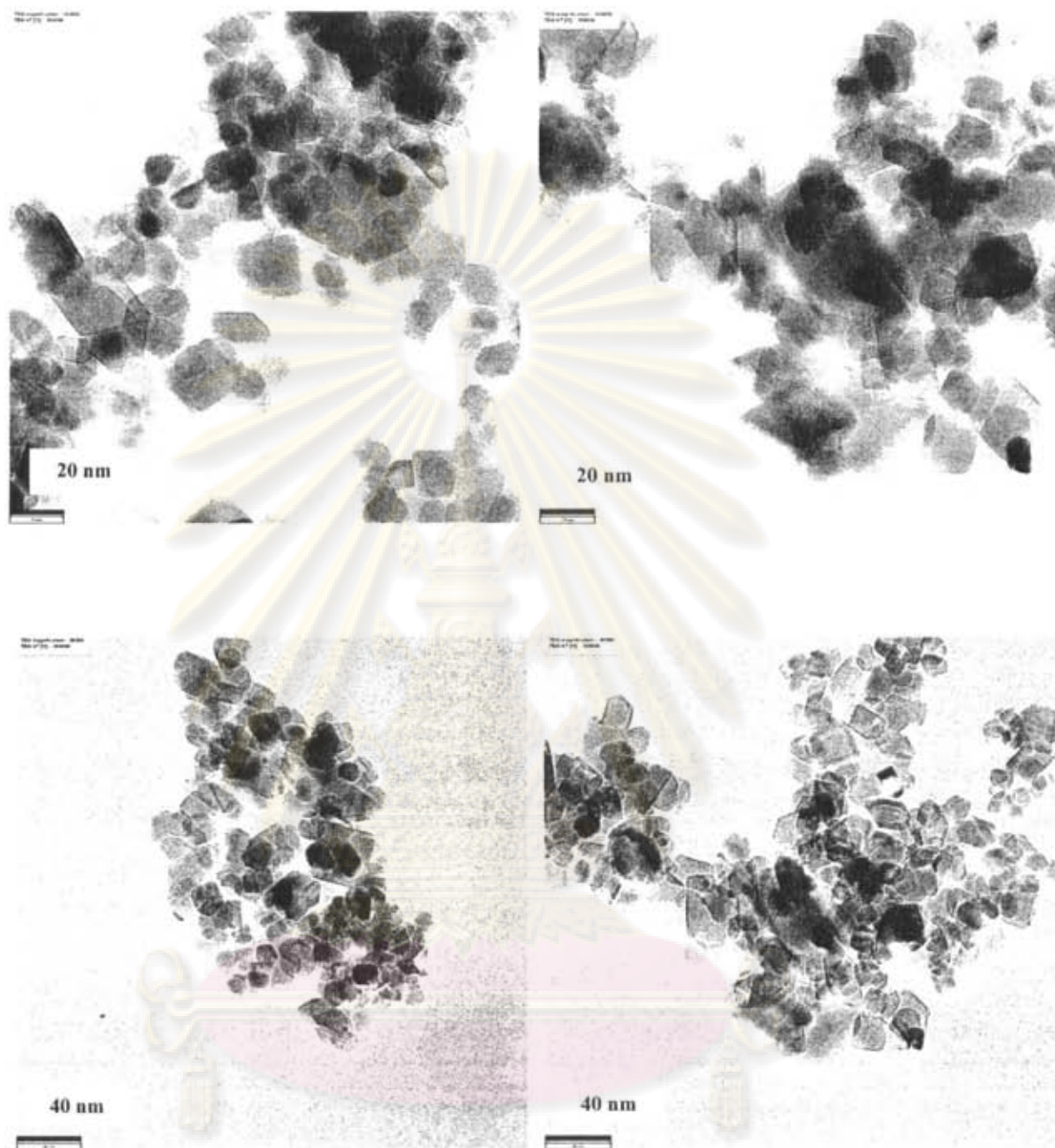
(E) 1%Pd/TiO$_2$-17 nm-R40   (F) 1%Pd/TiO$_2$-17 nm-R500
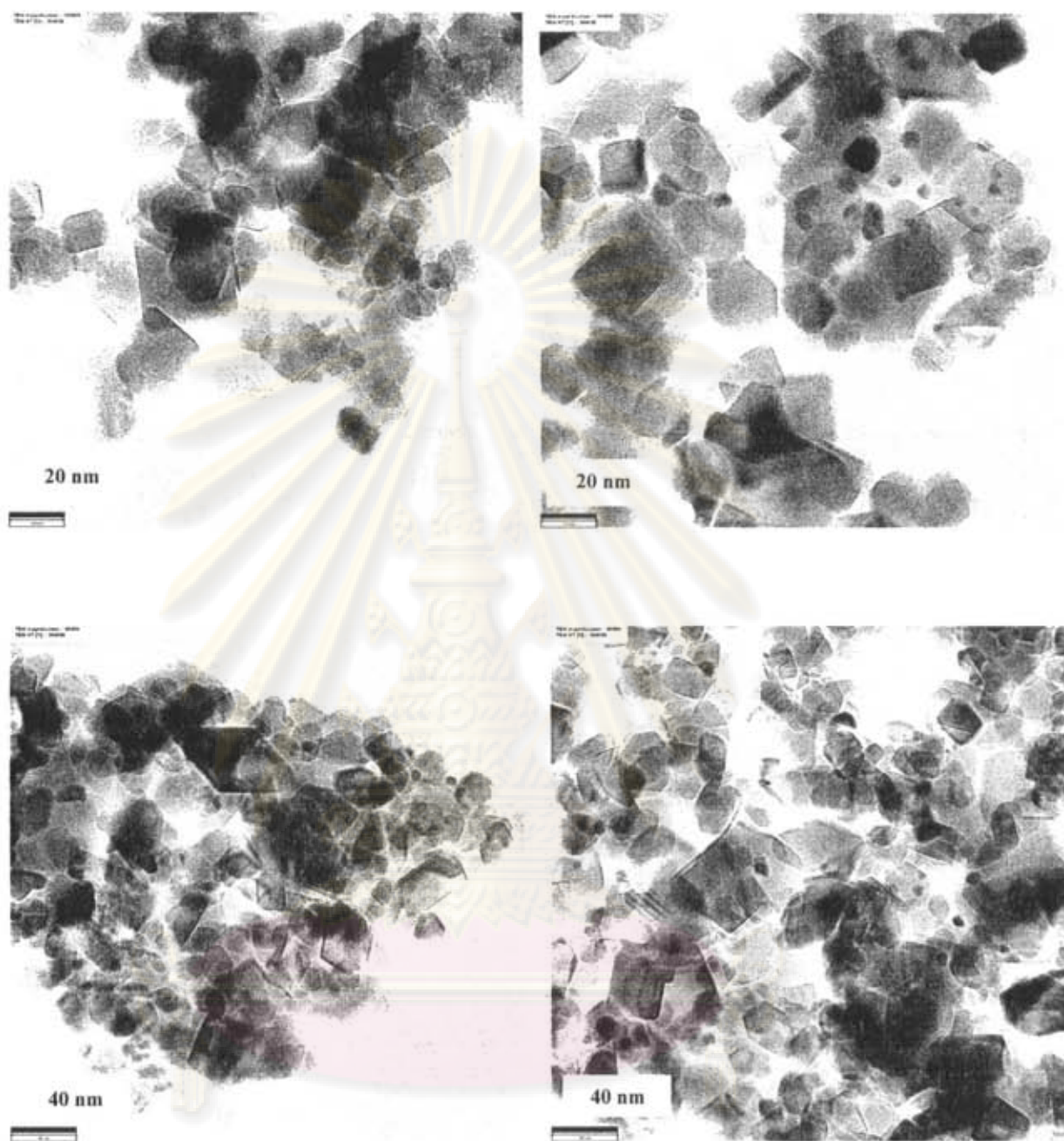
(E) 1%Pd/TiO$_2$-23 nm-R40   (F) 1%Pd/TiO$_2$-23 nm-R500

Figure5.25 TEM micrographs of 1%Pd/TiO$_2$ various crystallite sizes of TiO$_2$

5.2.2.5 CO-pulse chemisorption

5.2.2.5.1 Metal active sites

CO chemisorption technique provides the information on the number of palladium active sites and palladium particle sites. The total CO uptakes, palladium particle sites and the differences between the amount of CO chemisorbed on the catalysts reduced at $40^{\circ}C$ and $500^{\circ}C$ are reported in **Table 5.11**.

From the results, it was found that the amount of CO chemisorbed on Pd/TiO$_2$-9 nm reduced at $40^{\circ}C$ gave the highest CO chemisorption around 18.10×10^{18} molecule CO/g.cat whereas the amount of CO chemisorbed on the other catalysts reduced at $40^{\circ}C$ slightly decreased when increasing of TiO$_2$ crystallite sizes from 9 to 23 nm. The amount of CO chemisorbed were 15.60×10^{18}, 12.10×10^{18} and 9.73×10^{18} molecule CO/g.cat for 1%Pd/TiO$_2$-12nm-R40, 1%Pd/TiO$_2$-17nm-R40 and 1%Pd/TiO$_2$-23nm-R40, respectively. While the amount of CO chemisorbed of catalysts reduced at $500^{\circ}C$ were 1.31×10^{18}, 1.02×10^{18}, 0.90×10^{18} and 1.11×10^{18} for 1%Pd/TiO$_2$-9nm-R500, 1%Pd/TiO$_2$-12nm-R500, 1%Pd/TiO$_2$-17nm-R500 and 1%Pd/TiO$_2$-23nm-R500, respectively. It was clearly seen that the amount of CO chemisorbed on the Pd/TiO$_2$ catalysts dramatically decreased when the catalysts were reduced at $500^{\circ}C$ in all catalysts. The differences between the amount of CO chemisorbed on the catalysts reduced at $40^{\circ}C$ and $500^{\circ}C$ were larger when the crystallite size of the TiO$_2$ was small.

5.2.2.5.2 Strong Metal Support Interaction Test (SMSI Test)

The SMSI test was performed by measuring the amounts of CO chemisorption of the re-calcined (at $450^{\circ}C$) and re-reduced (at $40^{\circ}C$) catalysts after they were subjected to reduction at $500^{\circ}C$. This effect was confirmed by totally recovered the metal active site after being reduced at $500^{\circ}C$, re-calcined and re-reduced at $40^{\circ}C$.

The recovery of palladium active sites on all Pd/TiO$_2$ catalysts after being reduced at $500^{\circ}C$, re-calcined and re-reduced at $40^{\circ}C$ are illustrated on **Figure 5.26**. This figure showed the amount of CO chemisorbed can be totally restored for all

catalysts. The results exhibited the strong metal-support interaction or SMSI for all catalysts and suggested that there was no Pd sintering during high temperature reduction at 500°C. The Pd^0 metal particles calculated from CO chemisorption results (for the catalysts reduced at 40°C) increased with increasing TiO$_2$ crystallite size and were in the range of 3.2-5.9 nm. The results were consistent with TEM analysis.

Table5.11 CO chemisorptions results of the Pd/TiO$_2$ catalysts

Catalysts	CO chemisorption (x10^{-18} molecule CO/g cat.)	ΔCO (red.40-red.500)	d$_p$ Pd^0 (nm)
1%Pd/TiO$_2$-9 nm-R40	18.10	16.8	3.2
1%Pd/TiO$_2$-9 nm-R500	1.31		
1%Pd/TiO$_2$-12 nm-R40	15.60	14.6	3.7
1%Pd/TiO$_2$-12 nm-R500	1.02		
1%Pd/TiO$_2$-17 nm-R40	12.10	11.2	4.7
1%Pd/TiO$_2$-17 nm-R500	0.90		
1%Pd/TiO$_2$-23 nm-R40	9.73	8.6	5.9
1%Pd/TiO$_2$-23 nm-R500	1.11		
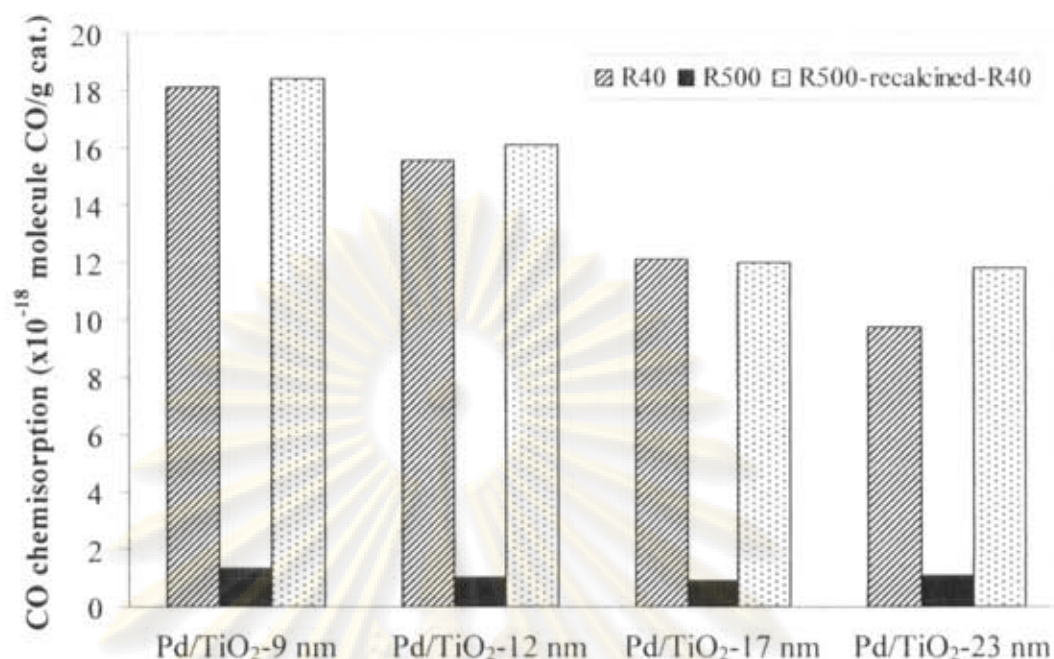
Figure5.26 The results of SMSI test on 1%Pd/TiO$_2$ catalysts which various TiO$_2$ crystallite sizes

5.2.2.6 Atomic Absorption Spectroscopy (AAS)

The percentage of palladium loading was determined by atomic absorption spectroscopy (AAS) to confirm the actual amount of palladium loading in the fresh catalysts. The actual amount of palladium loading in the fresh catalysts, 1%Pd/TiO$_2$ various crystallite sizes of TiO$_2$ in range 9 nm to 23 nm are shown in **Table5.12**. The results corresponded with amount of palladium loading at 1%palladium.

Table5.12 The actual amount of palladium loading in fresh catalysts by AAS

Catalysts	Actual amount of palladium loading (%)
1%Pd/TiO$_2$-9 nm	1.2
1%Pd/TiO$_2$-12 nm	1.1
1%Pd/TiO$_2$-17 nm	1.2
1%Pd/TiO$_2$-23 nm	1.2

5.2.3 Reaction Study of Pd/TiO₂ which various nanocrystallite sizes of TiO₂ supports in Liquid Phase Selective Hydrogenation of Phenylacetylene.

The performance of Pd/TiO$_2$ catalysts was evaluated in the liquid-phase selective hydrogenation of phenylacetylene to styrene in a batch-type stainless steel reactor. The reaction was carried out in ethanol solvent at 30°C and H$_2$ pressures 5 bars. The substrate: ethanol ratio was 1: 9 and amount of substrate was 0.5 ml. The products are analyzed by gas chromatography with flame ionization (GC-FID) using GS-alumina column.

The performance of Pd/TiO$_2$ catalysts was exhibited in the concentration profile of phenylacetyrene, styrene and ethylbenzene with various reaction time from 5 to 60 minutes and are shown in **Figure5.27 (a-d)**. The X-axis shows the reaction time and Y-axis shows the concentration of substrate and products. Comparing Pd/TiO$_2$ with similar TiO$_2$ crystallite size, phenylacetylene hydrogenation rate for the catalyst reduced at 500°C was lower that those reduced at 40°C. Such effect was more pronounced for the smaller TiO$_2$ crystallite size supported Pd catalysts. Moreover, the smaller crystallite sizes of TiO$_2$, the slower the reaction rate for phenylacetylene hydrogenation and are shown in **Figure5.28**. This was probably due to the fact that on small crystallite size TiO$_2$ the Pd^0 particle size was relatively small. It has been reported that specific activity (turnover frequencies) of Pd^0 decreases as metal particle size decreases especially when the average Pd particle size is very small ($\leq$ 3-5 nm) (Marin-Astroga, N. *et al.*, 2005, Molnar, A. *et al.*, 2001, Albers, P. *et al.*, 1999).

However, the performance of the Pd/TiO$_2$ catalysts in this study show typical profile compared to other Pd catalyst systems such as Pd/SiO$_2$ (Nijhuis, T. A. *et al.*, 2003), Pd/C (S. D. Jackson and L. A. Shaw, 1996), and commercial Lindlar catalyst for alkynes semihydrogenation reaction. **Figure5.27(a)** shows the performance of Pd/TiO$_2$-9nm, the styrene selectivity at 100% phenylacetylene conversion was significantly improved when it was reduced at 500°C. Such results suggest that the strong metal-support interaction on Pd/TiO$_2$ produced great beneficial effect on the catalyst performance. However, for the catalyst supported on larger TiO$_2$ crystallite size, Pd/TiO$_2$-12nm, Pd/TiO$_2$-17nm and Pd/TiO$_2$-23 nm (**Figure 5.27(b-d)**), the styrene selectivity for Pd/TiO$_2$ reduced at 500°C were dramatically decrease until

similar to that reduced at 40°C especially when the reaction time was prolonged. Based on CO chemsisorption results, all the Pd/TiO$_2$ catalysts appeared to exhibit the strong metal-support interaction when reduced at 500°C. However, the catalyst performance reveals that the SMSI effect may decrease with increasing TiO$_2$ crystallite size. A number of study has also shown the absence of SMSI effect on Pd/TiO$_2$ during high temperature reduction when the TiO$_2$ particle size is very large ($\geq$ 100 nm) (Weerachawanasak, P. *et al.*, 2007, Musolino *et al.*, 2004). Moreover, Panagiotopoulou et al. (Panagiotopoulou *et al.*, 2006) reported that formation of substoichiometric TiO$_x$ species was more facile over Pt/TiO$_2$ for small TiO$_2$ particle sizes (around 10 nm).

Generally, the mechanism of phenylacetylene hydrogenation pronounced in two pathways. In the first way, phenylacetylene will be hydrogenated to styrene and ethybenzene in two steps. As in the second way, phenylacetylene will be hydrogenated directly to ethylbenzene. In this research, it was found that the first pathway usually occur more than the second pathway. Under the reaction conditions used, the phenylacetylene was hydrogenated up to nearly 100% conversion within 20 min. When the concentration of phenylacetylene was sufficiently low, the hydrogenation of styrene to ethylbenzene was then occurred. This indicates a slower parallel reaction pathway for the direct hydrogenation of phenylacetylene to ethylbenzene.
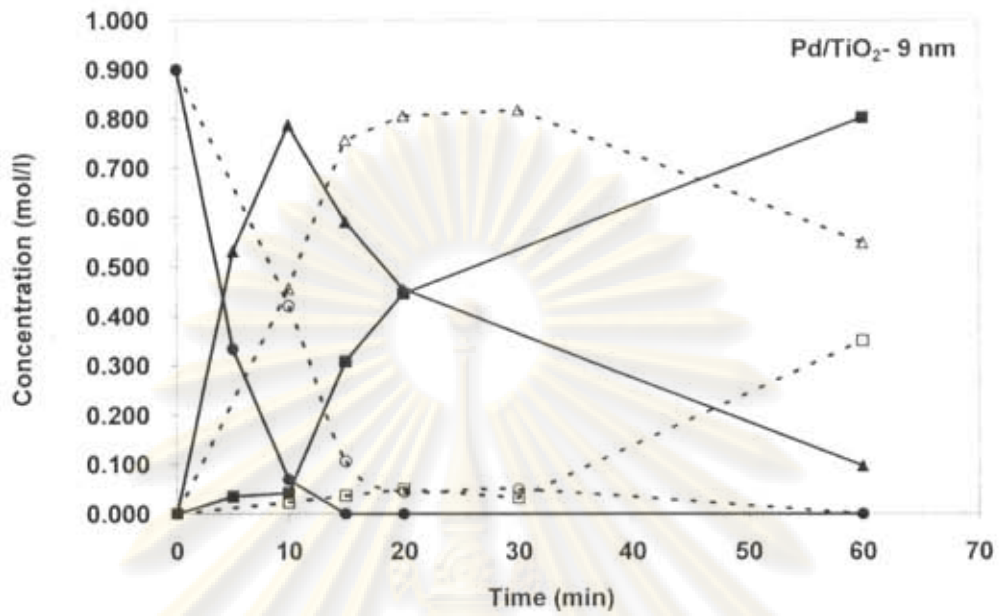
(a) 1%Pd/TiO$_2$-9 nm
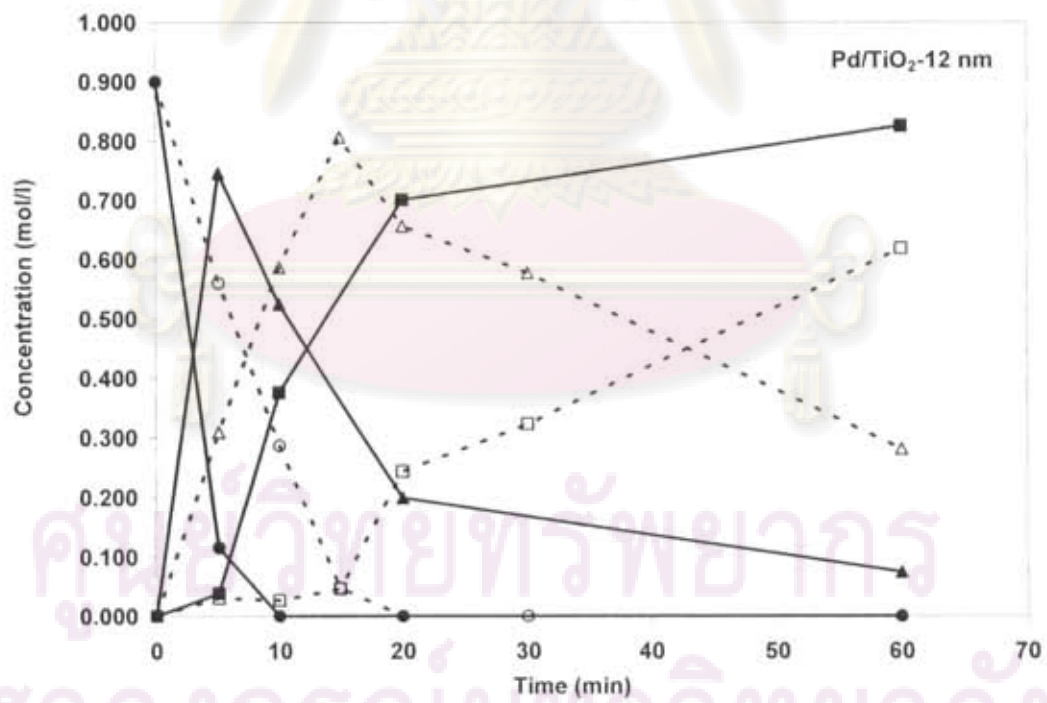
(b) 1%Pd/TiO$_2$-12 nm
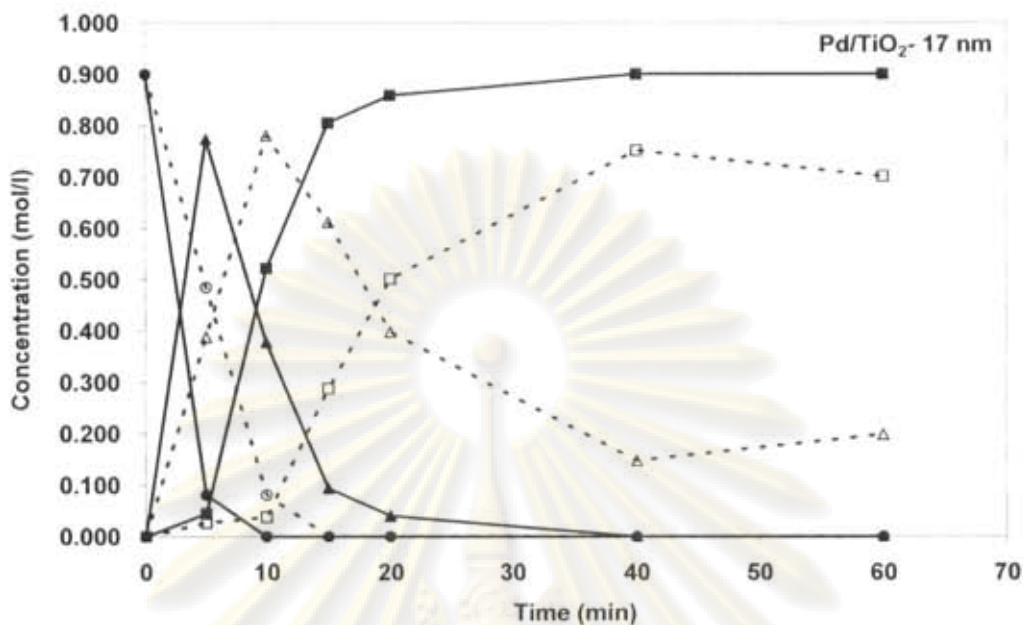
(c) 1%Pd/TiO$_2$-17 nm
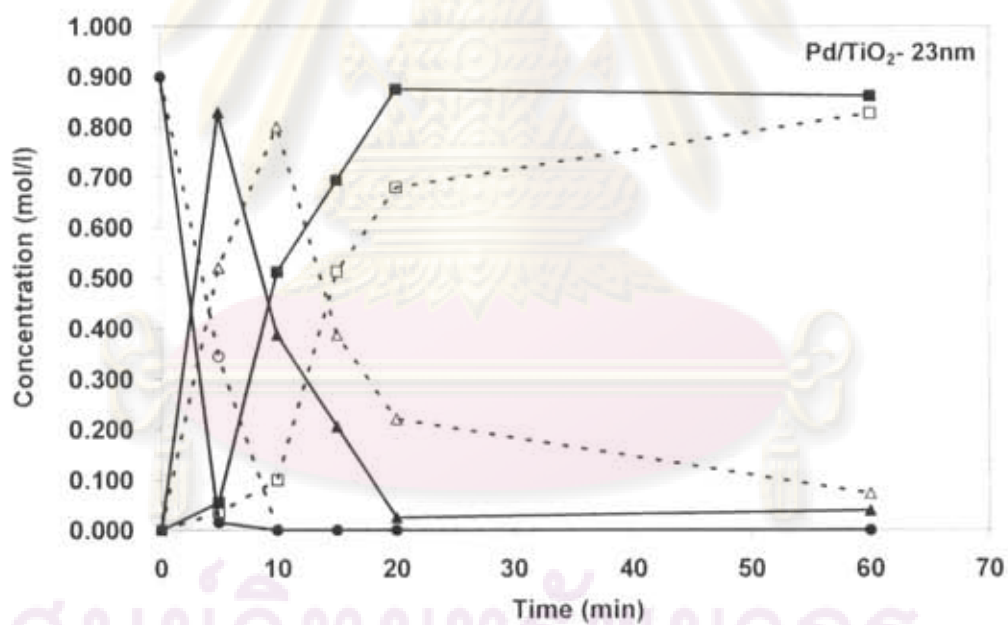
(d) 1%Pd/TiO$_2$-23 nm

Figure5.27 The effect of various nanocrystallite sizes of TiO$_2$ on the liquid phase

selective hydrogenation of phenylacetylene :

(o : phenylacetylene concentration); (Δ : styrene concentration);

(□ : ethylbenzene concentration). Closed symbols: Pd/TiO$_2$ catalyst

reduced at 40°C and Open symbols: Pd/TiO$_2$ catalyst reduced at 500°C.
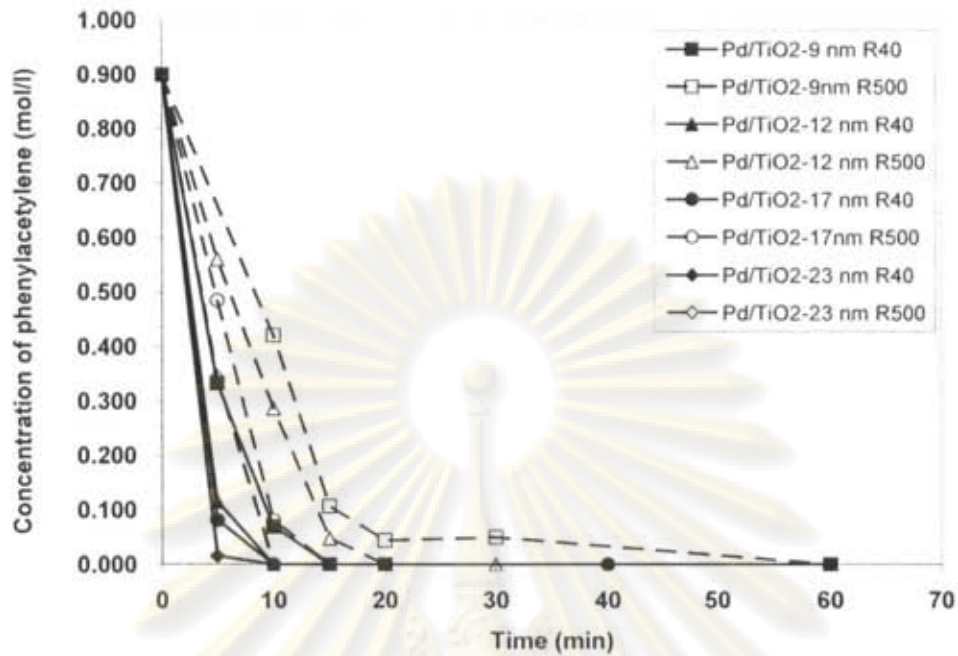
Figure5.28 Hydrogenation rate of phenylacetylene over Pd/TiO₂ catalysts which reduced at 40°C and 500°C

CHAPTER VI

CONCLUSIONS AND RECOMMENDATIONS

In this chapter, section 6.1 provides the conclusions obtained from the experimental results of Pd/TiO$_2$ catalysts prepared with various crystallite sizes of TiO$_2$ supports in both of micron (1 μm) and nano scales (9-23 nm) in the liquid phase selective hydrogenation of phenylacetylene. Section 6.2 suggested the recommendations in this work.

6.1 Conclusions

6.1.1 Comparative study of Pd catalysts supported on micron and nano-sized TiO$_2$

Based on the results from various characterization techniques such as CO pulse chemisorption, X-ray photoelectron spectroscopy (XPS), transmission electron microscopy (TEM), and CO-temperature program desorption. The nano-sized TiO$_2$ supported Pd catalyst exhibited strong metal-support interaction (SMSI) exhibited when the catalyst was reduced at 500°C. Such effect was not found on the micron-sized TiO$_2$ supported one; sintering of Pd^{0*} metal was observed instead. The SMSI effect appeared to be necessary for high catalytic performance of the Pd/TiO$_2$ catalysts in liquid phase selective hydrogenation of phenylacetylene to styrene. The presence of SMSI effect may result in an inhibition of the adsorption of the product styrene hence styrene selectivity was improved especially high phynelacetylene conversion.

6.1.2 Catalytic Properties of Pd catalysts supported on a series of solvothermal-derived TiO$_2$ (TiO$_2$ crystallite size 9-23 nm)

For the series of nanocrystalline TiO$_2$ supported Pd catalysts (TiO$_2$ crystallite size 9-23 nm) higher Pd dispersion and smaller Pd particles were obtained on the catalysts with smaller TiO$_2$ crystallite size. Phenylacetylene hydrogenation rate for the

catalysts reduced at $500^{\circ}C$ was lower than those reduced at $40^{\circ}C$. This effect was more pronounced for the smaller TiO_2 crystallite size supported Pd catalysts. All the catalysts exhibited the strong metal-support interaction effect since styrene selectivity at 100% phenylacetylene conversion was improved when the catalysts were reduced at $500^{\circ}C$. However, the SMSI effect may decrease with increasing TiO_2 crystallite size. The SMSI effect became less pronounced for larger crystallite size TiO_2.

6.2 Recommendations

1. The SMSI effect on various nanocrystallite sizes of TiO_2 supports palladium catalysts in the range of 30-100 nm should be investigated for the optimum of TiO_2 crystallite size.

2. The presence/absence of SMSI effect of Pd/TiO_2 should be investigated in other catalytic reactions, i.e., selective oxidation.

3. The presence of Ti^{3+} on the surface of TiO_2 should be confirmed by other techniques such as X-ray photoelectron spectroscopy (XPS).

4. The nano-sized commercial TiO_2 supported Pd catalyst should be investigated the characteristic and catalytic performance in the liquid phase selective hydrogenation of phenylacetylene for comparative with the solvothermal derived nano-sized TiO_2 supported one.

REFERENCES

Albers, P., Seibold, K., Prescher, G., and Muller, H. XPS and SIMS studies of carbon deposits on Pt/Al$_2$O$_3$ and Pd/SiO$_2$ catalysts applied in the synthesis of hydrogen cyanide and selective hydrogenation of acetylene. Appl. Catal. A. 176 (1999): 135-146.

Ali, S. H., and Goodwin, J. G., Jr. SSITKA Investigation of Palladium Precursor and Support Effects on CO Hydrogenation over Supported Pd Catalysts. J. Catal. 176 (1998): 3-13.

Anderson, A. B., and Onwood, D. P. Why carbon monoxide is stable lying down on a negatively charged Ru(001) surface but not on Pt (111). Surface Science Letters. 154(1985): L261-L267.

Angel, G. D., and Benitez, J.L. Ammonia and sulfur poisoning effects on hydrogenation of phenylacetylene over Pd supported catalysts. J. Mol. Catal. A. 94 (1994): 409-416.

Arena, F., Cum, G., Gallo, R., Parmaliana, A. Palladium catalysts supported on oligomeric aramides in the liquid-phase hydrogenation of phenylacetylene. J. Mol. Catal. A. 110 (1996): 235-242.

Bond, G.C. Metal-Support and Metal-Additive Effects in Catalysis. Platinum Metals Rev. 21 (1983): 16-18.

Carturan, G., Facchin, G., Cocco, G., Enzo, S., and Navazio, G. Influence of metal dispersion on selectivity and kinetics of phenylacetylene hydrogenation catalyzed by supported palladium. J. Catal. 76 (1982): 405-417.

Duca, D., Liotta, L.F., and Deganello, G. Liquid phase hydrogenation of phenylacetylene on pumice supported palladium catalysts. Catal. Today. 24 (1995): 15-21.

Fujishima, A., Hashimoto, K. and Watanabe, T. TiO$_2$ photocatalysis: fundamental and applications. 1 st ed. Tokyo: BKC, 1999.

Guczi, L., Borkó, L., and Schay, Z. Some problems on environmental catalysis Studies in Surface Science and Catalysis.113 (1998): 69-80.

How, R. F., and Gratzel, M. EPR Observeation of Trapped Electrons in Colloidal TiO$_2$. J. Phys.Chem. 89 (1985): 4495-4499.

Huang, X., Wilhite, B., McCready, M. J., Varma, A. Phenylacetylene hydrogenation in a three-phase catalytic packed-bed reactor: experiments and model. Chem. Eng. Sci. 58 (2003): 3465 – 3471.

Ikeda, S., Sugiyama, N., Murakami, S., Kominami, H., Kera, Y., Noguchi, H., Uosaki, K., Torimoto, T., and Ohtani, B. Quantity analysis of defective sites in titanium (IV) oxide photocatalyst powders. Phys. Chem. Chem. Phys. 5 (2003): 778-783.

Jackson, S. D., and Shaw, L.A. The liquid phase hydrogenation of phenylacetylene and styrene on palladium/carbon catalyst. Appl. Catal. A.134 (1996):161-168.

Kang, M., Lee, S. Y., Chung, C.H., Cho, S. M., Han,G. Y., Kim, B.W., Yoon, K. J. Characterization of a TiO₂ photocatalyst synthesized by the solvothermal method and its catalytic performance for CHCl₃ decomposition. J. Photochem. Photobiol. A 144 (2001): 185–191.

Kang, M. Synthesis of Fe/TiO₂ photocatalyst with nanometer size by solvothermal method and the effect of H₂O addition on structural stability and potodecomposition of methanol. J. Mol.Catal.A.197 (2003): 173–183.

Kim, C. S., Moon, B. K., Park, J. H., Chung, S. T., and Son, S. M. Synthesis of nanocrystalline TiO₂ in toluene by a solvothermal route. J. Crystal Growth. 254 (2003): 405–410.

Kim, C.S., Kwon., I.M., Moon, B. K., Jeong, J. H., Choi,B.C. Kim, J. H., Choi, H., Yi,S. S., Yoo,D. H., Hong, K.S., Park, J.H., Lee, H. S. Synthesis and particle size effect on the phase transformation of nanocrystalline TiO₂. Mat.Sci.Eng. C. 27 (2007):1343–1346.

Kominami, H., Kohno, M., Takada, Y., Inoue, M., Inui, T., and Kera, Y. Hydrothermal of Titanium Alkoxide in Organic Solvent at High Temperatures: A New Synthetic Method for Nanosized, Thermally Stable Titanium (IV) Oxide. Ind. Eng. Chem. Res. 38 (1999): 3925-3931.

Kongsuebchart, W., Praserthdam, P., Panpranot, J., Sirisuk, A., Supphasrirongjaroen, P., and Satayaprasert, C. Effect of crystallite size on the surface defect of nano-TiO₂ prepared via solvothermal synthesis. J. Crys. Growth. 297 (2006): 234-238.

Kumar P. M., Badrinarayanan, S., Sastry, M. Nanocrystalline TiO₂ studied by optical, FTIR and X-ray photoelectron spectroscopy: correlation to presence of surface states. Thin Solid Films 358 (2000): 122-130.

Li, Y., Xu, B., Fan, Y., Feng, N., Qiu, A., He, J. M. J., Yang H., and Chen, Y. The effect of titania polymorph on the strong metal-support interaction of Pd/TiO$_2$ catalysts and their application in the liquid phase selective hydrogenation of long chain alkadienes. J. Mol. Catal.A. 216 (2004): 107–114.

Liqianga, J., Xiaojuna, S., Weimina, C., Zilic, X. Yaoguoc, D., Honggangb, F. The preparation and characterization of nanoparticle TiO$_2$/Ti films and their photocatalytic activity. J. Phy. Chem. Solid. 64 (2003): 615–623.

Lee, D. C., Kim, H., Kim, W. J., Kang, J. H. and Moon, S. H., Selective hydrogenation of 1,3-butadiene on TiO$_2$-modified Pd/SiO$_2$ catalysts. Appl. Catal. A. 244 (2003): 83-91.

Mahata, N., and Vishwanathan, V. Influence of Palladium Precursors on Structural Properties and Phenol Hydrogenation Characteristics of Supported Palladium. Catalysts. J. Catal. 196 (2000): 262–270.

Marin-Astorga, N., Alvez-Manoli, G., Reyes, P. Stereoselective hydrogenation of phenyl alkyl acetylenes on pillared clays supported palladium catalysts. J. Mol. Catal. A 226 (2005): 81-88.

Molnár, Á.; Sárkany, A.; and varga, M. Hydrogenation of carbon-carbon multiple bonds: chemo-, region- and stereo-selectivity. J. Mol. Catal. 173 (2001): 185-221.

Musolino, M.G., De Maio, P., Donato, A., Pietropaolo, R. Hydrogenation versus isomerization in α,β-unsaturated alcohols reactions over Pd/TiO$_2$ catalysts. J. Mol. Catal. A. 208 (2004): 219–224.

Musolino, M. G., De Maio, P., Donato, A., and Pietropaolo, R. Hydrogenation versus isomerization in α, β-unsaturated alcohols reactions over Pd/TiO$_2$ catalysts. J. Mol. Catal. A.208 (2004): 219-224.

Nijhuis, T.A., Koten, G. van., Moulijn, J.A., Optimized palladium catalyst systems for the selective liquid-phase hydrogenation of functionalyzed alkynes. Appl. Catal. A.238 (2003): 259–271.

Panagiotopoulou, P., Christodoulakis, A., Kondarides, D. I., and Boghosian, S. Particle size effects on the reducibility of titanium dioxide and its relation to the water-gas shift activity of Pt/TiO$_2$ catalysts. J. Catal 240 (2006):114-125.

Panpranot, J., Pattamakomsan, K., Praserthdam, P. and Goodwin, G.J. A comparative study of Pd/SiO₂ and Pd/MCM-41 catalysts in liquid-phase hydrogenation. Catal. Com. 5 (2004): 583-590.

Panpranot, J., Phandinthong, K., Praserthdam, P., Hasegawa, M., Fujita, S., Arai, M. A comparative study of liquid-phase hydrogenation on Pd/SiO₂ in organic solvents and under pressurized carbon dioxide: Activity change and metal leaching/sintering. J. Mol. Catal. A. 253 (2006): 20–24.

Reyes, P., Rojas, H., Fierro, J.L.G. Effect of Fe/Ir ratio on the surface and catalytic properties in citral hydrogenation on Fe-Ir/TiO₂ catalysts. J. Mol.Catal.A. 203 (2003): 203–211.

Sales, E.A., Bugli, G., Ensuque, A., Mendes, M. J. and Bozon-Verduraz, F. Phys. Chem. Chem. Phys. 1(1999): 491.

Sarkany, A., Weiss, A.H., and Guczi, L. Structure sensitivity of acetylene-ethylene hydrogenation over Pd catalysts. J. Catal. 98 (1986): 550-553.

Tauster, S.J., Fung, S.C., Garten, R.L. Strong Metal-Support Interactions Group 8 Noble Metals Supported on TiO₂. J. Ame.Chem.Soc.(1978): 170-174.

Wagner, C. D., Riggs,W. M., Davis, L. E., Moulder, J. F. Handbook of X-ray Photoelectron Spectroscopy, G. E. Muilenberg, Ed. Perkin-Elmer Corporation, Eden Prairie, MN, 1978.

Weerachawanasak, P., Praserthdam, P., Arai, M., Panpranot, P. A comparative study of strong metal–support interaction and catalytic behavior of Pd catalysts supported on micron- and nano-sized TiO₂ in liquid-phase selective hydrogenation of phenylacetylene. J. Mol. Catal. A.279 (2008): 133-139.

Xu, J., Sun, K., Zhang, L., Ren, Y., Xu, X. A highly efficient and selective catalyst for liquid phase hydrogenation of maleic anhydride to butyric acid. Catal. Comm. 6 (2005): 462-465.

Zhang, F., Zheng, Z., Liu, D., Mao, Y., Chen, Y., Zhou, Z., Yang, S., and Liu, X. Synthesis of titanium dioxide films by ion beam enhanced deposition. Nuclear Instruments and Methods in Physics Research Section B: Beam Interactions with Materials and Atoms. 132 (1997): 620-626.

APPENDICES

APPENDIX A

CALCULATION FOR CATALYST PREPARATION

Preparation of 1%Pd/TiO$_2$ catalysts by the incipient wetness impregnation method are shown as follows:

Reagent: - Palladium (II) nitrate hexahydrate (Pd (NO$_3$)$_2 \cdot$ 6H$_2$O)

              Molecular weight = 338.52

         - Support: Titania [TiO$_2$]

Example Calculation for the preparation of 1%Pd/TiO$_2$

Based on 100 g of catalyst used, the composition of the catalyst will be as follows:

     Palladium   =   1 g

     Titania   =   100-1   =   99 g

For 3 g of titania

Palladium required   =   3×(1/99)   =   0.0303 g

Palladium 0.0303 g was prepared from Pd (NO$_3$)$_2 \cdot$ 6H$_2$O and molecular weight of Pd is 106.42

$$\text{Pd (NO}_3)_2 \cdot \text{6H}_2\text{O required} = \frac{\text{MW of Pd(NO}_3)_2 \cdot \text{6H}_2\text{O} \times \text{palladium required}}{\text{MW of Pd}}$$

$$= (338.52/106.42) \times 0.0303 = 0.0964 \text{ g}$$

Since the pore volume of the titania support is 0.4 ml/g. Thus, the total volume of impregnation solution which must be used is 1.2 ml for titania by the requirement of incipient wetness impregnation method, the de-ionized water is added until equal pore volume for dissolve Palladium (II) nitrate hexahydrate.

APPENDIX B

CALCULATION OF THE CRYSTALLITE SIZE

Calculation of the crystallite size by Debye-Scherrer equation

The crystallite size was calculated from the half-height width of the diffraction peak of XRD pattern using the Debye-Scherrer equation.

From Scherrer equation:

$$D = \frac{K\lambda}{\beta \cos \theta} \qquad \text{(B.1)}$$

where
D = Crystallite size, Å

K = Crystallite-shape factor = 0.9

λ = X-ray wavelength, 1.5418 Å for CuKα

θ = Observed peak angle, degree

β = X-ray diffraction broadening, radian

The X-ray diffraction broadening (β) is the pure width of a powder diffraction free from all broadening due to the experimental equipment. α-Alumina is used as a standard sample to observe the instrumental broadening since its crystallite size is larger than 2000 Å. The X-ray diffraction broadening (β) can be obtained by using Warren's formula.

From Warren's formula:

$$\beta = \sqrt{B_M^2 - B_S^2} \qquad \text{(B.2)}$$

Where
B_M = The measured peak width in radians at half peak height.

B_S = The corresponding width of the standard material.

Example: Calculation of the crystallite size of TiO_2-micron

The half-height width of peak $= 0.23°$ (from Figure B.1)

$= (2\pi \times 0.23)/360$

$= 0.00401$ radian

The corresponding half-height width of peak of α-alumina $= 0.00383$ radian

The pure width $= \sqrt{B_M^2 - B_S^2}$

$= \sqrt{0.00401^2 - 0.00383^2}$

$= 0.0012$ radian

$\beta = 0.0012$ radian

$2\theta = 25.28°$

$\theta = 12.64°$

$\lambda = 1.5418$ Å

The crystallite size $= \dfrac{0.9 \times 1.5418}{0.0012 \cos 12.64} = 1185.07$ Å

$= 118.5$ nm
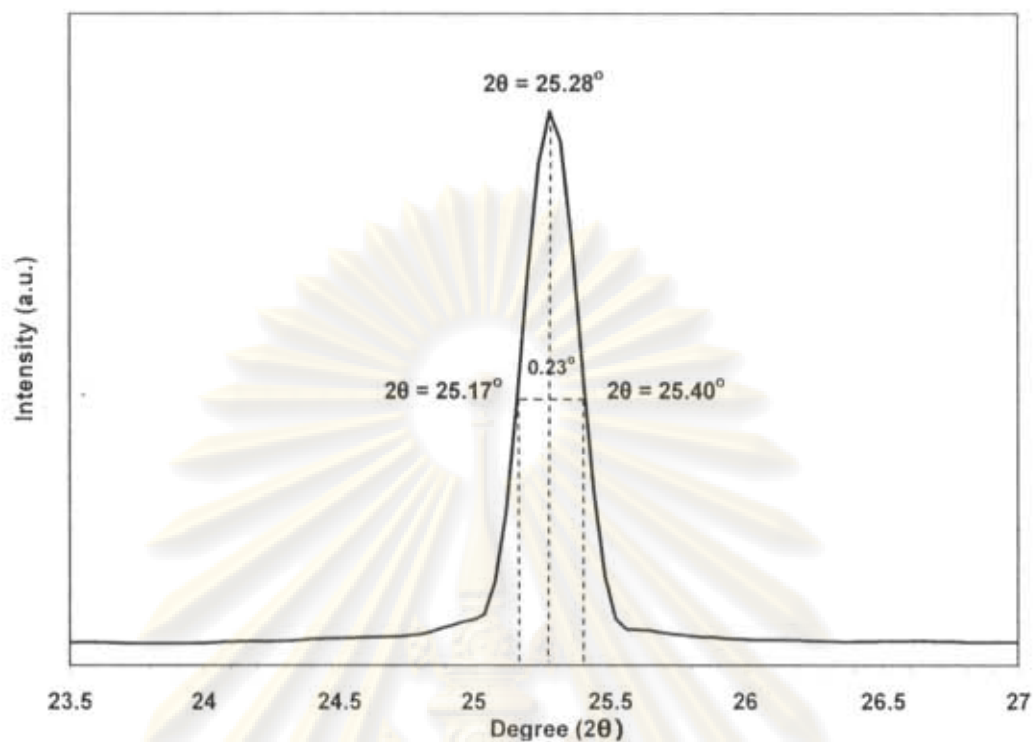
Figure B.1 The measured peak of TiO$_2$-micron for calculation the crystallite size.

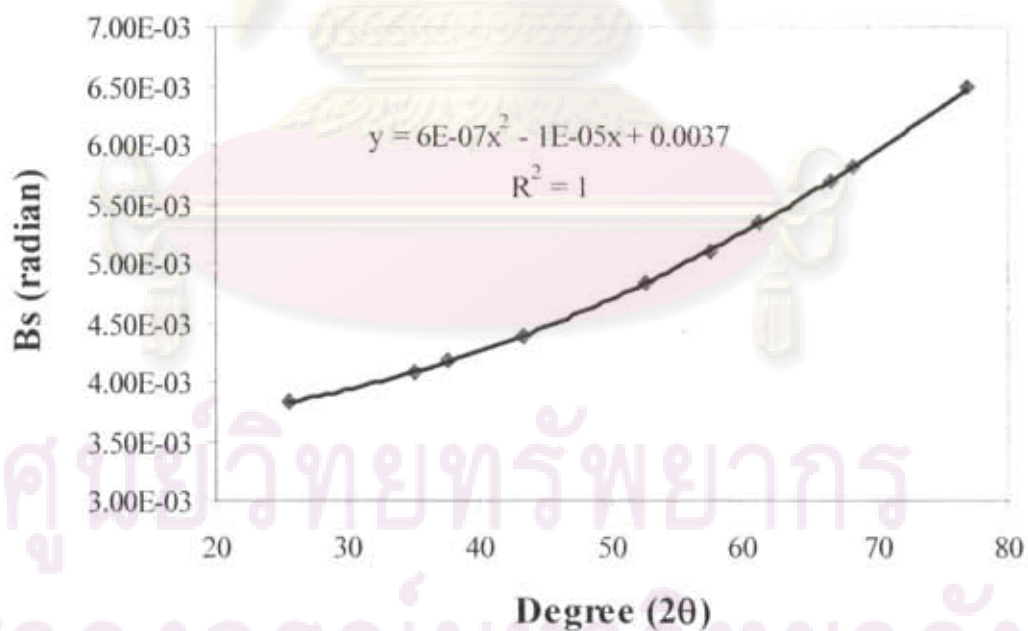$$y = 6E\text{-}07x^2 - 1E\text{-}05x + 0.0037$$
$$R^2 = 1$$

Figure B.2 The plot indicating the value of line broadening due to the equipment. The data were obtained by using α-alumina as standard

APPENDIX C

CALCULATION FOR METAL ACTIVE SITES AND DISPERSION

Calculation of the metal active sites and metal dispersion of the catalyst measured by CO adsorption is as follows:

Calculation of metal active site

Let the weight of catalyst used	= W	g
Integral area of CO peak after adsorption	= A	unit
Integral area of 75 μl of standard CO peak	= B	unit
Amounts of CO adsorbed on catalyst	= B-A	unit
Volume of CO adsorbed on catalyst	= $75 \times [(B-A)/B]$	μl
Volume of 1 mole of CO at 30°C	= 24.86×10^6	μl

Mole of CO adsorbed on catalyst $= [(B-A)/B] \times [75/24.86 \times 10^6]$ mole

Molecule of CO adsorbed on catalyst $= [3.02 \times 10^{-6}] \times [6.02 \times 10^{23}] \times [(B-A)/B]$ molecules

Metal active sites $= 1.82 \times 10^{18} \times [(B-A)/B] \times [1/W]$ molecules of CO/g of catalyst

Calculation of %metal dispersion

Definition of % metal dispersion :

Metal dispersion (%) = 100×[molecules of Pd from CO adsorption/molecules of Pd loaded]

In this study, the formula from Chemisorb 2750 Operator's Manual can used for determined the % metal dispersion as follow:

$$\%D = S_f \times [\frac{Vads}{Vg}] \times [\frac{m.w.}{\%M}] \times 100\% \times 100\% \dots\dots\dots\dots(1)$$

Where

%D	=	%metal dispersion	
S_f	=	stoichiometry factor, (CO on Pd* =1)	
V_{ads}	=	volume adsorbed	(cm^3/g)

V_g	=	molar volume of gas at STP = 22414 (cm^3/mol)
$m.w.$	=	molecular weight of the metal (a.m.u.)
$\%M$	=	%metal loading

Example: %Dispersion of 1%Pd/TiO$_2$-micron-R40

- Calculation Volume Chemisorbed (V_{ads})

$$V_{ads}(cm^3) \quad = \quad [\frac{Vinj}{m}] \times \sum_{i=1}^{n}(1-\frac{Ai}{Af})\ \text{.........................(2)}$$

Where:

V_{ing}	=	volumn injected (cm^3) = 0.075 cm^3
m	=	mass of sample (g)
Ai	=	area of peak i
Af	=	area of last peak

To replace values in equation (1) and (2);

$$V_{ads} \quad = \quad [\frac{0.075}{0.0235}] \times [(1-\frac{0.010}{0.143})+ (1-\frac{0.142}{0.143})]$$

$$= \quad 0.345\ cm^3$$

$$\%D \quad = \quad 1 \times [\frac{0.345}{22414}] \times [\frac{106}{1}] \times 100\% \times 100\%$$

$$= \quad \mathbf{16.4\%}$$

So that %Pd dispersion is 16.4%

ศูนย์วิทยทรัพยากร

จุฬาลงกรณ์มหาวิทยาลัย

Calculation of Average Crystallite Size

Average Crystallite Size of Palladium metal can be calculated base on active metal surface area per gram of metal

$$d_p^o = [\frac{Fg}{p \times MSAm}] \times [\frac{m^3}{10^6 cm^3}] \times \frac{10^9}{m} nm \dots\dots(3)$$

Where:

d_p^o = average crystallite size of Palladium metal

Fg = crystallite geometry factor (hemisphere = 6)

p = specific gravity of the active metal (Palladium = 12.0 g/cm^3)

$MSAm$ = active metal surface area per gram of metal (m^2/g_{metal})

Example: Average Crystallite Size of 1%Pd/TiO$_2$-micron-R40

- Calculation of active metal surface area

$$MSAm = S_f \times [\frac{Vads}{Vg}] \times [\frac{100\%}{\%M}] \times N_A \times \sigma_m \times [\frac{m^2}{10^{18} nm^2}] \dots\dots(4)$$

Where:

N_A = Avogado's number (6.02×10^{23} molecules/mol)

σ_m = cross-sectional area of active metal atom (Palladium = 0.0787 nm^2)

To replace values in equation (3) and (4);

$$MSAm = 1 \times [\frac{0.345}{22414}] \times [\frac{100\%}{1\%}] \times 6.02 \times 10^{23} \times 0.0787 \times 10^{-18}$$

$$= 72.92 \ m^2/g_{metal}$$

$$d_p^o = \frac{6000}{(12 \times 72.92)}$$

$$= \mathbf{6.85 \ nm}$$

Average crystallite size of Palladium metal equal to 6.85 nm

APPENDIX D

CALIBRATION CURVES

This appendix showed the calibration curves for calculation of composition of reactant and products in phenylacetylene hydrogenation. The reactant is phenylacetylene and products are styrene and ethylbenzene.

The flame ionization detector (FID), gas chromatography Shimadzu modal 14B was used for analyzing the concentration of phenylacetylene, styrene and ethylbenzene by using GS-alumina column.

The GS-alumina column was used with a gas chromatography equipped with a flame ionization detector (FID), Shimadzu modal 14B, for analyzing the concentration of phenylacetylene, styrene and ethylbenzene. Conditions uses in GC are illustrated in **Table D.1**.

Mole of reagent in y-axis and area, which was reported by gas chromatography, in x-axis are exhibited in the curves. The calibration curves of phenylacetylene, styrene and ethylbenzene are shown in **FigureD.1**, **FigureD.2** and **FigureD.3**, respectively. The example of product and reactant peaks from GC shows in **FigureD.4**.

Table D.1 Conditions uses in Shimadzu modal GC-14B.

Parameters	Conditions of Shimadzu GC-14B
Width	5
Slope	29
Drift	0
Min. area	100
T.DBL	2.7
Stop time	30
Atten	1
Speed	2
Method	1
Format	1
SPL.WT	100
IS.WT	0

ศูนย์วิทยทรัพยากร

จุฬาลงกรณ์มหาวิทยาลัย
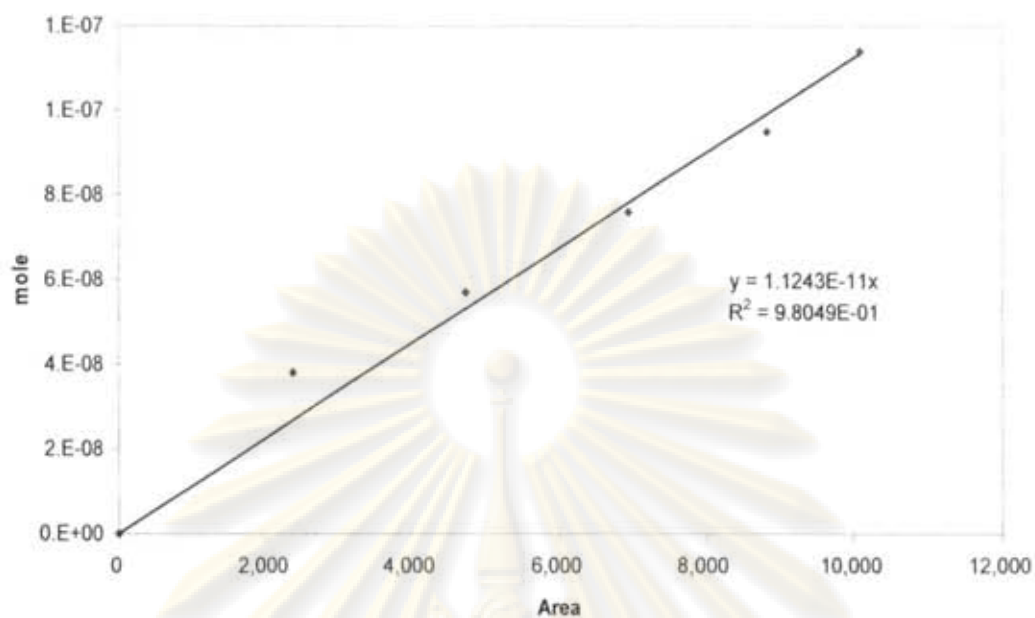
FigureD.1 The calibration curve of phenylacetylene

y = 1.1243E-11x
R^2 = 9.8049E-01
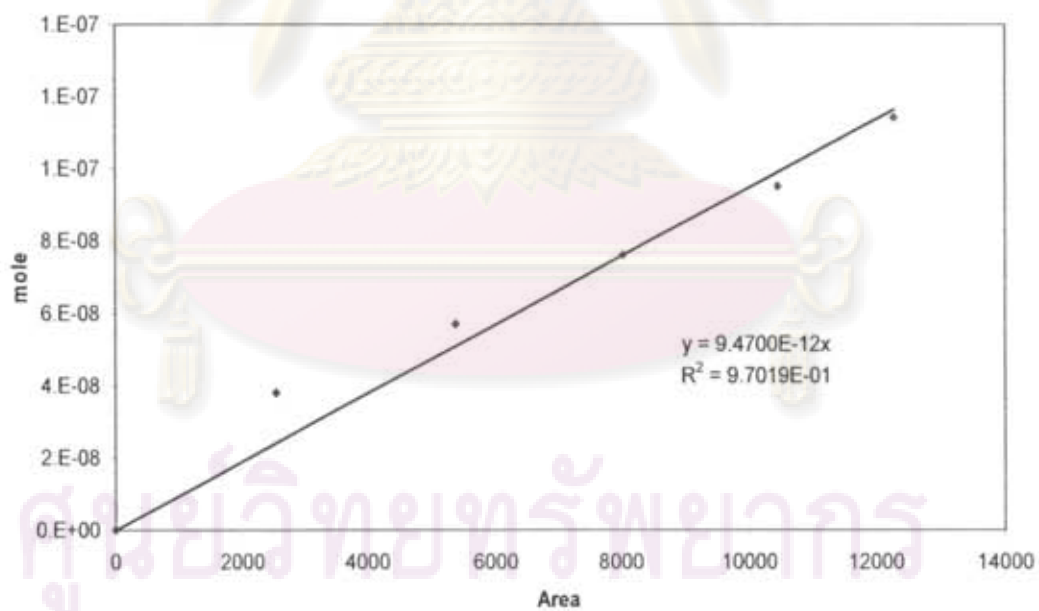
FigureD.2 The calibration curve of styrene

y = 9.4700E-12x
R^2 = 9.7019E-01
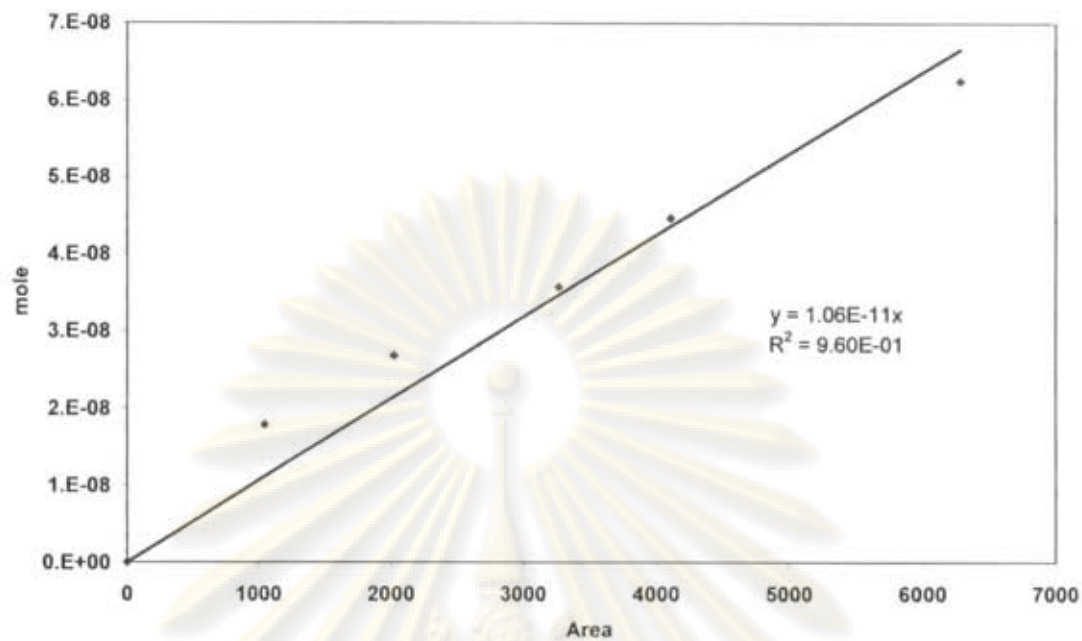
FigureD.3 The calibration curve of ethylbenzene
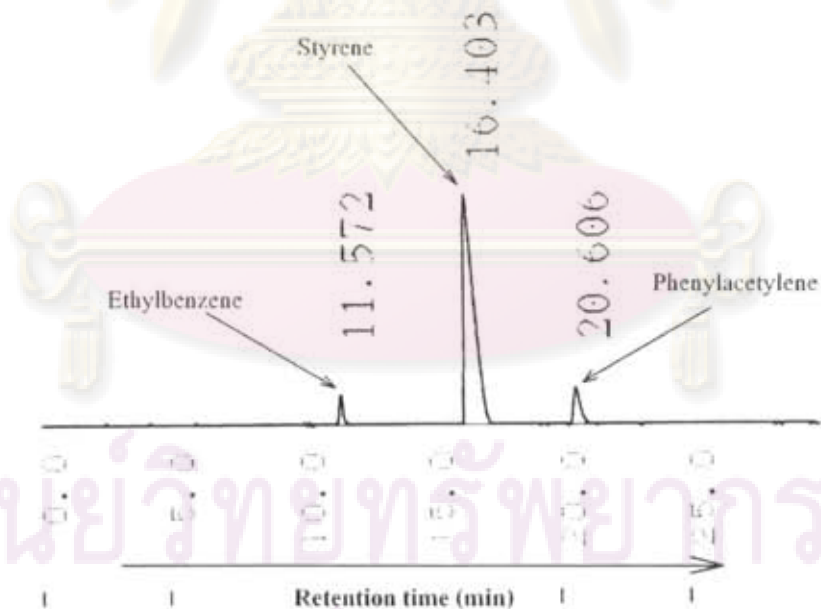
FigureD.4 The GC peaks of phenylacetylene, styrene and ethylbenzene

APPENDIX E

CALCULATION OF PHENYLACTYLENE CONVERSION
AND STYRENE SELECTIVITY

The catalytic performance for the phenylacetylene (PA) hydrogenation was evaluated in terms of activity for phenylacetylene conversion and styrene selectivity.

Activity of the catalyst performed in term of phenylacetylene conversion. Phenylacetylene conversion is defined as moles of phenylacetylene converted with respect to phenylacetylene in feed:

$$\text{PA conversion (\%)} = \frac{\text{mole of PA in feed - mole of PA in product}}{\text{mole of PA in feed}} \times 100$$

Where mole of phenylacetylene can be measured employing the calibration curve of phenylacetylene in Figure D.1, Appendix D., i.e.

$$\text{Mole of PA} = (\text{Area of PA peak from integrator plot on GC - 14B}) \times 1.1243 \times 10^{-11}$$

Selectivity of product is defined as mole of styrene (ST) formed with respect to mole of styrene and ethylbenzene was obtained:

$$\text{Selectivity of ST (\%)} = \frac{\text{mole of ST formed}}{\text{mole of total product}} \times 100$$

Where mole of styrene and ethylbenzene can be measured employing the calibration curve of styrene in Figure D.2 and Figure D.3, in Appendix D, respectively.

$$\text{Mole of styrene} = (\text{Area of styrene peak from integrator plot on GC - 14B}) \times 9.47 \times 10^{-12}$$
$$\text{Mole of ethylbenzene} = (\text{Area of styrene peak from integrator plot on GC - 14B}) \times 1.06 \times 10^{-11}$$

APPENDIX F

LIST OF PUBLICATIONS

1. Patcharaporn Weerachawanasak, and Joongjai Panpranot, "Liquid Phase Semihydrogenation of Phenylacetylene on Micron and Nano-sized TiO$_2$ supported Pd Catalysts", Proceedings of the Regional Symposium on Chemical Engineering , 3-5 Dec. (2006), Singapore.

2. Patcharaporn Weerachawanasak, Joongjai Panpranot, Piyasan Praserthadam, and Masahiko Arai, " A Comparative Study of Strong Metal-Support Interaction and Catalytic Behaviors of Pd Catalysts Supported on Micron-and Nano-sized TiO$_2$ in Liquid-Phase Selective Hydrogenation of Phenylacetylene", Journal of Molecular Catalysis A (2008).

ศูนย์วิทยทรัพยากร
จุฬาลงกรณ์มหาวิทยาลัย

VITA

Miss Patcharaporn Weerachawanasak was born in July 13th, 1982 in Nakhonsawan, Thailand. She finished high school from Satrinakhonsawan School, Nakhonsawan in 2001, and received bachelor's degree in Chemistry Science from the department of Chemistry, Faculty of Science, Kasetsart University, Bangkok, Thailand in 2005.